Effects of Salt and pH

on Binding and Catalysis by Ribonuclease A

by

Chiwook Park

A dissertation submitted in partial fulfillment

of the requirements for the degree of

Doctor of Philosophy

(Biochemistry)

at the

University of Wisconsin–Madison

2000

A dissertation entitled

Effects of Salt and pH

on Binding and Catalysis by Ribonuclease A

submitted to the Graduate School of the

University of Wisconsin-Madison

in partial fulfillment of the requirements for the
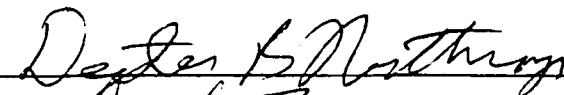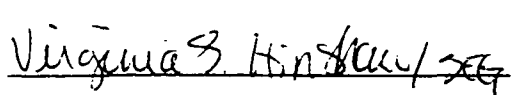
degree of Doctor of Philosophy

by

Chiwook Park

Date of Final Oral Examination: December 1, 2000

Month & Year Degree to be awarded: **December** 2000 **May** **August**

* *

Approval Signatures of Dissertation Readers: **Signature, Dean of Graduate School**

ACKNOWLEDGEMENTS

First, I thank my advisor, Dr. Ronald T. Raines for his mentoring. My research as a graduate student has overflowed with unsolved mysteries and inexplicable abnormalities. He was always patient with my perplexing results, enjoyed the moments of breakthrough together, and never doubted my experimental skills. I appreciate all the help from former and present members of Raines lab as colleague scientists and warmest friends. Dr. L. Wayne Schultz helped me in the crystallization of H12A and H119A RNase A. Dr. Byung-Moon Kim passed me the fail-proof mutagenesis technique. I am greatly indebted to Dr. Barbra M. Fisher for providing invaluable foundation of salt effects and Dr. Bradley R. Kelemen for his fascinating fluorogenic substrates indispensable for this dissertation. I also owe them a big Thank you for the guidance they provided me when I initiated my graduate work in this lab. I thank Kenneth J. Woychechowsky, Marcia C. Haigis, Dr. Tony A. Klink for insightful discussions on my research and encouragement on rainy days. I thank Dr. Sang-Hyun Park for his everlasting friendship.

I cannot thank my family too much, especially my parents, my lovely wife, Sookkyung, and Esther, for their immeasurable support and love. I also thank my friends in belief for their prayers for my family. Finally, I praise the Lord for His guidance and comfort in my life. I realized His power is indeed made perfect in my weakness (2 Corinthians 12:9).

ABSTRACT

Salt concentration and pH have dramatic effects on enzymatic catalysis. A quantitative description on these effects is important to elucidate the energetics and mechanisms of catalysis. Here, the effects of salt concentration and pH on binding and catalysis are analyzed with Ribonuclease A (RNase A) as a model system.

The effects of pH and mutagenesis on the stability of RNase A•nucleic acids complexes were studied by biophysical methods (Chapter 2). The thermodynamic information indicates that the active-site histidine residues make a significant contribution to nucleic acid binding as well as to catalytic turnover. The origin of RNase A "inactivation" at low salt concentration is scrutinized by kinetic studies (Chapter 3). The results show that inactivation results from the inhibition of RNase A activity by low-level contaminants from common buffer solutions. The salt effect on RNase A catalysis is analyzed with a novel quantitative model (Chapter 4). This model is applied successfully to explain salt–rate profiles of RNase A. The energetics of RNase A catalysis is re-examined by the effects of pH, salt concentration, and solvent isotope, which show that substrate association limits catalysis by RNase A (Chapter 5). By protein complementation with H12A RNase A and H119A RNase A, dimerization by RNase A is detected and analyzed, providing clues for the mechanism of dimer evolution (Chapter 6). Finally, adjacent cysteine residues were introduced into RNase A as a redox switch (Chapter 7). The catalytic activity of the RNase A variant is regulated by the redox potential of the medium.

TABLE OF CONTENTS

LIST OF TABLES

LIST OF TABLES

LIST OF FIGURES

ABBREVIATIONS

3′–CMP ....cytidine 3′-phosphate

3′–UMP ....uridine 3′-phosphate

4-DABCYL ....4-((4-(dimethylamino)phenyl)azo)benzoic acid

6-FAM 6-carboxyfluorescein

6-TAMRA 6-carboxyteteramethylrhodamine

Bistris..........................[bis(2-hydroxyethyl)amino]tris(hydroxymethyl)methane

BS-RNase ....bovine seminal ribonuclease

cCMP..........................cytidine 2′,3′-cyclic phosphate

C_f ....forward commitment factor

CpA ....cytidylyl(3′→5′)adenosine

cUMP ....uridine 2′,3′-cyclic phosphate

DTNB..........................5,5′-dithiobis(2-nitrobenzoic acid)

DTT............................dithiothreitol

FRET ....fluorescence resonance energy transfer

GSH............................reduced glutathione

GSSG..........................oxidized glutathione

hRI..............................human ribonuclease inhibitor

ITC..............................isothermal titration calorimetry

K_a .... acid dissociation constant

K_d .... equilibrium dissociation constant

MES .... 2-morpholinoethanesulfonic acid

MOPS .... 3-morpholinopropanesulfonic acid

NMR .... nuclear magnetic resonance

PDB .... protein data bank

pI .... isoelectric point

poly(C) .... poly(cytidylic acid)

RNase A .... bovine pancreatic ribonuclease A

T_m .... temperature at the midpoint of thermal denaturation

Tris .... tris(hydroxymethyl)aminomethane

UpA .... uridylyl(3'→5')adenosine

UpU .... uridylyl(3'→5')uridine

UV .... ultraviolet

Chapter 1

Introduction

Overview. The main focus of enzymology is to understand how enzymes provide enormous rate enhancements for chemical reactions (Fersht, 1985; Jencks, 1987). Information on the energetics of enzymatic catalysis is a key to achieving this goal. This information is obtained primarily by assessing the effects of variations in enzymes, substrates, and environment from many perspectives, using a wide range of tools (*e.g.*, site-directed mutagenesis, semisynthesis, isotope effects, and variation of pH, ionic strength, temperature, and viscosity). Bovine pancreatic ribonuclease A (RNase A; EC 3.1.27.5) (Richards & Wyckoff, 1971; Eftink & Biltonen, 1987; D'Alessio & Riordan, 1997; Raines, 1998) has been an archetypal system to apply this 'assessment of the effect of variation' approach for scrutinizing catalytic mechanism and energetics (Findlay et al., 1961; Witzel & Barnard, 1962; Crestfield & Stein, 1963; Eftink & Biltonen, 1983a; Eftink & Biltonen, 1983b; Matta & Vo, 1986; Jackson et al., 1994; delCardayré et al., 1995; Thompson et al., 1995; Sowa et al., 1997), as well as protein chemistry, folding, and structure (Kartha et al., 1967; Anfinsen, 1973; Moore & Stein, 1973; Merrifield, 1984). This dissertation is focused on developing tools for assessing the effect of salt and pH on binding and catalysis with RNase A as a model system. The wealth of information on the structure and mechanism of this enzyme serves as a great foundation for expanding the scope of understanding the effects of these two fundamental parameters on biochemical systems.

Effects of Salt and pH on the Properties of Biomolecules. Most biochemical reactions occur in an aqueous environment. Ionic properties of biomolecules have essential roles in regulating their interaction, stability, structures, and localization in this aqueous environment. Some examples of ionic groups in biomolecules are lipid molecules with ionic

head groups (phosphatidyl serine, phosphatidyl ethanolamine, and phosphatidyl choline), seven amino acids with ionizable side chains (lysine, arginine, histidine, aspartate, glutamate, cysteine, and tyrosine), and the phosphoryl groups of nucleic acids. Enzymatic catalysis exploits these ionic groups of biomolecules extensively. Enzymic active-sites are often comprised of the seven amino acids with ionizable side-chains, which stabilize ionic transition states and serve as Brønsted acids, Brønsted bases, and nucleophiles (Perutz, 1978; Jencks, 1987; Jackson & Fersht, 1993; Warshel, 1998). The ionic groups also provide both the specificity and driving force for complex formation (Record et al., 1976; Perutz, 1978; Honig & Nicholls, 1995; Schreiber & Fersht, 1996; Carbeck et al., 1998). The effects of salt and pH in biochemical systems can be defined as moderators of the thermodynamic properties of ionic groups in biomolecules. Therefore, salt and pH are powerful probes for revealing the energetics of enzymatic catalysis.

The effects of salt on ionic groups can be simply viewed as the modification of their activity coefficients by screening charges, as described by the Debye–Hückel limiting law:

$$\log \gamma_{\pm} = -|z_{+}z_{-}| A I^{1/2} \tag{1.1}$$

where $\gamma_{\pm}$ is a mean activity coefficient, z_{+} and z_{-} are charge numbers, and I is the ionic strength of medium. A is a proportionality coefficient that depends on the relative permittivity and the temperature (Atkins, 1990). Because this equation assumes the absence of specific interactions between ionic species, the ionic environment of a medium is

described as a composition variable, ionic strength, which ignores the nature of salts (Record et al., 1998). Salt effects on biomolecules, however, frequently involve specific interactions, which could depend on the nature or valences of ions.

Salt effects on biomolecules are prominent in interactions involving nucleic acids (Record et al., 1976; Lohman, 1986). The phosphoryl groups of a nucleic acid bestow on this molecule the special property of being a polyelectrolyte. The continuous charge density of a nucleic acid causes cations to accumulate on its surface. When a ligand binds to the anionic surface, the condensed cations are released, which increases the entropy of the system. Because of this ionic property of nucleic acids, the stability of a complex of a protein and a nucleic acid is strongly dependent on salt concentration (Jensen & von Hippel, 1976). This 'polyelectrolyte effect' is not dependent on the nature of salt, but on the valences of its constituent ions (Record et al., 1998).

Another prominent example of salt effects is on the conformational stability of proteins (von Hippel & Schleich, 1969a). The effectiveness of salts in stabilizing or destabilizing the native conformation of a protein is distinct between different types of salts. This effectiveness follows the Hofmeister series, which ranks the effectiveness of ions in salting-out proteins. This order for anions is: $SO_4^{2-} < CH_3COO^- < Cl^- < Br^- < ClO_4^- < CNS^-$; this order for cations is: $(CH_3)_4N^+, NH_4^+, K^+, Na^+ < Li^+ < Ca^{2+}$ (von Hippel & Schleich, 1969a; Cacace et al., 1997).

Salts also influence enzymatic catalysis. Salt can inhibit catalysis by binding directly to an active site (Fridovich, 1963) or by disrupting the local structures of active sites (Warren & Cheatum, 1966; Warren et al., 1966), as following the order of Hofmeister series.

Enzymes requiring monovalent cations for their catalysis also show salt-dependent catalytic

activities (Suelter, 1970). Specific binding sites for cations for catalysis and allostery have

been found in this class of enzymes (Toney et al., 1993; Larsen et al., 1994; Di Cera et al.,

1995). A rigorous quantitative description of salt effects on enzymatic catalysis is, however,

nonexistent.

pH influences the catalysis and conformational stability of enzymes by the modifying

the protonation states of titratable groups. The effect of pH on ionizable groups is described

by the Henderson–Hasselbalch equation:

$$pH = pK + \log\frac{[A^-]}{[HA]} \qquad (1.2)$$

Assessment of the effect of pH on enzymatic catalysis has been a useful tool, both to

identify catalytically important residues and to reveal the catalytic mechanisms of enzymes

(Tipton & Dixon, 1979; Cleland, 1982). When a specific protonation state of an enzyme is

required for catalysis, pH affects catalysis by varying the availability of the catalytically

competent protonation state. The effect of pH on the conformational stability of a protein is

also significant. At extremes of pH, proteins are destabilized by the Coulombic repulsion of

the accumulated charged functional groups. When a protein is stabilized by salt bridges or

ionic hydrogen bonds, the variation of protonation state of the involved groups results in the

destabilization of the native conformation of the protein (Anderson et al., 1990; Quirk et al.,

1998).

Catalysis by Ribonuclease A. RNase A depolymerizes RNA substrates by cleaving a

P–O$^{5'}$ bond after a pyrimidine base using a general acid–base mechanism (Figure 1.1)

(Findlay et al., 1961; Thompson & Raines, 1995). Two active-site histidine residues, His12

and His119, are involved in this catalytic mechanism. His12 abstracts a proton from the 2'

hydroxyl group of a ribose group, and His119 donates a proton to the 5' oxygen of the

leaving group. The catalytic significance of these histidine residues has been revealed by

chemical modification (Crestfield & Stein, 1963) and site-directed mutagenesis (Thompson

& Raines, 1995). When either histidine residue is replaced by an alanine residue, the enzyme

suffers more than a 10^4-fold decrease in k_{cat}/K_M. Lys41 also has a significant contribution to

stabilization of the transition state by donating an ionic hydrogen bond (Messmore et al.,

1995). There has been a debate between the classical concerted mechanism and the triester-

like mechanism for RNase A catalysis. A triester-like mechanism has been proposed, based

on kinetic studies of nonenzymatic catalysis of cleavage of UpU by imidazole buffer

(Anslyn & Breslow, 1989). In this mechanism, His119 protonates non-bridging oxygen to

facilitate the nucleophilic attack of 2' hydroxy group to the phosphoryl group. The classical

concerted mechanism, however, has been corroborated by thio-effects (Herschlag, 1994),

site-directed mutagenesis (Thompson & Raines, 1995), and isotope effects (Sowa et al.,

1997).

Interaction of RNase A with an RNA substrate is not limited to its active site. The

substrate-binding cleft of RNase A provides various contacts with phosphoryl groups and

nucleobases of an RNA substrate (Figure 1.2) (McPherson et al., 1986; Fontecilla-Camps et

al., 1994). The contribution of the residues comprising these substrate-binding sites to

catalysis and specificity has also been studied in detail (Boix et al., 1994; delCardayré et al.,

1994; delCardayré & Raines, 1995; Moussaoui et al., 1995; Fisher et al., 1998a; Fisher et al.,

1998b; Kelemen et al., 2000). A series of cationic residues comprise the phosphoryl group

binding sites: P(-1) (Arg85), P0 (Lys66), P1 (His12, His119, and Lys41), and P2 (Lys 7

and Arg 10). The P1 subsite is the active site for catalysis, which binds to the scissile

phosphoryl group. The other phosphoryl group binding sites contribute to catalysis mainly

through Coulombic interactions with the phosphoryl groups of an RNA substrate (Fisher et

al., 1998a; Fisher et al., 1998b). The base-binding sites determine the specificity for

nucleobases: B1 (Thr45, Asp83, and Phe120) for a pyrimidine base, B2 (Asn71 and Glu111)

for adenosine, and B3 (residues unknown) for a purine base (Witzel & Barnard, 1962;

McPherson et al., 1986; delCardayré et al., 1994).

Previous Studies on the Effects of Salt and pH on ribonuclease A. The intimate

involvement of histidine residues and Coulombic interactions in catalysis makes RNase A a

prominent model system for studying the effects of pH and salts on enzymatic catalysis.

RNase A has been a model system for studying salt effects on protein–nucleic acid

interactions and the conformational stability of proteins. The Coulombic nature of RNase A–

nucleic acid interaction results in a strong salt effect on ligand binding by RNase A. By

applying the polyelectrolyte theory to this salt effect, Record and coworkers showed that

RNase A forms ~7 ion pairs with a single-stranded DNA (Record et al., 1976). von Hippel

and coworkers also used RNase A as a model system to show that salt effects on the

conformational stability of proteins follows the order of the Hofmeister series (von Hippel &

Wong, 1965; von Hippel & Schleich, 1969b). Salt concentration also influences the catalytic

activity of RNase A. Studies of the salt effect on RNase A catalysis have shown that

RNase A has an apparent bell-shaped salt–rate profile (Davis & Allen, 1955; Dickman et al.,

1956; Edelhoch & Coleman, 1956; Dickman & Ring, 1958; Kalnitsky et al., 1959; Irie,

1965; Winstead & Wold, 1965; Libonati & Sorrentino, 1992). The physical basis of this salt

effect has, however, been controversial. Salt has also been shown to affect the protonation

state of the active-site histidine residues. Proximal cationic residues make the pK_a values of

its histidine residues sensitive to the ionic environment. A shift of these pK_a values has been

observed from both pH–rate profiles and NMR determination of the pK_a values of the

active-site histidines at varying salt concentrations (Irie, 1965; Eftink & Biltonen, 1983a;

Fisher et al., 1998c).

The bell-shaped pH–rate profile of RNase A is a classic example of the pH-dependence

of enzyme catalysis. The general acid–base mechanism of RNase A shown in Figure 1.1 was

initially supported by this bell-shaped pH–rate profile (Findlay et al., 1961). Two

macroscopic pK_a values have been reported to be ~6 from pH–k_{cat}/K_M profiles with various

substrates (Herries et al., 1962; Witzel, 1963; del Rosario & Hammes, 1969; Eftink &

Biltonen, 1983a; Schultz et al., 1998). pH also affects the stability of RNase A•nucleotide

complexes by changing the protonation state of active-site histidines and nucleotides (Flogel

et al., 1975; Flogel & Biltonen, 1975a; Flogel & Biltonen, 1975b). pH also influences the

conformational stability of RNase A (Quirk et al., 1998). As RNase A is cationic (pI =9.3

(Ui, 1971)), its conformational stability decreases at acidic pH because of repulsive

Coulombic forces and loss of ion pairs.

Scope of this Work. This dissertation assesses the effects of pH and salt on binding and catalysis by RNase A, based on a series of biochemical and biophysical studies, and exploits these effects as tools to obtain an advanced portrait of the energetics of RNase A catalysis.

Chapter 2 addresses the contribution of active-site histidine residues to nucleic acid binding. Studies on the effects of mutagenesis and pH on the stability of RNase A•nucleic acid complexes show that His12 and His119 have roles not only in catalytic turnover of RNA substrate, but also in nucleic acid binding. In addition, the structures of crystalline H12A RNase A and H119A RNase A are analyzed by X-ray diffraction analysis.

In Chapter 3, the origin of RNase A "inactivation" at low salt concentration is scrutinized. Surprisingly, the inactivation results from the inhibition of RNase A activity by low-level contaminants from buffer solutions at low salt conditions. By using an uncontaminated buffer or adding H12A RNase A to absorb the contaminants, k_{cat}/K_M was observed to be as high as 10^9 $M^{-1}s^{-1}$ at low salt. This result shows that catalytic activity of RNase A is maximal at low salt.

The salt effect on RNase A catalysis is analyzed with a quantitative model developed using the polyelectrolyte theory in Chapter 4. This model is applied to salt–rate profiles of wild-type RNase A and its variants to show the importance of salt effects on enzymatic catalysis as a modulator of uniform binding. These analyses reveal that the dependence of k_{cat}/K_M on salt concentration can reveal the extent of Coulombic interactions in enzyme–substrate complexes.

In Chapter 5, the energetics of RNase A catalysis is re-examined using optimal substrates. Analysis of the effects of pH, salt concentration, and solvent isotope indicates

that substrate association limits catalysis by RNase A. A qualitative method for analyzing

pH–k_{cat}/K_M profiles in a kinetic mechanism with parallel pathways is presented. Based on

these results, a mechanism for substrate binding by RNase A is proposed. The energetics of

RNase A catalysis indicates that RNase A is a perfect enzyme.

Chapter 6 describes dimer formation by RNase A. Dimerization of RNase A is detected

and analyzed by protein complementation experiments with H12A RNase A and H119A

RNase A. Based on this analysis and dimer formation by bovine seminal ribonuclease, a

homologous protein in the RNase A superfamily, a putative mechanism for dimer evolution

is proposed.

In Chapter 7, adjacent cysteine residues are discussed and exploited as a redox switch.

Adjacent cysteine residues form a strained eight-membered ring upon oxidation to a cystine.

As a switch to regulate enzymatic activity by the redox potential of the medium, adjacent

cysteine residues were introduced into RNase A. Characterization of variants with adjacent

cysteine residues shows that the efficiency of this engineered switch is dependent on their

structural context.

Figure 1.1   Mechanism for the transphosphorylation reaction (A) and the hydrolysis

reaction (B) catalyzed by ribonuclease A. B and A depict His12 and His119,

respectively.

A
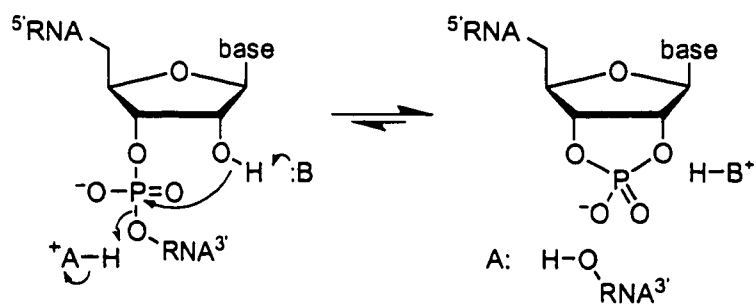
B
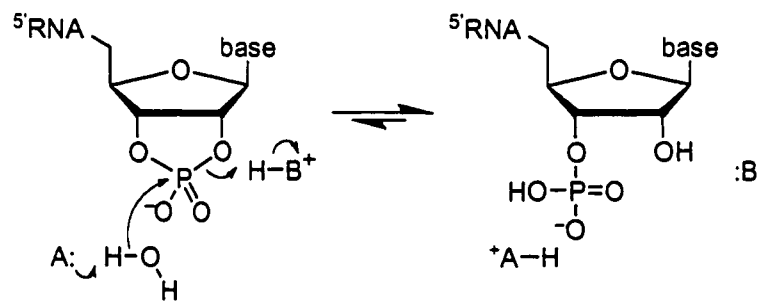
Figure 1.2   Interactions between ribonuclease A subsites and an RNA substrate. B and P

refer to base-binding and phosphoryl group-binding sites, respectively.

Residues comprising each site are represented in boxes. The scissile bond (P–

$O^{5'}$) is indicated by an arrow. Nucleobases of the RNA molecule indicate the

base preference of RNase A.

Lys66

P0 subsite

Cyt
Ura

Thr45
Asp83

B1 subsite

OH

Gln11
His12
Lys41
His119
Asp121

P1 subsite
(active site)

scissile
bond

Ade

Asn71
Glu111

B2 subsite

OH

Lys7
Arg10

P2 subsite

Ade
Gua

?

B3 subsite

OH
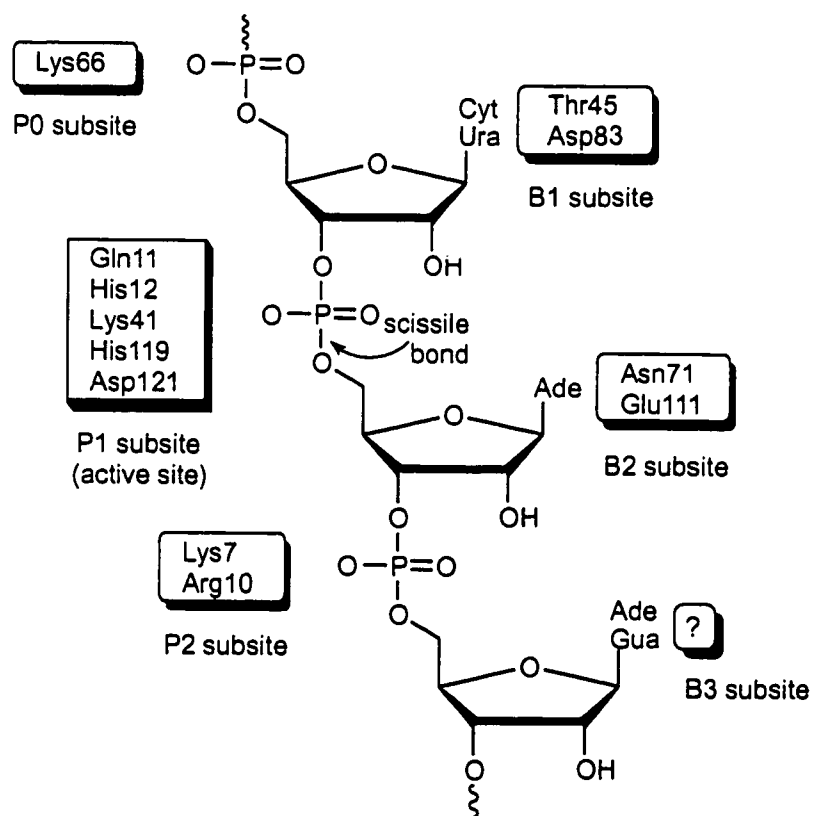
Chapter 2

Contribution of the Active-Site Histidine Residues of Ribonuclease A

to Nucleic Acid Binding

ABSTRACT

The imidazole/imidazolium side chains of His12 and His119 of ribonuclease A

(RNase A) are critical for catalysis of RNA cleavage by this enzyme. Substitution of either

residue with an alanine decreases the value of k_{cat}/K_M by more than 10^4-fold. His12 and

His119 are proximal to the scissile phosphoryl group of an RNA substrate in enzyme-

substrate complexes. Here, the role of these active-site histidines in RNA binding was

investigated by monitoring the effect of mutagenesis and pH on the stability of enzyme-

ligand complexes. X-Ray diffraction analysis of the H12A and H119A variants shows that

the amino acid substitutions do not perturb the overall structure of the variants. Isothermal

titration calorimetric studies on the complexation of wild-type RNase A and the variants

with 3'-UMP at pH 6.0 show that His12 and His119 contribute 1.4 kcal/mol and 1.1

kcal/mol to complex stability, respectively. Determination of the stability of the complex of

wild-type RNase A and 6-carboxyfluorescein~d(AUAA) at varying pH's by fluorescence

anisotropy spectroscopy shows that the complex stability is sensitive to pH, increasing by

2.4 kcal/mol as pH decreases from 8.0 to 4.0. Substitution of His12 with an alanine residue

lessens the stability of the complex with 6-carboxyfluorescein~d(AUAA) by 2.3 kcal/mol at

pH 4.0. These structural and thermodynamic observations indicate that His12 and His119

have a significant role in substrate binding as well as catalytic turnover of substrates to

products.

INTRODUCTION

Ribonuclease A (RNase A; EC 3.1.27.5) is a pyrimidine-specific endoribonuclease from

bovine pancreas (D'Alessio & Riordan, 1997; Raines, 1998). Decades of studies on catalysis

and interaction with nucleic acid by RNase A have made this enzyme one of the most

important model systems in enzymology and protein chemistry. RNase A depolymerizes an

RNA substrate by cleaving a P–O$^{5'}$ bond after a pyrimidine base. The mechanism of the

cleavage reaction catalyzed by RNase A employs two renown histidine residues, His12 and

His119. In the transphosphorylation reaction, His12 acts as a base to abstract a proton from

2' hydroxyl group of a ribose ring, and His119 acts as an acid to donate a proton to the 5'

oxygen of the leaving group (Figure 1.1). Replacing either histidine residue with an alanine

greatly impairs the catalytic activity of the enzyme. The k_{cat}/K_M values of H12A and H119A

RNase A for cleavage of UpA are >10^{4}-fold less than that of wild-type RNase A (Thompson

& Raines, 1995). Catalysis by RNase A necessitates another active-site residue, Lys41.

Lys41 facilitates catalysis by donating a hydrogen bond to a phosphoryl oxygen in the

transition state (Messmore et al., 1995). Replacing Lys41 with an alanine also decreases the

k_{cat}/K_M for cleavage of UpA by 10^{4}-fold (Messmore, 1999).

Interactions with RNA substrates by RNase A extend beyond the active site. Phosphoryl

group binding sites of RNase A have been studied in detail by X-ray crystallography

(McPherson et al., 1986; Fontecilla-Camps et al., 1994) and site-directed mutagenesis (Boix

et al., 1994; Fisher et al., 1998a; Fisher et al., 1998b). These binding sites are composed of

cationic residues that use Coulombic forces to attract the anionic phosphoryl groups of

nucleic acid (Record et al., 1976). Arg85 and Lys66 comprise the P(-1) and the P0 site,

respectively. Lys7 and Arg10 comprise the P2 site. The active-site residues also comprise

one of the phosphoryl group binding sites, P1.

Physical characterization of complex formation by wild-type RNase A suggests the

involvement of active-site residues in phosphoryl group binding. The structure of crystalline

complexes of wild-type RNase A and nucleotide ligands shows that the active-site histidine

residues are proximal to the phosphoryl group in the active site (Fontecilla-Camps et al.,

1994; Zegers et al.. 1994). The stability of the complex of wild-type RNase A and cytidine

3'-phosphate (3'–CMP) is sensitive to the ionization state of these histidines (Flogel et al.,

1975; Flogel & Biltonen, 1975a; Flogel & Biltonen, 1975b). Binding of uridine 3'-phosphate

(3'–UMP) to wild-type RNase A alters the microscopic pK_a values of the histidines, as

revealed by NMR spectroscopy (Quirk & Raines, 1999).

We sought a quantitative assessment of the contribution of His12 and His119 to nucleic

acid binding by RNase A. First, we used X-ray crystallography to assess the integrity of the

structure of histidine variants. Then, we studied the thermodynamics of complex formation

by wild-type RNase A and the histidine variants by isothermal titration calorimetry and

fluorescence anisotropy. The results provide a thorough picture of the interaction of two

histidine side chains with the phosphoryl group of a nucleic acid.

MATERIALS AND METHODS

Materials. Wild-type RNase A and the H12A and H119A variants were produced, folded, and purified as described elsewhere (delCardayré et al., 1995; Park & Raines, 2000a). Concentrations of wild-type RNase A and its variants were determined by ultraviolet spectroscopy using $\varepsilon = 0.72$ mL mg^{-1}cm^{-1} at 277.5 nm (Sela et al., 1957). 6-Carboxyfluorescein~d(AUAA) (6-FAM~d(AUAA)) was from Promega (Madison, WI). The concentration of 6-FAM~d(AUAA) was determined by using $\varepsilon = 66,300$ M^{-1}cm^{-1} at 260 nm. 3'-UMP was from Sigma Chemical (St. Louis, MO). The concentration of 3'-UMP was determined by using $\varepsilon = 10,000$ M^{-1}cm^{-1} at 260 nm (Beaven et al., 1955).

Protein Crystallization. Crystals of H12A and H119A RNase A were prepared by vapor diffusion using the hanging drop method. Drops (6 μL) of 0.050 M sodium acetate buffer (pH 6.0), containing H12A RNase A (33 mg/mL), saturated sodium chloride (25% v/v), and saturated ammonium sulfate (15% v/v) were suspended over 1.0-mL wells of 0.10 M sodium acetate buffer (pH 6.0) containing saturated sodium chloride (50% v/v) and saturated ammonium sulfate (30% v/v). Single trigonal crystals were grown at 20 °C, appeared within several weeks, and grew to a final size of 0.6 × 0.6 × 0.5 mm.

Drops (6 μL) of 0.050 M sodium acetate buffer (pH 6.0), containing H119A RNase A (30 mg/mL), saturated sodium chloride (22.5% v/v), and saturated ammonium sulfate (14.5% v/v) were suspended over 1.0-mL wells of 0.10 M sodium acetate buffer (pH 6.0) containing saturated sodium chloride (45% v/v) and saturated ammonium sulfate (29% v/v).

Single trigonal crystals were grown at 20 °C, appeared within 1 week, and grew to a final

size of 0.6 × 0.6 × 0.6 mm.

Data Collection. Crystals of H12A RNase A were of space group $P3_221$, with a = 64.54

Å c = 65.08 Å, $\alpha = \beta = 90°$, $\gamma = 120°$. Crystals of H119A RNase A were of space group

$P3_221$, with a = 64.53 Å c = 65.04 Å, $\alpha = \beta = 90°$, $\gamma = 120°$. All X-ray data were collected

with a Siemens HI-STAR detector mounted on a Rigaku rotating anode operating at 50 kV

and 90 mA with a 300 μm focal spot. The X-ray beam was collimated by double-focusing

mirrors. The crystal-to-detector distance was 12.0 cm. Data were obtained in 512 × 512

pixel format, processed with the program XDS (Kabsch, 1988; Kabsch, 1998), and scaled

using the program XSCALIBRE (G. Wesenberg and I. Rayment, unpublished results). For

each protein, frames of data (135°) were collected from a single crystal using a combination

of ω and φ-scans. Reflections with $I/\sigma < 0.33$ were rejected. The crystals were cooled in a 2

°C air stream, resulting in negligible crystal decay for both data collections. Full

crystallographic details are listed in Tables 2.1 and 2.2.

Refinement of the H12A Structure. The structure was solved by difference fourier using

PDB entry 4RSD stripped of solvent, as a starting model (Ala121 was replaced by Asp and

His12 by Ala). A rigid body refinement resulted in an *R*-factor of 0.369. Prior to least-

squares refinement $2|F_o| - |F_c|$, $|F_o| - |F_c|$, and σ_A [Collaborative Computational Project,

1994 #915], difference maps were calculated using the data from 30–3.0 Å. The model

(residues 1–11 and 13–124) was examined and was continuous in electron density for the

entire chain. Residue 12 was clearly identified as alanine. The starting model was subjected

to 10 cycles of least-squares refinement using the program TNT (Tronrud et al., 1987) and

the data from 30–2.0 Å, giving an initial R-factor of 0.238. Manual adjustments to the model

were performed using the program TURBO-FRODO (Cambillau et al., 1997). The

resolution was extended to 1.7 Å after several cycles of manual adjustments and least-

squares refinement. The peak-searching algorithm in TNT was used to place ordered water

molecules. Water molecules were retained if they had at least 1σ of 2$|F_o|$ − $|F_c|$ density, 3σ

of $|F_o|$ − $|F_c|$ density, and were within hydrogen bonding distance of the protein or other

water molecules. The final model contains the complete protein (residues 1–124), 96 water

molecules, and two chloride ions.

Refinement of the H119A Structure. The structure was solved by difference fourier using

PDB entry 4RSD stripped of solvent, as a starting model (Ala121 was replaced by Asp and

His119 by Ala). A rigid body refinement resulted in an R-factor of 0.345. Prior to least-

squares refinement 2$|F_o|$ − $|F_c|$, $|F_o|$ − $|F_c|$ and σ$_A$ [Collaborative Computational Project;

Number 4, 1994 #915], difference maps were calculated using the data from 30–3.0 Å. The

model (residues 1–118 and 120–124) was examined and was continuous in the density for

the entire chain. Residue 119 was clearly identified as alanine. The starting model was

subjected to 10 cycles of least-squares refinement using the program TNT (Tronrud et al.,

1987) and the data from 30–2.0 Å, giving an initial R-factor of 0.220. Manual adjustments to

the model were performed using the program TURBO-FRODO (Cambillau et al., 1997).

The resolution was extended to 1.8 Å after several cycles of manual adjustments and least-

squares refinement. Water molecules from the H12A structure were used as a starting

solvent model. Water molecules were retained if they had at least 1σ of $2|F_o| - |F_c|$ density, 3σ of $|F_o| - |F_c|$ density, and were within hydrogen bonding distance of the protein or other water molecules. The final model contains the complete protein (residues 1–124), 102 water molecules, and three chloride ions.

Atomic coordinates for H12A and H119A RNase A have been deposited in the PDB with accession codes 1C9V and 1C9X, respectively.

Determination of K_d for RNase A•3'-UMP complexes. The stability of the complexes of 3'-UMP with wild-type RNase A and the H12A and H119A variants was determined by using a Micro Calorimetry System isothermal titration calorimeter from MicroCal (Northampton, MA). The proteins and 3'-UMP solutions were prepared with 0.10 M MES-NaOH (pH 6.0) containing 0.10 M NaCl and were degassed prior to use. For wild-type RNase A, the initial concentration of the protein solution in the cell was 0.12 mM. Aliquots (5 μl) of 2.8 mM 3'-UMP solution were injected into the cell at 240-s intervals. For H12A and H119A variants, the initial concentrations of protein in the cell were 0.64 mM and 0.65 mM, respectively. Aliquots (5 μl) of 22 mM 3'-UMP were injected into the cell. The heat evolved from complex formation was recorded and analyzed to determine K_d values by using the program ORIGIN (MicroCal Software; Northampton, MA) (Wiseman et al., 1989).

Determination of K_d for RNase A•6-FAM~d(AUAA) Complexes at Varying pH's. The stability of the complex between RNase A and an oligonucleotide was determined by fluorescence anisotropy (Fisher et al., 1998b; Kelemen et al., 2000). The ligand, 6-FAM~d(AUAA), is a DNA oligonucleotide with a fluorescein molecule attached to its

5′-end via a 6-carbon spacer. Wild-type RNase A was prepared in 2.0 mL of buffers with pH

4.0–8.0, as listed in Table 2.4. H12A RNase A was prepared in 2.0 mL of 0.10 M sodium

acetate buffer (pH 4.0) containing 0.050 M NaCl. Determination of the K_d values of the

complex of H12A RNase A and 6-FAM~d(AUAA) at other than pH 4.0 was not attempted

with this method because of the reduced affinity of the variant to the ligand. The buffers

used for this study were designed to have an identical ionic strength of 0.15. The RNase A

solutions was divided to prepare 1.0 mL of a sample solution and a blank solution in

silanized borosilicate glass tubes. Both solution contained the same concentration of wild-

type RNase A (1.9–3.4 mM) or H12A RNase A (5.7 mM), but only the sample solution had

the ligand (2.5–5.0 nM). Fluorescence anisotropy was measured at 23 °C on a Beacon

Fluorescence Polarization System from PanVera (Madison, WI) with excitation at 488 nm

and emission at 520 nm. Anisotropy values of the sample solution were determined 5 times

with a blank reading before each sample reading. After each measurement, the sample

solution was diluted by dispensing 0.25 mL of the sample and adding 0.25 mL of buffer

containing the same concentration of the ligand as the sample solution to reduce protein

concentration for subsequent measurements. The blank solution was also diluted with buffer

by the same procedure. The measurement was continued until the anisotropy values reached

the minimum and did not change any more. Equilibrium dissociation constants at each pH

were determined by eq 2.1.

$$A = \frac{\Delta A \cdot [\text{RNaseA}]}{K_d + [\text{RNaseA}]} + A_{min} \qquad (2.1)$$

A_{mun} is the anisotropy of free ligand. ΔA is the difference in the anisotropy between free

ligand and the bound ligand. Nonlinear regression analyses were performed with the

program SIGMAPLOT 5.0 (SPSS; Chicago, IL).

RESULTS

Structure of H12A RNase A. The structure of H12A RNase A was solved by difference

fourier and refined to an R-factor of 0.182 using the data from 30–1.7 Å. The RMS

deviations from target geometries are 0.012 Å for bond lengths and 2.31° for bond angles.

Average B-factors for the main chain and side chain are 30.4 and 36.7 Å^2, respectively. The

electron density is continuous for the main chain and most of the side chains. The

conformation of residue 12 was unambiguous and clearly defined in both $2|F_o| - |F_c|$ density

and annealed omit $|F_o| - |F_c|$ density (Figure 2.1).

Structure of H119A RNase A. The structure of H119A RNase A was solved by

difference fourier and refined to an R-factor of 0.164 using the data from 30–1.8 Å. The

RMS deviations from target geometries are 0.011 Å for bond lengths and 2.41° for bond

angles. Average B-factors for the main chain and side chain are 25.5 and 32.1 Å^2,

respectively. The electron density is continuous for the main chain and most of the side

chains. The conformation of residue 119 was unambiguous and clearly defined in both $2|F_o|$

$- |F_c|$ density and annealed omit $|F_o| - |F_c|$ density (Figure 2.2).

Binding of 3'–UMP to Wild-Type RNase A and its Histidine Variants. To assess the role of active-site histidine residues in binding to 3'–UMP, the values of the equilibrium dissociation constant (K_d) of the complex with ligand were determined by using isothermal titration calorimetry (Table 2.3). The K_d of the complex of wild-type RNase A and 3'–UMP was 0.054 mM, which is identical to a value reported previously (Fisher et al., 1998c). The K_d's for H12A RNase A and H119A RNase A with the same ligand were determined as 0.55 mM and 0.37 mM, respectively. These increases in K_d values correspond to decreases in the stability of the complexes with the H12A and H119A variants by 1.4 kcal/mol and 1.1 kcal/mol, respectively.

Effect of pH on the Stability of the RNase A•6-FAM–d(AUAA) Complex. The effect of pH on the stability of the complex of RNase A and an oligonucleotide was determined by using fluorescence anisotropy. The values of K_d with fluorescein-tagged tetranucleotide, 6-FAM–d(AUAA), as a ligand were obtained at pH 4.0–8.0 (Table 2.4). The stability of the complex was maximal at acidic pH. As the pH was increased, the K_d of the complex also increased. At pH 8.0, the K_d was ~60-fold higher than the K_d determined at pH 4.0. The K_d value of the complex with H12A RNase A (2.0 ± 0.4 mM) at pH 4.0 was significantly greater than that for the complex with wild-type RNase A (0.038 ± 0.005 mM).

DISCUSSION

Structural Comparison of H12A RNase A and H119A RNase A to Wild-Type RNase A.

H12A RNase A and H119A have overall structures almost identical to that of the wild-type enzyme. The main-chain atoms of the H12A and H119A variants have an average RMS deviation of 0.31 Å and 0.24 Å from those of wild-type RNase A [PDB entry 1RPH (Zegers et al., 1994)]. The main-chain conformations of Ala12 and Ala119 are similar to those of the analogous residues in wild-type RNase A. H12A RNase A shows the greatest deviations, which occur in residues 66 and 67, with the main chain deviating up to 0.5 Å.

Active-Site Structures in H12A RNase A and H119A RNase A. A water molecule (W153) occupies the position of the imidazole ring of His12 in wild-type RNase A. W153 forms a hydrogen bond to the main-chain O of Thr45 (2.95 Å) analogous to the bond formed between $N_{\delta1}$ of His12 and the main-chain O of Thr45 in the wild-type enzyme. W153 is part of a water network in the active site and is within hydrogen bonding distance of W195 (2.79 Å), a solvent molecule that is replaced by a chloride ion in the H119A RNase A structure as well as that of T45G RNase A (Kelemen et al., 2000). His12 occupies a similar position in the wild-type and H119A RNase A.

In H12A RNase A, the electron density surrounding the side chain of His119 is diffuse due to some disorder in this residue. Although it was possible to define χ_1, it was difficult to assess χ_2 because of weak density. His119 occupies two positions in the H12A RNase A structure, commonly defined as A and B (Borkakoti et al., 1982). In wild-type RNase A, the A position brings the side-chain $N_{\epsilon2}$ of His119 within hydrogen bonding distance of the

side-chain $O_{\delta 1}$ of Asp121 (2.97 Å) and $O_{\delta 2}$ of Asp121 forms a hydrogen bond with the

main-chain N of Lys66 (3.35 Å). However, in H12A RNase A, a shift of the Asp121 side

chain positions the side-chain $N_{\epsilon 2}$ of His119 3.71 Å from the side-chain $O_{\delta 1}$ of Asp121.

Instead, $O_{\delta 1}$ of Asp121 is involved in a hydrogen bond with the main-chain N of Lys66

(3.03 Å). These conformational changes may have resulted in the 0.5 Å shift of residues 66

and 67 away from the active site with respect to wild-type RNase A.

In the H119A RNase A structure, a water molecule (W246) forms a hydrogen bond with

the side-chain $O_{\delta 1}$ of Asp121 (2.74 Å) in place of the His119 side chain. $O_{\delta 2}$ of Asp121

forms a hydrogen bond with the main-chain N of Lys66 (3.12 Å).

In wild-type RNase A, the side chain of Phe120 is in contact with the side chain of

His12. In the H12A RNase A structure, Phe120 becomes slightly disordered and occupies

two distinct positions (χ_1, χ_2 angles are $-174°$, $97°$ and $-140°$, $128°$). The first is very similar

to that of wild-type RNase A (χ_1, χ_2 angles are $-164°$, $93°$) and the second position fills

space in the absence of the side chain at residue 12.

Effects of Ionization of Active-Site Histidines on Ligand Binding. To investigate the

effect of pH on substrate binding by RNase A, the K_d value of the

RNase A•6-FAM~d(AUAA) complex was determined at varying pH's. DNA

oligonucleotides have been used previously as substrate analogues for crystallographic and

biophysical studies (Record et al., 1976; Fontecilla-Camps et al., 1994). The effect of pH on

ligand binding by RNase A has been studied with 3'-UMP (Flogel et al., 1975; Flogel &

Biltonen, 1975a; Flogel & Biltonen, 1975b). This analysis, however, was not

straightforward because of the titration of the ligand near pH 6. The use of a DNA

oligonucleotide as a ligand obviates this complication, as the ionization state of the

phosphoryl groups of DNA does not change in the range of pH used for this study. Within

this range of pH, we assume that the only titratable groups affecting the K_d value are those

of His12 and His119. Scheme 2.1 shows a thermodynamic cycle for ligand binding with

macroscopic acid dissociation constants and K_d values.

$$
\begin{array}{ccc}
EH_2{}^{2+} & \xrightleftharpoons[K_d{}^1]{} & EH_2{}^{2+}{\cdot}L \\[1em]
K_a{}^1 \updownarrow & & K_a{}^3 \updownarrow \\[1em]
EH^+ & \xrightleftharpoons[K_d{}^2]{} & EH^+{\cdot}L \\[1em]
K_a{}^2 \updownarrow & & K_a{}^4 \updownarrow \\[1em]
E & \xrightleftharpoons[K_d{}^3]{} & E{\cdot}L
\end{array}
$$
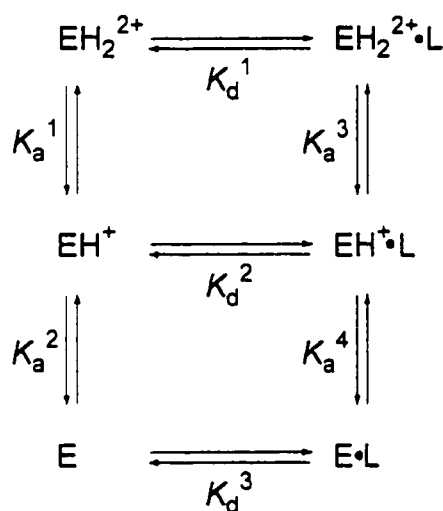
Scheme 2.1

K_a^1 and K_a^2 are macroscopic acid equilibrium constants for the free enzyme. K_a^3 and K_a^4

are macroscopic acid dissociation constants for the enzyme bound to the ligand. K_d^1, K_d^2,

and K_d^3 are equilibrium dissociation constants for each complex of the ligand and the

enzyme with different ionization status. Given this thermodynamic cycle, the apparent

equilibrium dissociation constant, $K_{d,app}$, can be written:

$$K_{d,app} = K_d^1 \cdot \frac{1 + \dfrac{K_a^1}{[H^+]} + \dfrac{K_a^1 K_a^2}{[H^+]^2}}{1 + \dfrac{K_a^3}{[H^+]} + \dfrac{K_a^3 K_a^4}{[H^+]^2}}$$

(2.2)

To reduce the number of parameters, the K_a values of His12 and His119 are assumed to be

the same and not to affect one another. This approximation seems to be valid for the analysis

here, because the data in Table 2.4 could not resolve the difference in pK_a's of His12 and

His119. By assigning K_a of His12 and His119 as K_a^f in the free enzyme and K_a^b in the

bound enzyme, the four macroscopic acid equilibrium constants, K_a^1, K_a^2, K_a^3, and K_a^4 in

eq 2.2 can be expressed as $2 K_a^f$, $K_a^f/2$, $2 K_a^b$, and $K_a^b/2$. Then, eq 2.2 can be rewritten:

$$K_{d,app} = K_d^1 \cdot \frac{1 + \dfrac{2K_a^f}{[H^+]} + \left(\dfrac{K_a^f}{[H^+]}\right)^2}{1 + \dfrac{2K_a^b}{[H^+]} + \left(\dfrac{K_a^b}{[H^+]}\right)^2}$$

(2.3)

which can be converted into an equation for free energy as a function of pH:

$$\Delta G_{\text{binding}}{}^{\circ} = \Delta G^{1} + RT \ln \frac{1 + 2 \cdot 10^{pH-pK_{a}^{f}} + 10^{2(pH-pK_{a}^{f})}}{1 + 2 \cdot 10^{pH-pK_{a}^{b}} + 10^{2(pH-pK_{a}^{b})}} \tag{2.4}$$

where $\Delta G_{\text{binding}}{}^{\circ}$ is the apparent change in free energy at each pH and ΔG^{1} is the change in

the free energy when the histidine residues are pully protonated. Eq 2.4 was used to fit the

data in Table 2.4 by nonlinear regression (Figure 2.3). Thus, the value of pK_{a}^{f} and pK_{a}^{b} are

determined to be 6.14 ± 0.03 and 7.08 ± 0.03, and ΔG^{1} is determined to be (-6.03 ± 0.02)

kcal/mol. From these parameters, $\Delta G^{3} - \Delta G^{1}$, the difference in the stability of the complex

between its protonated form and unprotonated form is calculated as (-2.5 ± 0.1) kcal/mol.

Therefore, the protonation of each histidine residue contributes approximately 1.3 kcal/mol

to the stability of the complex.

The increase in the pK_{a} values of the active-site histidine residues suggests that the

binding of the ligand stabilizes the imidazolium form of the side chain by Coulombic

interactions. The microscopic pK_{a} values of the histidines have been shown to increase by

0.5-0.8 unit upon binding to 3'–UMP (Quirk & Raines, 1999). The macroscopic pK_{a}'s

determined from pH-k_{cat}/K_{M} profiles and pH-k_{cat} profiles also have shown that the binding

of substrate to the active site of RNase A increases the pK_{a} values of these histidine residues

(Findlay et al., 1961; Eftink & Biltonen, 1983a).

Effect of Replacing Active-Site Histidine Residues on Ligand Binding. The effect of

replacing the active-site histidine residues on ligand binding is depicted in Figure 2.4. When

wild-type RNase A forms a complex with 3'–UMP at pH 6.0, the active-site histidines form

Coulombic interactions with the phosphoryl group of 3'-UMP. When His12 or His119 is

replaced with an alanine residue, the complex stability is decreased by 1.4 kcal/mol or 1.1

kcal/mol, respectively (Figure 2.4A). Direct assignment of the decrease in stability to

specific interactions are not feasible because of the partial protonation states of the histidine

residues and 3'-UMP at pH 6.0. The substitution of His12 with an alanine residue also

affects the stability of the complex with 6-FAM~d(AUAA) significantly. At pH 4.0, where

the complex with wild-type RNase A most stable, the K_d for the complex was (2.0 ± 0.4)

mM. The $\Delta G_{binding}°$ was calculated to (−3.7 ± 0.1) kcal/mol, which is higher by 2.3 kcal/mole

than the stability of the complex with wild-type RNase A at the same pH. This $\Delta G_{binding}°$ of

the complex with H12A RNase A at pH 4.0 is comparable to that of the complex with wild-

type RNase A at pH 8.0 (Figure 2.4B). When the pH is increased from 4.0 to 8.0, the wild-

type RNase A•6-FAM~d(AUAA) complex loses 2.4 kcal/mol in stability or, presumably,

~1.2 kcal/mol per histidine residue. When protonated His12 is replaced with an alanine

residue, the complex loses 2.3 kcal/mol in stability. Therefore, the neutral His12 still

contributes ~1.1 kcal/mol to the stability of the complex at pH 8.0. These energetic

considerations imply that the interaction between His12 and the ligand at pH 4.0 does not

rely only on ionic hydrogen bonding between the protonated histidine and the non-bridging

oxygens but also on other types of interactions even neutral histidines and the ligand can

form at pH 8.0, such as a stacking interaction with a nucleobase.

The contribution of protonated His12 to complex stability, 2.3 kcal/mol, is prominent.

Lys66 and Lys7/Arg10 comprise the enzymic P0 and P2 subsites, respectively. Like His12,

Lys66 and Lys7/Arg10 interact with a phosphoryl group of a bound nucleic acid (Fisher et al., 1998b). K66A RNase A forms a complex that is 0.9 kcal/mol less stable in the same solution condition (0.10 M MES–NaOH buffer, pH 6.0, containing 0.10 M NaCl). K7A/R10A RNase A forms a complex that is 1.2 kcal/mol less stable in this solution condition. Thus, the contribution of protonated His12 to binding is greater by 1.1–1.4 kcal/mol than that of the P0 or P2 subsite residue.

Interaction of Active-Site Histidine Residues with Ligands. The structure of the crystalline wild-type RNase A•3'–CMP complex [PDB entry 1RPF (Zegers et al., 1994)] shows that His12 and His119 are both within hydrogen bonding distance of the phosphoryl group of 3'–CMP. Specifically, $N_{\varepsilon 2}$ of His12 is 2.7 Å from an oxygen atom of the phosphoryl group of 3'–CMP and $N_{\delta 1}$ of His119 is in 3.1 Å from another oxygen atom. Rotation about the P–$O^{3'}$ bond of the 3'–CMP molecule varies the lengths of these hydrogen bonds. In the structure of the crystalline complex of K7A/R10A/K66A RNase A and 3'–UMP [PDB entry 4RSK (Fisher et al., 1998c)], $N_{\varepsilon 2}$ of His12 does form a longer hydrogen bond with a phosphoryl oxygen atom (3.0 Å) and $N_{\delta 1}$ of His119 forms a shorter hydrogen bond (2.7 Å).

The structure of the crystalline complex of wild-type RNase A and d(ATAAG) [PDB entry 1RCN (Fontecilla-Camps et al., 1994)] can be used to explain our thermodynamic data on the stability on the complex of RNase A and 6-FAM–d(AUAA). $N_{\varepsilon 2}$ of His12 is within hydrogen bonding distance of non-bridging oxygen atoms of the ligand, 3.2 Å from one oxygen and 3.3 Å from the other oxygen, which explains the pH dependence of the complex

stability. The side chain of His12 is also in contact with the thymine nucleobase of the ligand, which could be responsible for the contribution of neutral histidine to the complex stability. $N_{\delta1}$ of His119 also forms hydrogen bonds with a non-bridging oxygen and 5' oxygen of the phosphoryl group in the active site, each with a length of 3.0 Å. These hydrogen bonds are also likely to be responsible for the pH dependence of the stability of the complex. His119 makes a stacking interaction with the adenine nucleobase in the B2 subsite. Therefore, His119 can interact with the ligand even when its side chain is neutral. These extended interactions with other moieties of the ligand beyond the phosphoryl group in the active site make the protonated active-site histidines more significant in ligand binding than the cationic residues in the P0 and P2 subsites, which mainly rely on Coulombic interactions.

Implications for Catalysis by RNase A. His12 and His119 of RNase A have roles not only in nucleic acid turnover, but also in nucleic acid binding. The contributions of these histidine residues to ground state stabilization is comparable or higher than the contributions of the arginine and lysine residues comprising the P0 and P2 subsites (Fisher et al., 1998b), even at pH 6.0. At acidic pH, the contributions of the histidine residues are maximal. Because the transphosphorylation reaction catalyzed by RNase A requires neutral His12 as a base (Figure 1.1), the catalysis is impaired at acidic pH. Ground state stabilization is, however, maximal at acidic pH. Therefore, nonproductive enzyme–substrate complexes with improper ionization states of active-site histidines are expected to be prevalent at acidic pH. This consideration is consistent with the bell-shaped pH–k_{cat} profiles of RNase A. If

RNase A binds to a substrate only when His12 and His119 are in a catalytically competent ionization state, then its value of k_{cat} should be pH-independent, as only one ionization state would be possible in the enzyme–substrate complex. The bell-shaped pH–k_{cat} profile, therefore, shows that catalytically incompetent ionization states of active-site histidines are allowed in an enzyme–substrate complex, which is consistent with the effect of pH on the complex stability reported herein.

Table 2.1: X-Ray Diffraction Analysis Statistics of H12A RNase A.

Crystal data	H12A RNase A
Space group	P3$_2$21
Cell dimensions (Å)	a = 64.54 (1)
	b = 64.54 (1)
	c = 65.08 (2)
Protein mols/unit cell	6
Data collection statistics	
Resolution (Å)	1.7
No. of measured reflections (I/σ > 0.33)	50643
No. of unique reflections	20142
Average redundancy	2.5
Average I/σ	24
Completeness (30 – 1.7) (%)	96
Completeness high-resolution shell (%)	(1.8–1.7 Å) 88
R_{sym}	0.030
R_{sym} high-resolution shell	(1.8–1.7 Å) 0.13
Final refinement statistics	
H12A RNase A atoms	960
Solvent atoms	99
R-factor	(30–1.7 Å) 0.182
RMS deviation from ideal geometry	
Bond distances (Å)	0.012
Bond angles (°)	2.31
Average B-factors (Å^2)	
Main-chain atoms	30.4
Side-chain atoms	36.7
Chloride atoms	32.6

Table 2.2: X-Ray Diffraction Analysis Statistics of H119A RNase A.

Crystal data	H119A RNase A
Space group	$P3_221$
Cell dimensions (Å)	$a = 64.53$ (1)
	$b = 64.53$ (1)
	$c = 65.04$ (2)
Protein mols/unit cell	6
Data collection statistics	
Resolution (Å)	1.8
No. of measured reflections ($I/\sigma > 0.33$)	68047
No. of unique reflections	23009
Average redundancy	3.0
Average I/σ	19
Completeness (30 – 1.8) (%)	94
Completeness high-resolution shell (%)	(1.9–1.8 Å) 90
R_{sym}	0.033
R_{sym} high-resolution shell	(1.9–1.8 Å) 0.149
Final refinement statistics	
H119A RNase A atoms	960
Solvent atoms	99
R-factor	(30–1.8 Å) 0.164
RMS deviation from ideal geometry	
Bond distances (Å)	0.011
Bond angles (°)	2.41
Average B-factors ($Å^2$)	
Main-chain atoms	25.5
Side-chain atoms	32.1
Chloride atoms	29.5

Table 2.3: Thermodynamic Stabilities of the 3'-UMP Complexes with Wild-Type

Ribonuclease A and the H12A and H119A Variants.

RNase A	K_d (mM)[a]	$\Delta G°$ (kcal/mol)
Wild-type	0.054	−5.8
H12A	0.55	−4.4
H119A	0.37	−4.7

[a]Data were obtained at 25 °C in 0.10 M MES–NaOH buffer (pH 6.0) containing 0.10 M

NaCl by isothermal titration calorimetry.

Table 2.4: Thermodynamic Stability of the Complex of 6-FAM~d(AUAA) with Wild-Type

Ribonuclease A and the H12A Variant.

Proteins	pH	Buffer condition	K_d (mM)[a]	$\Delta G_{binding}°$ (kcal/mol)
Wild-type RNase A	4.0	0.10 M Sodium Acetate 0.050 M NaCl	0.038 ± 0.005	−5.99 ± 0.08
	5.0	0.10 M Sodium Acetate 0.050 M NaCl	0.040 ± 0.002	−5.96 ± 0.03
	6.0[b]	0.10 M MES-NaOH 0.10 M NaCl	0.088 ± 0.008	−5.50 ± 0.05
	7.2	0.10 M MOPS–HCl 0.10 M NaCl	1.1 ± 0.1	−4.01 ± 0.05
	8.0	0.10 M TrisHCl–NaOH 0.050 M NaCl	2.2 ± 0.2	−3.60 ± 0.05
H12A RNase A	4.0	0.10 M Sodium Acetate 0.050 M NaCl	2.0 ± 0.4	−3.7 ± 0.1

[a]Data were obtained at 23 °C in the designated buffer conditions by fluorescence anisotropy.

[b]Data from (Fisher et al., 1998c).

Figure 2.1   Stereoview of the active site of H12A ribonuclease A. The electron density is

$2|F_o| - |F_c|$ contoured at 1.0 σ. Loss of the side chain at residue 12 has

resulted in disorder in residues Asn67, His119, and Phe120. A water

molecule (W153) is occupying the position of the side-chain imidazole of

His12.
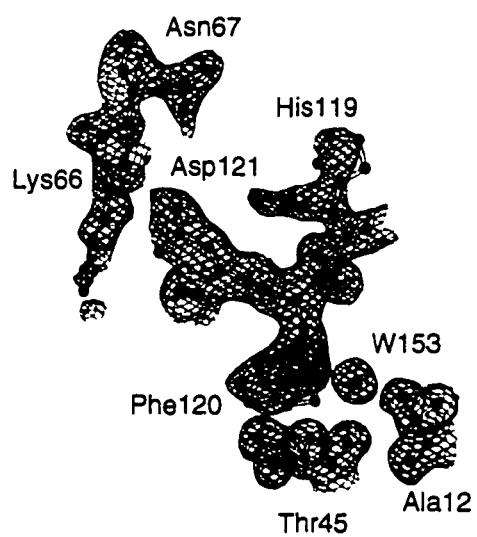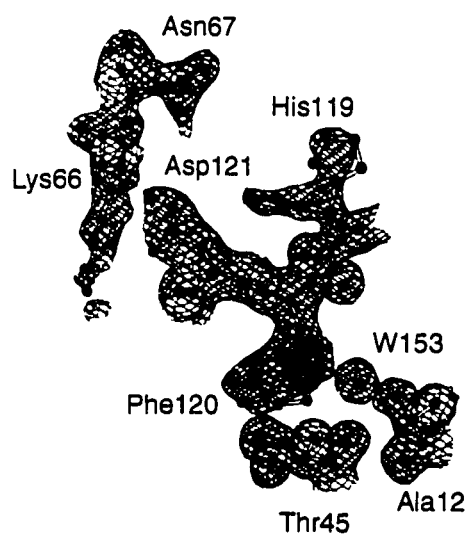
Figure 2.2   Stereoview of the active site of H119A ribonuclease A. The electron density

is $2|F_o| - |F_c|$ contoured at 1.0 σ. Loss of the side chain at residue 119 has

little effect on the structure. A water molecule (W246) forms a hydrogen

bond with the side chain of Asp121 in place of the His119 side chain.

Asn67 Asn67
Lys66 Asp121 Ala119 Lys66 Asp121 Ala119
W246 W246
Phe120 Phe120
Thr45 His12 Thr45 His12
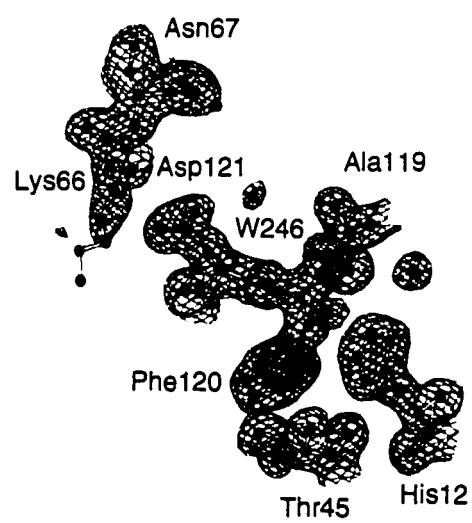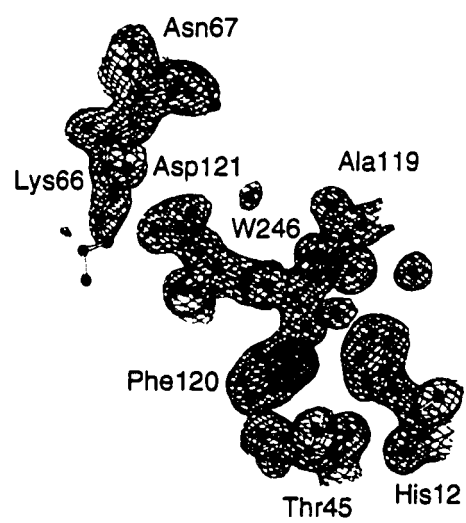
Figure 2.3 Effect of pH on the stability of the complex of wild-type ribonuclease A and

6-FAM~d(AUAA). Non-linear regression of data in Table 2.4 with eq 2.4

determines $pK_a^f = 6.14 \pm 0.03$, $pK_a^b = 7.08 \pm 0.03$, and $\Delta G^1 = (-6.03 \pm 0.02)$

kcal/mol.
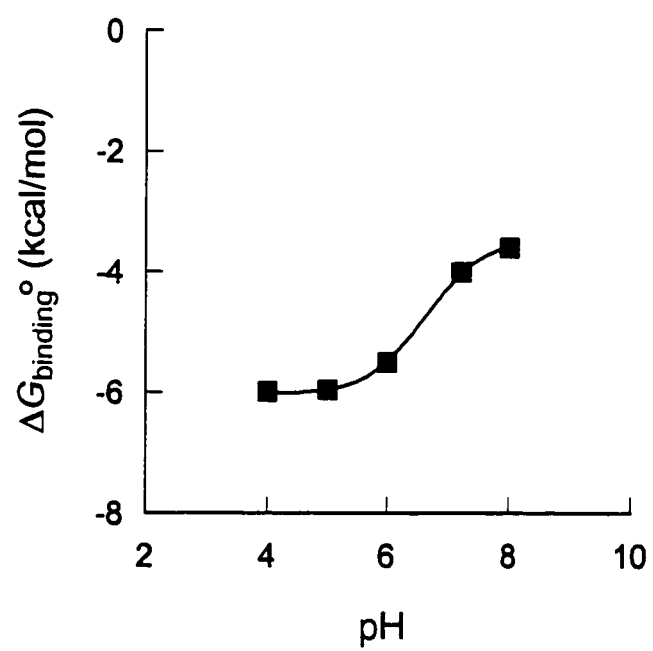
Figure 2.4   Schematic diagrams depicting the effect of replacing the active-site histidine

residues on the stability of the complexes with 3'-UMP (A) and 6-

FAM~d(AUAA) (B). Phosphoryl groups are depicted as circles. His12 and

His119 are depicted as squares with a concave surface facing the phosphoryl

groups. Numbers in shapes present formal charges of each group.
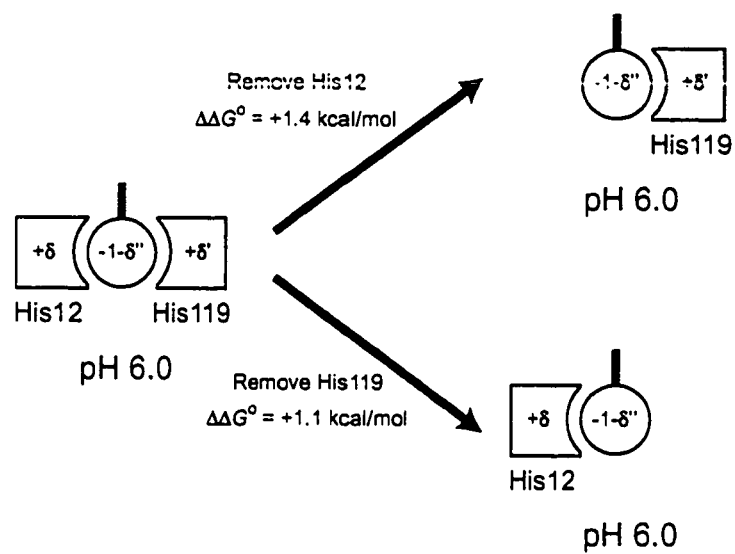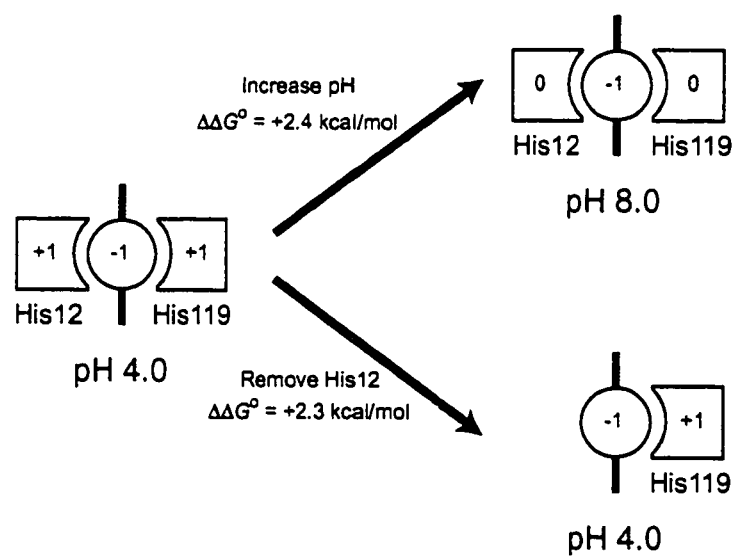
Chapter 3

Origin of the "Inactivation" of Ribonuclease A at Low Salt Concentration

ABSTRACT

The effect of salt concentration on catalysis by ribonuclease A (RNase A) has been reexamined. At low salt concentration, the enzyme is inhibited by low-level contaminants in common buffers. When an uncontaminated buffer system is used or H12A RNase A, an inactive variant, is added to absorb inhibitory contaminants, enzymatic activity is manifested fully at low salt concentration. Catalysis by RNase A does not have an optimal salt concentration. Instead, $k_{cat}/K_M > 10^9$ $M^{-1}s^{-1}$ for RNA cleavage at low salt concentration. These findings highlight the care that must accompany the determination of meaningful salt–rate profiles for enzymatic catalysis.

INTRODUCTION

Salt concentration, like pH and temperature, is a solution condition that can have a

dramatic affect on enzymatic catalysis. Despite the importance of salt effects on catalysis,

their chemical origins are unknown for most enzymes. For decades, bovine pancreatic

ribonuclease A (RNase A; EC 3.1.27.5 (D'Alessio & Riordan, 1997; Raines, 1998)) has been

the object of much study in this area (Davis & Allen, 1955; Dickman et al., 1956; Edelhoch

& Coleman, 1956; Dickman & Ring, 1958; Kalnitsky et al., 1959; Irie, 1965; Winstead &

Wold, 1965; Libonati & Sorrentino, 1992; Boix et al., 1996). Numerous workers have

reported that the enzyme has a bell-shaped salt–rate profile with a salt concentration

optimum. Surprisingly, there has been no consensus as to either the optimal concentration of

salt or the origin of the decrease in catalytic activity at low salt concentration.

Various explanations have been proposed to explain the decrease in the catalytic activity

of RNase A at low salt concentration. These explanations include intramolecular interactions

between the binding sites of the enzyme (Edelhoch & Coleman, 1956), a conformational

change of the enzyme or substrates (Irie, 1965), a decrease in "specific" interactions with

substrates due to increased rigidity of the enzyme (Libonati & Sorrentino, 1992), and so

forth. Here, we use a series of kinetic experiments with a sensitive fluorogenic substrate and

enzyme variants to demonstrate that the inactivation of RNase A at low salt concentration is

caused by inhibitory contaminants of buffer solutions commonly used for enzymatic assays.

Rather than having an optimum, ribonucleolytic activity continues to increase as salt

concentration decreases. Moreover, in solutions of low salt concentration, RNase A has

$k_{cat}/K_m > 10^9$ $M^{-1}s^{-1}$ for the cleavage of an RNA substrate.

MATERIALS AND METHODS

Materials. Wild-type RNase A and its H12A and K7A/R10A/K66A variants were

produced, folded, and purified as described elsewhere (delCardayré et al., 1995; Fisher et al.,

1998b). The substrate

6-carboxyfluorescein~dAdArUdAdAdA~6-carboxytetramethylrhodamine

[6-FAM~(dA)$_2$rU(dA)$_3$~6-TAMRA] was from Integrated DNA Technologies (Coralville,

IA). A large increase in fluorescence occurs upon cleavage of the P–O$^{5'}$ bond on the 3' side

of the single ribonucleotide residue embedded within this substrate (Kelemen et al., 1999).

2-Morpholinoethanesulfonic acid (MES) and citric acid (trisodium salt) were from Sigma

Chemical (St. Louis, MO). [bis(2-Hydroxyethyl)amino]tris(hydroxymethyl)methane

(Bistris) was from ICN Biomedicals (Aurora, OH). The concentration of solutions of the

wild-type, H12A and K7A/R10A/K66A enzymes was determined spectrophotometrically by

using $\varepsilon = 0.72$ mL mg^{-1}cm^{-1} at 277.5 nm (Sela et al., 1957). Concentrations of the substrate

were also determined spectrophotometrically by using $\varepsilon = 126,400$ M^{-1}cm^{-1} at 260 nm

(Kelemen et al., 1999).

Assays of Catalytic Activity. Ribonucleolytic activity was assessed at 23 °C in 2.00 mL

of 10 mM or 50 mM MES-NaOH buffer (pH 6.0), or 25 mM or 50 mM Bistris-HCl buffer

(pH 6.0). The buffered solutions contained NaCl (0 – 1.0 M),

6-FAM~(dA)$_2$rU(dA)$_3$~6-TAMRA (19 – 38 nM), and enzyme (0.50 – 500 pM).

Fluorescence was measured with a QuantaMaster 1 photon-counting fluorescence

spectrometer from Photon Technology International (South Brunswick, NJ) using quartz or

glass cuvettes (1.0-cm pathlength; 3.5-mL volume) from Starna Cells (Atascadero, CA) and

493 nm and 515 nm as the excitation and emission wavelengths, respectively.

Kinetic parameters were determined by regression analysis of the fluorescence intensity

change as described previously (Kelemen et al., 1999). Briefly, when the rate was fast

enough to reach completion, pseudo-first order rate constants were determined by fitting the

observed fluorescence intensity to an exponential equation:

$$F = F_0 + (F_{max} - F_0)(1 - e^{-kt})$$ (3.1)

where F is the observed fluorescence intensity, F_0 is the initial intensity before the

reaction is initiated, F_{max} is the final fluorescence intensity after the reaction has reached

completion. The values of F_{max}, F_0, and k were determined by nonlinear regression analysis.

When substrate concentration is sufficiently smaller than K_M, the pseudo-first order rate

constant k from this regression can be regarded as $V K$. When a reaction was too slow to

achieve completion, $V K$ was determined with eq 3.2 instead of eq 3.1.

$$V / K = \frac{(\Delta F / \Delta t)}{F_{max} - F_0}$$ (3.2)

where $\Delta F/\Delta t$ is the slope from linear regression analysis. The slope was determined from

linear regression analysis of fluorescence intensity change for a linear region. The value of

F_{max} was determined by completing the reaction by adding an excess of enzyme. The value

of the apparent k_{cat}/K_M was calculated by dividing $V K$ by the enzyme concentration.

Rescue of Catalytic Activity by Increasing Protein Concentration. The effect of protein

concentration on the catalytic activity of wild-type RNase A was assessed by measuring the

activity at varying concentrations of H12A RNase A. After a reaction was initiated at 23 °C

with wild-type RNase A (0.5 nM) in 50 mM MES-NaOH buffer (pH 6.0) as described

above, the total concentration of protein was increased by adding aliquots of a concentrated

solution of H12A RNase A dissolved in the assay buffer. In a control experiment with H12A

RNase A alone, there was no detectable ribonucleolytic activity under identical reaction

conditions.

RESULTS AND DISCUSSION

Salt–Rate Profiles of Catalysis. The effect of salt concentration on the catalytic activity

of wild-type RNase A and the K7A/R10A/K66A variant were determined in MES-NaOH

buffer (pH 6.0) containing different concentrations of NaCl. The K7A/R10A/K66A variant

has three fewer cationic residues than does the wild-type enzyme (Fisher et al., 1998b;

Fisher et al., 1998c), and is effectively missing two of the four known subsites for

phosphoryl group binding (Fisher et al., 1998b; Nogues et al., 1998). The two enzymes appear to have salt–rate profiles of similar shape (Figure 3.1). Both enzymes lose their catalytic activity at low salt with an identical steep slope. The apparent salt optima for catalysis by the two enzymes are, however, distinct. The apparent salt optimum for catalysis by wild-type RNase A is 120 mM Na^+, whereas that for K7A/R10A/K66A RNase A is 14 mM Na^+. As a consequence, wild-type RNase A appears to have only 1% of the catalytic activity of the K7A/R10A/K66A variant at low salt concentration. This result is consistent with the previously reported observation that the salt optimum for catalysis by a ribonuclease depends on the basicity of the enzyme (Libonati & Sorrentino, 1992).

At high salt concentration, the salt–rate profile of the wild-type enzyme has a steeper slope than does that of K7A/R10A/K66A RNase A. The decline in activity at high salt concentration is likely due to the decrease in the strength of the Coulombic interaction between the enzymes and the substrate. This explanation is consistent with our previous observation that the binding of a single-stranded nucleic acid to wild-type RNase A is more sensitive to salt concentration than is the binding to the K7A/R10A/K66A variant (Fisher et al., 1998b). What then is the origin of the observed decline in activity at low salt concentration?

Dependence of Salt–Rate Profiles on Buffer Type. Salt effects on catalysis by RNase A were found to be dependent on the buffer system used for an assay. The salt–rate profile in Bistris-HCl buffer (pH 6.0) is markedly different from that in MES-NaOH buffer (pH 6.0) (Figure 3.2A). Although the salt–rate profile determined with MES-NaOH buffer has a bell-shaped curve with a salt optimum, the profile with Bistris-HCl buffer does not show a salt

optimum. Rather, the rate continues to increase as the salt concentration decreases. In 25

mM Bistris-HCl buffer (pH 6.0) without added NaCl, the apparent value of k_{cat}/K_M was 2.8 ×

10^9 $M^{-1}s^{-1}$, which is 50-fold greater than the apparent value of k_{cat}/K_M at the salt optimum in

MES-NaOH buffer (pH 6.0). The activities measured with the two different buffers coincide

only when the salt concentration is >0.10 M. This result suggests that the "inactivation" of

RNase A at low salt concentration is due to buffer contaminants rather than to an intrinsic

property of the enzyme. Moreover, the true k_{cat}/K_M for catalysis of RNA cleavage by

RNase A does not have a salt optimum.

To demonstrate directly the inhibitory effect of MES-NaOH buffer at low salt, small

amounts of MES-NaOH buffer (pH 6.0) were added to an enzymatic reaction occurring in

Bistris-HCl buffer (pH 6.0) (Figure 3.2B). The reaction was quenched completely by the

addition of the MES-NaOH buffer to a final concentration of only 0.5 mM. Citrate-HCl

buffer (pH 6.0) also effected a similar inhibition. The reaction in Bistris-HCl buffer (pH 6.0)

was quenched when citrate-HCl buffer (pH 6.0) was added to a final concentration of 5 mM

(data not shown).

Dependence of Salt–Rate Profile on Enzyme Concentration. A distinctive characteristic

of the catalytic activity of RNase A in a MES-NaOH buffer (pH 6.0) with a low salt

concentration is the presence of a burst. Specifically, the addition of enzyme to a reaction

mixture produces a sharp increase in fluorescence intensity followed by a slow phase

(Figure 3.3A). This burst is consistent with the enzyme being active in the stock solution but

becoming inactive quickly upon addition to the reaction mixture. Moreover, the degree of

inhibition is related to the concentration of enzyme in the reaction mixture. These results were unexpected because both the stock solution and the reaction mixture were made of the same buffer—50 mM MES-NaOH buffer (pH 6.0).

H12A RNase A was used to elucidate the origin of the apparent burst kinetics. His12 is an active-site residue of RNase A, and the H12A variant has 10^5-fold less ribonucleolytic activity than does the wild-type enzyme (Thompson & Raines, 1995). Hence, the addition of small quantities of H12A RNase A to a reaction mixture increases the total protein concentration without introducing significant catalytic activity. Surprisingly, the H12A variant was able to revive the catalytic activity of wild-type RNase A when added to reactions occurring in 50 mM MES-NaOH buffer (pH 6.0). Addition of H12A RNase A (to 80 nM) increased by $>10^4$-fold the apparent k_{cat}/K_m value for catalysis by the wild-type enzyme (at 0.5 nM) (Figure 3.3B). This result indicates that the inhibitor was not the MES-NaOH buffer itself, which was present at 50 mM, but low-level contaminants. In effect, the H12A variant is acting like a sponge that absorbs those Contaminants. Because the addition of H12A RNase A to 80 nM enabled the wild-type enzyme to regain almost all of its intrinsic catalytic activity (Figures 3.2A and 3.3B), the concentration of the inhibitory contaminants in 50 mM MES-NaOH buffer must be <80 nM, that is, <2 ppm. The enzyme is active in the stock solution because the enzyme concentration there (unlike in the reaction mixture) far exceeds the concentration of the inhibitory contaminants. Finally, neither RNase A with scrambled disulfide bonds nor the S-protein fragment (residues 21 – 124) can revive the catalytic activity of RNase A in 50 mM MES-NaOH buffer (pH 6.0) (data not

shown). Apparently, binding to the inhibitory contaminants requires the native structure of RNase A.

Nature of the inhibitory contaminants. The inhibitory contaminants are likely to be highly charged because inhibition is sensitive to salt concentration. They are also likely to be anionic, because RNase A is cationic [pI = 9.3 (Ui, 1971)]. This proposal is consistent with the observation that a less cationic variant, K7A/R10A/K66A RNase A, has less affinity for the contaminants (Figure 3.1). The contaminants do not seem to be polymeric, as the salt dependence of inhibition is similar for wild-type RNase A and the K7A/R10A/K66A variant, which is missing two enzymic subsites for phosphoryl group binding.

Conclusions. The often reported "inactivation" of RNase A at low salt concentration is due to low levels of small anions in common buffer solutions. The degree of inhibition can vary according to the buffer system and enzyme concentration used in assays of catalytic activity. These variations could be responsible for the reported discrepancy in the optimal salt concentration for catalysis (Davis & Allen, 1955; Dickman et al., 1956; Edelhoch & Coleman, 1956; Dickman & Ring, 1958; Kalnitsky et al., 1959; Irie, 1965; Libonati & Sorrentino, 1992; Boix et al., 1996). pH–Rate profiles have been used often and with great success to reveal the role of acidic and basic functional groups in enzymatic catalysis (Knowles, 1976; Cleland, 1982; Brocklehurst, 1994). Likewise, salt–rate profiles can provide valuable insight into the role of Coulombic interactions, but only when proper care is used to avoid artifacts in their determination.

Figure 3.1   Apparent salt–rate profiles for wild-type RNase A and K7A/R10A/K66A

RNase A in MES-NaOH buffer. Salt–rate profiles for catalysis of the

cleavage of 6-FAM~(dA)$_2$rU(dA)$_3$~6-TAMRA by wild-type ribonuclease A

(●) in 50 mM MES-NaOH buffer (pH 6.0) and the K7A/R10A/K66A variant

(O) in 10 mM MES-NaOH buffer (pH 6.0). Apparent values of k_{cat}/K_M were

determined at 23 °C in buffer containing substrate (19 nM) and enzyme (0.50

nM). [Na$^+$] was calculated by summing the contribution from buffer and

added salt.
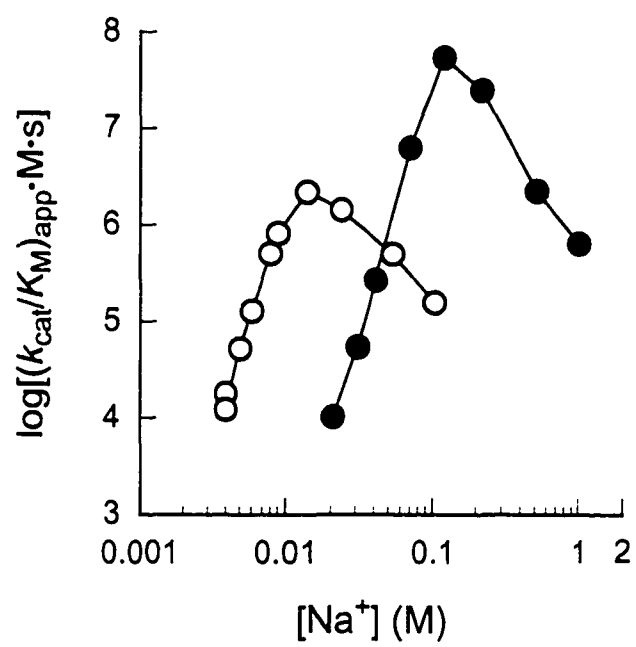
Figure 3.2 Effect of buffer on the salt dependence of catalysis. Effect of buffer on the

salt dependence of catalysis of the cleavage of

6-FAM~(dA)₂rU(dA)₃~6-TAMRA by wild-type ribonuclease A. A. Salt–rate

profiles at 23 °C in 25 mM or 50 mM Bistris-HCl buffer (■; pH 6.0) and 50

mM MES-NaOH buffer (●; pH 6.0). [Cation] is the sum of the concentration

of Bistris cation and Na⁺. B. Inhibition of catalytic activity by MES-NaOH

buffer. The reaction was initiated at 23 °C by the addition $t \approx 250$ s of wild-

type RNase A (1 µl of a 1 nM solution) to a final concentration of 0.50 pM in

2.00 mL of 50 mM Bistris-HCl buffer (pH 6.0) containing substrate (19 nM).

At $t \approx 450$ s, an aliquot (20 µL) of 50 mM MES-NaOH buffer (pH 6.0) was

added to the reaction mixture to give a final MES-NaOH concentration of

0.50 mM.

A

B
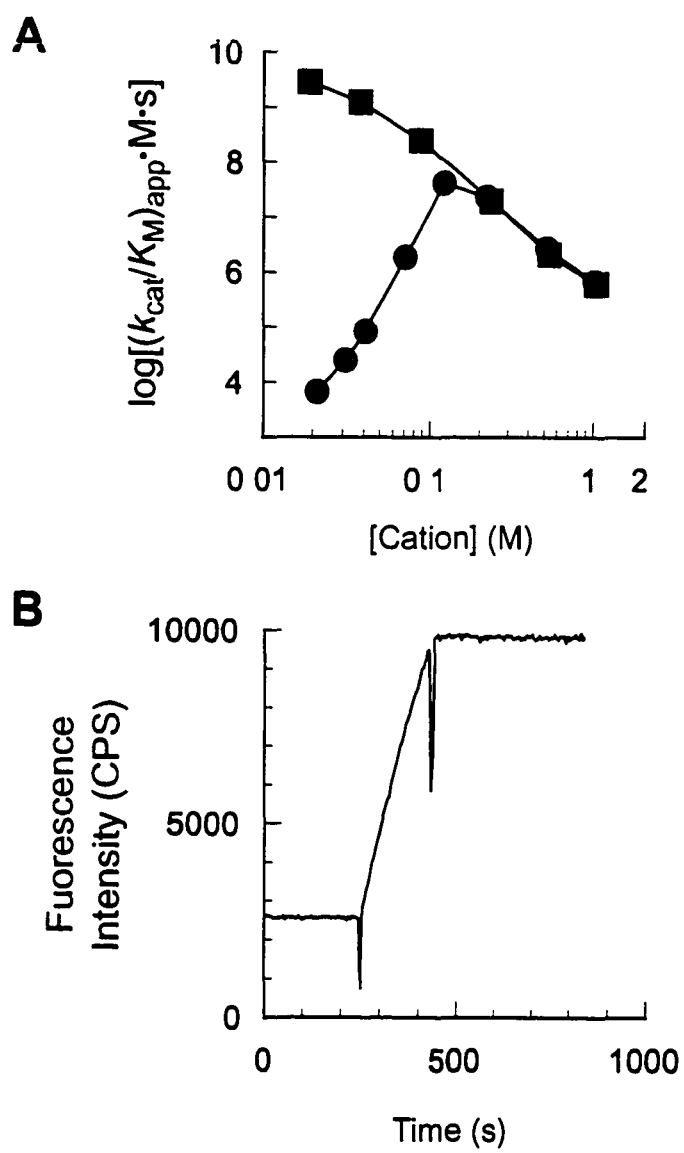
Figure 3.3   Effect of enzyme concentration on the "inactivation" of ribonuclease A at

low salt concentration. **A.** The reaction was performed at 23 °C in 50 mM

MES-NaOH buffer (pH 6.0) containing 6-FAM~(dA)$_2$rU(dA)$_3$~6-TAMRA

(19 nM). Bursts of catalytic activity were observed upon addition of aliquots

of wild-type RNase A (5 μL of a 0.31 nM solution) to the reaction mixture

(2.00 mL). **B.** The reaction was performed at 23 °C in 50 mM MES-NaOH

buffer (pH 6.0) containing 6-FAM~(dA)$_2$rU(dA)$_3$~6-TAMRA (19 nM),

wild-type RNase A (0.50 nM), and H12A RNase A (0 – 80 nM). [Enzyme] is

the sum of the concentrations of wild-type RNase A and H12A RNase A.
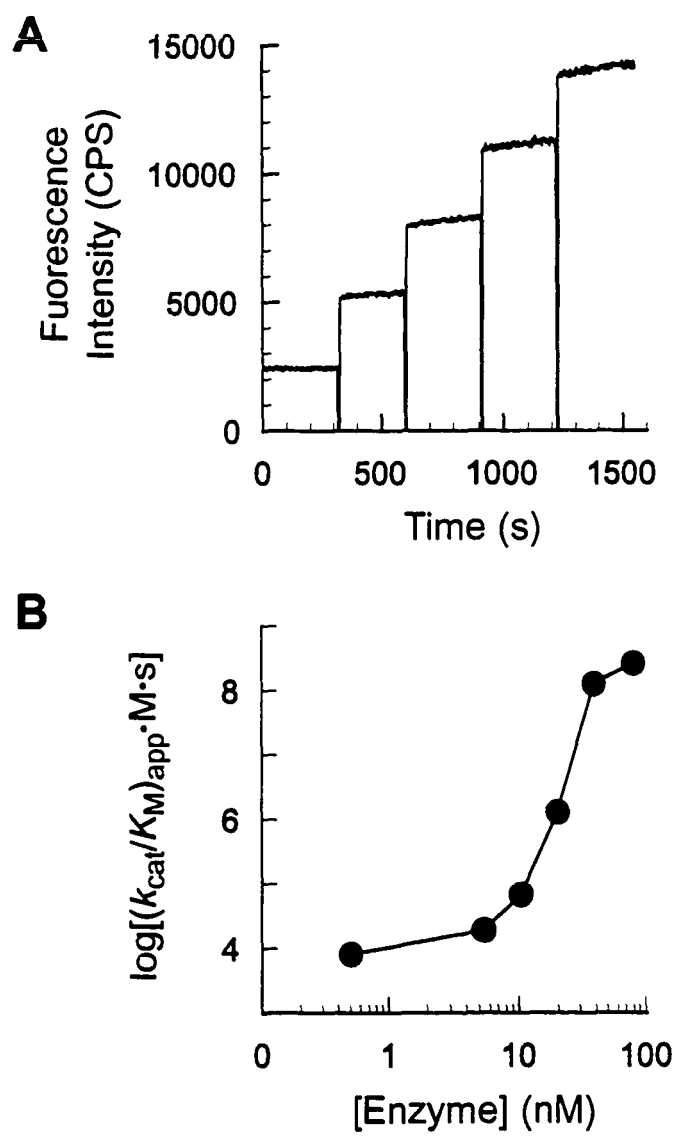
Chapter 4

Quantitative Analysis of the Effect of Salt Concentration

on Enzymatic Catalysis

ABSTRACT

Like pH, salt concentration can have a dramatic effect on enzymatic catalysis. Here, salt effects on catalysis by ribonuclease A (RNase A) were used to derive a quantitative model for salt–rate profiles. Salt–rate profiles were determined by measuring k_{cat}/K_M with fluorogenic substrates at varying salt concentrations. The analysis of salt–rate profiles of wild-type RNase A and its variants showed that the dependence of k_{cat}/K_M on salt concentration reflects the contribution of Coulombic interactions to uniform binding. The k_{cat}/K_M of K7A/R10A/K66A RNase A, a variant with three fewer positive charges at neutral pH, showed significantly reduced dependence on salt concentration, compared with that of wild-type RNase A. The salt–rate profiles of k_{cat}/K_M determined with three fluorogenic substrates with varing numbers of phosphoryl groups also showed that the dependence of k_{cat}/K_M on salt concentration correlates with the extent of Coulombic interactions in an enzyme–substrate complex. Quantitative analysis of salt–rate profiles is put forth as a useful tool for assessing the contribution of Coulombic interactions to catalysis.

INTRODUCTION

Catalysis by an enzyme depends on the environment in which the reaction occurs. Like pH, the ionic environment is a critical parameter for enzymatic catalysis, because the ionic environment determines the strength of Coulombic interactions in aqueous solution. Coulombic interaction is a major driving force in biomolecular recognition of enzyme–substrate, protein–ligand, and protein–protein interactions (Record et al., 1976; Perutz, 1978; Honig & Nicholls, 1995; Schreiber & Fersht, 1996; Carbeck et al., 1998).

Substrate binding by ribonuclease A (RNase A; EC 3.1.27.5) provides an archetypal example of Coulombic interactions between a protein and a single-stranded nucleic acid (Jensen & von Hippel, 1976; Record et al., 1976; Fisher et al., 1998b). RNase A is a pyrimidine-specific ribonuclease from bovine pancreas (Raines, 1998). A series of cationic residues on the surface of the enzyme form extensive Coulombic interactions with phosphoryl groups of nucleic acids. The cationic residues comprising phosphoryl group-binding sites have been identified by X-ray diffraction analyses (McPherson et al., 1986; Fontecilla-Camps et al., 1994) and site-directed mutagenesis (Fisher et al., 1998a; Fisher et al., 1998b). Four subsites have been identified: P(-1), P0, P1, and P2 (Figure 4.1). Arg85 and Lys66 comprise the P(-1) subsite and P0 site, respectively. The active-site residues, His12, Lys41, and His119 comprise the P1 subsite. These residues have roles in binding the phosphoryl group in the active site as well as in catalysis (Park et al., 2001). Finally, Lys1 and Arg7 comprise the P2 subsite.

Extensive Coulombic interactions in the complex of RNase A and nucleic acids are

responsible for the strong salt effects on the stability of RNase A–nucleic acid complexes.

Jensen and von Hippel showed that when denatured DNA was used as a ligand for RNase A,

the equilibrium association constant decreases from 5.6×10^5 M to 1.2×10^4 M as [Na$^+$] is

increased from 0.030 M to 0.070 M (Jensen & von Hippel, 1976). The logarithm of the

observed equilibrium constant shows a linear dependence on log[Na$^+$]. Record and

coworkers successfully applied the polyelectrolyte theory to explain this thermodynamic salt

effect (Record et al., 1976). Their analysis shows that the dependence of logK_{obs} on log[Na$^+$]

is linearly proportional to the number of ion pairs formed upon complex formation. The salt

effects on RNase A complex formation implicated the involvement of ~7 ion pairs in the

interaction of the enzyme with denatured DNA. Previously, we used this analysis to

characterize nucleic acid binding by RNase A variants with mutated phosphoryl group-

binding subsites (Fisher et al., 1998b).

The accumulated information on the structure and thermodynamics of Coulombic

interactions in RNase A makes this enzyme a promising model for studying salt effects on

enzymatic catalysis. Even though the contribution of Coulombic interactions to stabilizing

charged transition states in enzymatic catalysis has been appreciated (Perutz, 1978; Jackson

& Fersht, 1993), quantitative analyses of salt effects on enzymatic catalysis are nonexistent.

Here, we present a quantitative model for salt effects on catalysis by RNase A. We test the

validity of this model with salt–rate profiles of wild-type RNase A and its variants,

K7A/R10A/K66A RNase A and K41R RNase A. Because of the role of Lys7, Arg10, and

Lys66 in binding to the phosphoryl groups of substrates, K7A/R10A/K66A RNase A shows

significantly decreased Coulombic interactions with substrates (Fisher et al., 1998b). Lys41

is critical for catalysis by RNase A, as it donates a hydrogen bond to the transition state

(Messmore et al., 1995). Replacing Lys41 with an arginine residue does not impair the

Coulombic interactions with substrates, but impairs catalysis. We also analyze salt–rate

profiles with three analogous fluorogenic substrates with different numbers of phosphoryl

groups. The proposed quantitative model for salt effects on catalysis by RNase A explains

the salt–rate profiles successfully. We demonstrate that, with quantitative analysis, salt–rate

profiles can be as informative as pH-rate profiles, especially in assessing the role of

Coulombic interactions in uniform binding.

THEORY

A notional free energy profile of catalysis by RNase A is depicted Figure 4.2. The rate

constants, k_1, k_2, and k_3 are for association with a substrate, dissociation from the ES

complex, and conversion from the ES complex to the EP complex, respectively. The second-

order rate constant for the overall reaction, k_{cat}/K_M, is a function of these rate constants (see

Appendix):

$$k_{cat} / K_M = \frac{k_1 \cdot k_3}{k_2 + k_3}$$ (4.1)

The major effect of salt concentration on this free energy profile is the change of the

relative energy of bound states (ES complex and the transition state for the chemistry step)

to the energy of free states (free E and free S). According to studies of salt effects on the

stability of RNase A–nucleic acid complexes, the salt effect on the equilibrium association

constant for the ES complex, K_S, can be written:

$$\frac{\partial \log K_S}{\partial \log[\text{Na}^+]} = -n \qquad (4.2)$$

where n is the number of counterions released from substrate upon complex formation. For

simplicity, it is assumed that Na^+ is the only cation interacting with nucleic acid in the

system. By solving the differential equation:

$$K_S = K_S^{\ominus}[\text{Na}^+]^{-n} \qquad (4.3)$$

where $K_S^{\ominus}$ is the equilibrium association constant of ES complex when $[\text{Na}^+] = 1 \text{ M}$ ($\ominus$

denotes the state where $[\text{Na}^+] = 1 \text{ M}$). The change in the association free energy of the ES

complex, ΔG_S°, can be expressed as a function of $[\text{Na}^+]$ by eq 4.3.

$$\Delta G_S^{\circ} = \Delta G_S^{\ominus} + nRT \ln[\text{Na}^+] \qquad (4.4)$$

where $\Delta G_S^{\ominus}$ is again the change in the association free energy of the ES complex when

$[Na^+] = 1$ M. Now, define $\Delta\Delta G_S^{\circ}$ as the difference between ΔG_S° and $\Delta G_S^{\ominus}$:

$$\Delta\Delta G_S^{\circ} = \Delta G_S^{\circ} - \Delta G_S^{\ominus} = nRT\ln[Na^+] \qquad (4.5)$$

$\Delta\Delta G_S^{\circ}$ is the thermodynamic parameter representing the salt effect on the thermodynamic

stability of ES complex. By applying a linear free energy relationship, the change in

activation free energy for association ($\Delta\Delta G_1^{\ddagger}$) can be written:

$$\Delta\Delta G_1^{\ddagger} = \beta\Delta\Delta G_S^{\circ} \qquad (4.6)$$

β is a correlation parameter for the association step in Figure 4.2. By a simple arithmetic

relation, the changes in activation energy for dissociation ($\Delta\Delta G_2^{\ddagger}$) can be written:

$$\Delta\Delta G_2^{\ddagger} = \Delta\Delta G_1^{\ddagger} - \Delta\Delta G_S^{\circ} = (\beta - 1)\Delta\Delta G_S^{\circ} \qquad (4.7)$$

The rate constants for each elementary step can be written as functions of $[Na^+]$ from

eq 4.5–4.7:

$$k_1 = k_1^{\ominus}[Na^+]^{-\beta n} \qquad (4.8)$$

$$k_2 = k_2^{\ominus}[Na^+]^{(1-\beta)n} \qquad (4.9)$$

$k_1^\ominus$ and $k_2^\ominus$ are the rate constants when $[Na^+] = 1$ M. Because the number of counterions in

the ES complex is unlikely to change in the transition state of the chemistry step, salt effects

on k_3 are likely to be negligible compared with salt effects on k_1 and k_2. Indeed, it has been

reported that k_{cat} for hydrolysis of cytidine 2',3'-cyclic phosphate (cCMP) by RNase A is

insensitive to the ionic strength of the solution (Eftink & Biltonen, 1983a).

By eq 4.8 and 4.9, k_{cat}/K_M of the reaction in eq 4.1 can be expressed as a function of

$[Na^+]$:

$$k_{cat} K_M = k_1^\ominus [Na^+]^{-\beta n} \cdot \frac{C_f}{1 + C_f} \tag{4.10}$$

where

$$C_f = C_f^\ominus [Na^+]^{(\beta-1)n} \tag{4.11}$$

and C_f is a forward commitment factor, which is the ratio of the rate constant for the

chemistry step (k_3) to the rate constant for the dissociation step from the ES complex to E +

S (k_2). C_f is also a function of $[Na^+]$ as shown in eq 4.11. The dependence of k_{cat}/K_M on

$[Na^+]$, $\partial \log(k_{cat}/K_M)/\partial \log[Na^+]$ is calculated from eq 4.10 and 4.11:

$$\frac{\partial \log(k_{cat} / K_M)}{\partial \log[Na^+]} = \left((1-\beta)\frac{C_f}{1+C_f} - 1 \right) n \tag{4.12}$$

Because $0 < \dfrac{C_f}{1+C_f} < 1$,

$$-n < \frac{\partial \log(k_{cat}/K_M)}{\partial \log[\text{Na}^+]} < -\beta n \tag{4.13}$$

Therefore, the slope in a $\log(k_{cat}/K_M)$ versus $\log[\text{Na}^+]$ plot varies from $-n$ to $-\beta n$ according to C_f. For a sluggish enzyme with $C_f \ll 1$, the slope would be close to $-n$. If substrate association is rate-determining, the slope would be close to $-\beta n$.

Eq 4.10 is impractical to fit to a salt–rate profile, because β and n are not independent enough to be determined simultaneously in a regression analysis. For an actual regression analysis, however, $\partial \log(k_{cat}/K_M)/\partial \log[\text{Na}^+]$ could be approximated to be constant as in eq 4.14 with the assumption that $\dfrac{C_f}{1+C_f}$ is relatively insensitive to salt concentration:

$$\frac{\partial \log(k_{cat}/K_M)}{\partial \log[\text{Na}^+]} = -n' \tag{4.14}$$

where $\beta n < n' < n$. This assumption is valid if β is close to 1 or if either the dissociation step or the chemisty step is much slower than the other. By solving the differential equation, k_{cat}/K_M can be written:

$$k_{cat}/K_M = (k_{cat}/K_M)^{\ominus}[\text{Na}^+]^{-n'} \tag{4.15}$$

where $(k_{cat}/K_M)^\ominus$ is k_{cat}/K_M when $[Na^+] = 1$ M.

If catalysis approaches a physical limit, such as diffusion, then the linearity in eq 4.14 would fail at low $[Na^+]$ (Figure 4.3) and the k_{cat}/K_M would be written:

$$k_{cat}/K_M = \frac{(k_{cat}/K_M)_{MAX} \cdot (k_{cat}/K_M)^\ominus [Na^+]^{-n'}}{(k_{cat}/K_M)_{MAX} + (k_{cat}/K_M)^\ominus [Na^+]^{-n'}} \qquad (4.16)$$

where $(k_{cat}/K_M)_{MAX}$ is the k_{cat}/K_M at the physical limit. Eq 4.16 can be rewritten in a simpler form:

$$k_{cat}/K_M = \frac{(k_{cat}/K_M)_{MAX}}{1 + \left(\dfrac{[Na^+]}{K_{Na^-}}\right)^{n'}} \qquad (4.17)$$

where $K_{Na^-} = \sqrt[n']{\dfrac{(k_{cat}/K_M)^\ominus}{(k_{cat}/K_M)_{MAX}}}$. Eq 4.17 is reminiscent of an equation for a pH–rate profile.

The meaning of each parameter is presented graphically in Figure 4.3. $(k_{cat}/K_M)_{MAX}$ is the k_{cat}/K_M at the plateau. $-n'$ is the slope of the linear region. K_{Na^-} is the salt concentration where k_{cat}/K_M is half of its maximum.

MATERIALS AND METHODS

Materials. Wild-type RNase A, and the H12A and K41R variants were produced, folded

and purified as described elsewhere (delCardayré et al., 1995; Messmore et al., 1995; Park

& Raines, 2000a). K7A/R10A/K66A RNase A was a generous gift of Dr. B. M. Fisher.

Substrates 1–3 were from Integrated DNA Technologies (Coralville, IA).

Substrate 1	6-FAM~rUdA~6-TAMRA
Substrate 2	6-FAM~dArU(dA)$_2$~6-TAMRA
Substrate 3	6-FAM~(dA)$_2$rU(dA)$_3$~6-TAMRA

These substrates are DNA–RNA chimeras with a 5' 6-carboxyfluorescein label (6-FAM)

and 3' 6-carboxytetramethylrhodamine (6-TAMRA) label. When the substrate is intact, the

fluorescence of the fluorescein is minimal because of the quenching by fluorescence

resonance energy transfer (FRET) from 6-FAM to 6-TAMRA. A large increase in

fluorescence occurs upon cleavage of the P–O$^{5'}$ bond on the 3' side of the single

ribonucleotide residue embedded within the substrate (Kelemen et al., 1999; Park et al.,

2000).

[Bis(2-Hydroxyethyl)amino]tris(hydroxymethyl)methane (Bistris) was from ICN

Biomedicals (Aurora, OH). NaCl was from Fisher Scientific (Fair Lawn, NJ).

Concentrations of wild-type RNase A and its variants were determined

spectrophotometrically by using $\varepsilon = 0.72$ mL mg^{-1}cm^{-1} at 277.5 nm (Sela et al., 1957).

Concentrations of the substrates were determined spectrophotometrically by using ε = 76,340 $M^{-1}cm^{-1}$, ε = 102,400 $M^{-1}cm^{-1}$ and ε = 126,400 $M^{-1}cm^{-1}$ at 260 nm, respectively (Kelemen et al., 1999).

Assays of Enzymatic Activity. The ribonucleolytic activity of wild-type RNase A was determined at 23 °C with fluorogenic substrates 1-3 in 2.00 mL of 1.0 mM Bistris-HCl buffer (pH 6.0) containing NaCl (0.010 – 1.0 M), H12A RNase A (5.0 nM) and wild-type RNase A (0.050 nM). The concentrations of substrates 1-3 in the reactions were 4.3 nM, 20 nM, and 19 nM, respectively. Determination of enzymatic activity at low salt can be complicated from inhibition by possible contaminants in buffer solution (Park & Raines, 2000b). The addition of H12A RNase A (5.0 nM) to the assay mixture was used to absorb any inhibitory contaminants without affecting catalysis. Because H12A RNase A has 10^{4}-fold less ribonucleolytic activity than does wild-type RNase A (Thompson & Raines, 1995), its contribution to catalysis was negligible. The buffer concentration was low (1.0 mM) to minimize the concentration of possible contaminants. For the K41A and K7A/R10A/K66A variants, the enzyme concentration in the reactions was increased to 0.50 nM and 5.0 nM, respectively, because of the reduced catalytic activities of these variants. For the K7A/R10A/K66A RNase A variant, H12A RNase A was not used in the assay mixture because the enzyme concentration was already high enough to obviate inhibition by buffer contaminants.

Flourescence was measured with a QuantaMaster 1 photon-counting fluorescence spectrometer from Photon Technology International (South Brunswick, NJ) using 493 nm

and 515 nm as exitation and emission wavelengths, respectively. Quartz or glass cuvettes

(1.0 cm pathlengh; 3.5 mL volume) from Starna Cells (Atascadero, CA) were used in the

assay. The value of $V K$ for reactions was determined by regression analysis of the

fluorescence intensity change with eq 4.17 or 4.18, depending on whether the reaction

reaches completion or not, as described previously (Kelemen et al., 1999; Park et al., 2000).

$$F = F_0 + (F_{max} - F_0)(1 - e^{-(V/K)t}) \tag{4.17}$$

$$V/K = \frac{(\Delta F/\Delta t)}{F_{max} - F_0} \tag{4.18}$$

In eq 4.17 and 4.18, F_0 is the fluorescence intensity before a reaction is initiatied, F_{max} is the

maximum fluorescence intensity when the substrate in the reaction is fully cleaved, and

$\Delta F/\Delta t$ is the slope of fluorescence intensity change for an initial linear region. The value of

k_{cat}/K_M was calculated by dividing $V K$ by the enzyme concentration.

Regression Analysis of Salt–Rate Profiles. The salt–rate profile of wild-type and K41R

RNase A was analyzed with eq 4.16. Since k_{cat}/K_M of K7A/R10A/K66A RNase A did not

reach a plateau at low salt, eq 4.14 was used instead of eq 4.16. Log(k_{cat}/K_M) was used as a

dependent variable, rather than of k_{cat}/K_M, for the regression analysis of salt–rate profiles to

give more weight to small k_{cat}/K_M values. Nonlinear regression analyses were performed

with the program SIGMAPLOT 5.0 (SPSS; Chicago, IL).

RESULTS

Salt–rate Profiles of Wild-Type RNase A and the K7A R10A K66A and K41R variants.

The effect of salt concentration on catalysis by wild-type RNase A and two variants is

depicted in Figure 4.4. Each enzyme loses catalytic activity as salt concentration increases.

$Log(k_{cat}/K_M)$ shows a strong linear correlation to $log[Na^+]$, as proposed in the theoretical

model above. The salt–rate profiles of the enzymes do not show any decrease in activity at

low salt, as reported previously for wild-type RNase A (Park & Raines, 2000b). Parameters

determined by nonlinear regression analysis are listed in Table 4.1. Wild-type RNase A and

K41R RNase A reach half of their maximal activities at $[Na^+] = 0.025 \pm 0.002$ M and $[Na^+]$

$= 0.014 \pm 0.002$ M, respectively. The $(k_{cat}/K_M)_{MAX}$ value of wild-type RNase A is (3.3 ± 0.4)

$\times 10^9$ $M^{-1}s^{-1}$. The $(k_{cat}/K_M)_{MAX}$ value for K41R RNase A is $(0.7 \pm 0.2) \times 10^9$ $M^{-1}s^{-1}$. The

k_{cat}/K_M of K7A/R10A/K66A RNase A does not reach a plateau, even at low salt. Each

enzyme shows distinct slopes in the linear regions of the salt–rate profiles. Wild-type

RNase A has an n' value of 2.33 ± 0.05. K41R RNase A has an n' value of 2.66 ± 0.08,

which is slightly larger than that of wild-type RNase A. K7A/R10A/K66A RNase A has a

greatly reduced n' value of 1.37 ± 0.02.

Salt–Rate Profiles with Different Substrates. Substrates 1–3 were used to show that the

dependence of k_{cat}/K_M on salt concentration correlates with the extent of Coulombic

interactions (Figure 4.5A). The parameters from nonlinear regression analysis are listed in

Table 4.2. The n' values of the salt–rate profiles shows a monotonic increase in the order:

1.87 ± 0.07, 2.33 ± 0.05, and 2.71 ± 0.11 as the number of phosphoryl gourps in substrates

1–3 increases to 3, 5, and 7, respectively. A plot of n' values versus the number of

phosphoryl group in the substrates shows a linear correlation with a slope of 0.21 (Figure

4.5B). Substrate 2 has the highest $(k_{cat}/K_M)_{MAX}$ value of $(3.3 \pm 0.4) \times 10^9$ $M^{-1}s^{-1}$ and substrate

1 has the lowest $(k_{cat}/K_M)_{MAX}$ value of $(0.8 \pm 0.2) \times 10^9$ $M^{-1}s^{-1}$. Interestingly, k_{cat}/K_M values

for these substrates converge to the same value at $[Na^+] \sim 0.4$ M. When $[Na^+]$ is greater than

0.4 M, a longer substrate is a worse substrate. When $[Na^+]$ is less than 0.4 M, a longer

substrate is a better substrate. Substrate 3 has the biggest K_{Na^+} value of (0.044 ± 0.006) M,

and substrates 1 and 2 have the same K_{Na^+} of (0.025 ± 0.005) M and (0.025 ± 0.002) M,

respectively.

DISCUSSION

Assay Conditions for Salt–Rate Profiles. Buffers used for determining salt–rate profiles

should be chosen carefully. The pK_a value of a buffer could be sensitive to salt concentration.

If a buffer is a multivalent ion, the dependence of its pK_a on salt concentration is not

negligible. For example, the pK_a of sodium citrate buffer was observed to vary by 0.46 unit

when salt concentration was increased by 10-fold (data not shown). To check the salt effect

on the pK_a of a Bistris-HCl buffer system, the pH of the buffer solution was measured at the

salt concentrations used for salt–rate profile determinations. The variation of the pH was

determined to be less than 0.2 unit within the salt concentration range used in this study

$([Na^+] = 0.010-1.0$ M).

Only a minimal concentration of buffer (1.0 mM) was used herein for the following

reasons. First, buffer components or contaminants in the buffer could be inhibitory to the

reaction at low salt (Park & Raines, 2000b). Second, if the buffer has a cationic form, then

Na^+ is not the only cation in the reaction, which introduces a complication in salt–rate

profile analysis. Only when the concentration of buffer is much lower than $[Na^+]$ can the

contribution of the buffer cation be ignored and the salt–rate profile be analyzed as a

function of $[Na^+]$.

Salt Effects on the Conformational Stability of Ribonuclease A. Neutral salts can affect

the conformational stability of macromolecules (von Hippel & Schleich, 1969a; von Hippel

& Schleich, 1969b). Salt effects on the conformational stability of RNase A, in particular,

have been studied by measuring the changes in thermal denaturation behavior with various

salts (von Hippel & Wong, 1965). These studies showed that salt effects on the

conformational stability of proteins were related closely to the Hofmeister series, a rank of

the effectiveness of ions in salting-out proteins. Ions effective in salting-out are also

effective in stabilizing the native conformation of RNase A. Ions ineffective in salting-out

destabilize the native conformation of RNase A. This salt effect on the conformational

stability of the enzyme could introduce a complication in analyzing salt effects on catalysis.

NaCl, however, is one of the most inert salts in the Hofmeister series. No adverse effect on

the conformational stability of RNase A was observed to 2 M NaCl (von Hippel & Wong,

1965). Rather, NaCl stabilizes RNase A slightly. The temperature at the midpoint of thermal

denaturation (T_m) of RNase A increases monotonically from 59 °C to 63 °C as NaCl concentration changes from 0 M to 1.0 M (Mayr & Schmid, 1993). Coulombic repulsion between cationic residues on the surface of RNase A seems to cause the slight decrease in T_m at low salt (Grimsley et al., 1999), as RNase A is a cationic protein [pI = 9.3 (Ui, 1971)]. This slight change in the conformational stability of RNase A has little effect on catalysis by the enzyme at ambient temperature. Therefore, the salt effect on the conformational stability of RNase A is negligible in this study.

Salt Effect on pK$_a$'s of Aactive-Site Histidine Residues. Another factor affecting salt–rate profiles is the salt effect on the pK_a values of the active-site histidines. According to a pH titration experiment monitored by NMR spectroscopy (Fisher et al., 1998c), the microscopic pK_a values of the active-site histidines are increased by ~0.5 unit as the NaCl concentration is increased from 18 mM to 142 mM. The averaged pK_a of His12 and His119 of wild-type RNase A is 5.6 at 18 mM NaCl. The value is shifted to 6.1 at 142 mM NaCl. Nontheless, the contribution of the salt effect on the pK_a's of active-site histidines to salt–rate profiles is negligible compared with the intrinsic salt effect on k_{cat}/K_M, as salt–rate profiles were determined at pH 6.0 where k_{cat}/K_M is at maximal. Moreover, the salt effect on the pK_a's of the Bistris buffer is in the same direction as that on the pK_a's of the histidine residues, reducing the contribution of the salt effect on the pK_a's of the histidine residues to the overall salt–rate profiles.

Coulombic Interactions between Ribonuclease A and its Substrates. Eq 4.14 and 4.16 were applied to the salt–rate profiles of wild-type RNase A and its variants. The salt–rate profiles of k_{cat}/K_M for RNase A indicate that Coulombic interactions between the enzyme

and substrate are weakened at high salt. An n' value, the absolute value of the slope derived from a salt–rate profile is a useful parameter that indicates the extent of the Coulombic interactions in the enzyme–substrate complex. The n' value, however, is not always identical to n, the actual number of counterions released upon formation of the enzyme–substrate complex. As shown in eq 4.14, an n' would be identical to n only if the chemistry step were rate-limiting or $\beta = 1$. Otherwise, n' varies from βn to n.

The n' values were determined to 2.33 ± 0.05 and 2.66 ± 0.08 with wild-type RNase A and the K41R variant, respectively. Because K41R RNase A is a sluggish enzyme (Messmore et al., 1995), k_{cat}/K_M of this variant is limited by chemistry. The n' of K41R RNase A, therefore, seems to reflect n. Because a lysine to arginine substitution does not affect the formal charges of the enzyme at neutral pH, the extent of Coulombic interactions with substrates in the K41R variant should be close to that in wild-type RNase A. Therefore, wild-type RNase A and K41R variant can be assumed to have the same n value, 2.66 ± 0.08. The smaller n' value of the wild-type enzyme indicates that k_{cat}/K_M of RNase A is not limited solely by chemistry.

K7A/R10A/K66A RNase A is a variant with a reduced Coulombic component to substrate binding. Lys7, Arg10, and Lys66 are used to bind to the ground state and the transition state uniformly, and replacing these residues with alanine affects k_{cat}/K_m as well as K_m (Fisher et al., 1998b). The salt–rate profile of K7A/R10A/K66A RNase A in Figure 4.4 shows decreased catalysis by the variant. Moreover, the lower slope of the salt–rate profile compared to that of wild-type enzyme indicates reduced Coulombic interactions. The n'

value of the salt–rate profile of K7A/R10A/K66A RNase A was determined to be 1.37 ±

0.02 by nonlinear regression analysis, which is about 0.9 and 1.3 unit smaller than those of

wild-type RNase A and the K41R variant, respectively.

Comparison with Thermodynamic Salt Effects on Ligand Binding. The n value could be

determined directly by measuring the value of K_d for the complex of RNase A and a ligand

at varying salt concentrations. Fluorescence anisotropy spectroscopy was used to determine

K_d for the complex of RNase A and 6-carboxyfluorescein~d(AUAA) (6-FAM~d(AUAA)) at

varying salt concentrations (Fisher et al., 1998b). The slopes of plots of logK_d vs log[Na$^+$]

for wild-type RNase A and the K7A/R10A/K66A variant have been determined to be 2.3 ±

0.1 and 0.9 ± 0.2 with this ligand (Fisher et al., 1998b). The validity of the analysis of salt–

rate profiles can be tested by comparison of ∂logK_d/∂log[Na$^+$] with ∂log(k_{cat}/K_M)/∂log[Na$^+$].

Substrate 2 used for the salt–rate profiles in Figure 4.4 has 5 phosphoryl groups, whereas the

ligand 6-FAM~d(AUAA) has 4 phosphoryl groups. The greater dependence of k_{cat}/K_M on

salt concentrantion than that of K_d can be ascribed to this difference in the number of

possible ion pairs. Therefore, direct comparison of ∂logK_d/∂log[Na$^+$] with

∂log(k_{cat}/K_M)/∂log[Na$^+$] is not feasible. Mutation in K7A/R10A/K66A RNase A, however,

introduces the same decrease in the number of counterions released upon complex formation

with the ligand and the substrate. Specifically, ∂logK_d/∂log[Na$^+$] is decreased by 1.4 in

K7A/R10A/K66A RNase A, compared with the value for wild-type RNase A. This decrease

is consistent well with the decrease of 1.3 in ∂log(k_{cat}/K_M)/∂log[Na$^+$] of K7A/R10A/K66A

RNase A, compared with that of K41R RNase A (which is a more appropriate reference than

wild-type RNase A as discussed above). This consistency between $\partial \log K_d / \partial \log[\text{Na}^+]$ and

$\partial \log(k_{cat}/K_M)/\partial \log[\text{Na}^+]$ supports the validity of the quantitative analysis of salt–rate profile

developed herein.

The 4 phosphoryl groups of the ligand cover the known anion-binding subsites (P(-1),

P0, P1, P2). Still, it has been reported that RNase A can form ~7 ion pairs with polymeric

single-stranded DNA (Record et al., 1976). The salt–rate profiles of wild-type RNase A with

substrates of different lengths corroborate this observation. As the length of a substrate

increases, the slope of its salt–rate profile also increases (Table 4.2 and Figure 4.5). The

effect of increasing number of phosphoryl groups in the substrates seems to be additive. The

n' values for the substrates shows a linear dependence on the numbers of phosphoryl groups,

with a slope of 0.21 (Figure 4.5B). A quantitative interpretation of this slope is not apparent,

as the substrates are not long enough to assume a homogenous counterion density. Moreover,

n' is not the same as n for wild-type RNase A. It is clear, however, that increased Coulombic

interactions with a longer substrate is responsible for the increase in n' values.

Limit of Catalysis by Ribonuclease A. Salt–rate profiles of RNase A show that the

catalytic activity of the enzyme is maximal at low salt (Figure 4.4). The $(k_{cat}/K_M)_{\text{MAX}}$ for

wild-type RNase A with substrate 2 is $(3.3 \pm 0.4) \times 10^9$ $\text{M}^{-1}\text{s}^{-1}$ from the regression analysis

(Table 4.1). The average of k_{cat}/K_M from triplicate measurements at 0.010 M NaCl was

$(2.7 \pm 0.5) \times 10^9$ $\text{M}^{-1}\text{s}^{-1}$. This k_{cat}/K_M is one of the largest known. Only a few other enzymes

are known to have $k_{cat}/K_M > 10^9$ $\text{M}^{-1}\text{s}^{-1}$. Superoxide dismutase catalyzes the

disproportionation of superoxide with a k_{cat}/K_M of 3.5×10^9 $\text{M}^{-1}\text{s}^{-1}$ (Klug et al., 1972).

Acetylcholinesterase cleaves acetylthiocholine with a k_{cat}/K_M of 1.6×10^9 $M^{-1}s^{-1}$ (Nolte et al.,

1980). Both of these k_{cat}/K_M values were determined at low salt condition (≤ 0.010 M), where

catalysis by superoxide dismutase and acetylcholinesterase is maximal. Catalysis by these

two enzymes is limited by diffusion. The k_{cat}/K_M for RNase A compared to these enzymes

implies that catalysis by RNase A is likely to be limited by diffusion at low salt

concentration.

Postulation on the Salt Effect on k_{cat}. The salt–rate profile of RNase A shows that

RNase A does not have a salt optimum in k_{cat}/K_M. Rather, k_{cat}/K_M of RNase A is maximal at

low salt and decreases monotonically as salt concentration increases. The salt–rate profile of

k_{cat} for the cleavage of the same substrate by RNase A is also of interest. The determination

of salt–rate profile of k_{cat} with the substrate is challenging because of substrate inhibiton at

low salt (Dickman & Ring, 1958; Cleland, 1979) as well as the need for an impractically

high concentration of the substrate. Nontheless, based on the model used to analyze salt

effects on k_{cat}/K_M, we can postulate the shape of a salt–rate profile for k_{cat}. Two steps in

catalysis by RNase A determine k_{cat}: a chemistry step and a product-release step. The rate of

the chemistry step itself seems to be insensitive to salt concentration, as discussed above.

Therefore, salt effects on k_{cat} are determined mainly by the contribution of the rate of the

product release to k_{cat}. If product release is faster than chemistry, then k_{cat} would be

insensitive to salt concentration. If product release is slower than chemistry, then k_{cat} would

show a monotonic increase as salt concentration increases. Therefore, it is certain that the

salt–rate profile of k_{cat} would be distinct from the salt–rate profile of k_{cat}/K_M. Indeed, k_{cat} for

the hydrolysis of cCMP by RNase A is constant with ionic strength from 0.05 M to 1.0 M

(Eftink & Biltonen, 1983a).

What is the Salt Optimum for Catalysis by Ribonuclease A? The salt–rate profile of

RNase A activity *in vivo* is likely to be different from the salt–rate profile of k_{cat}/K_M and that

of k_{cat}. Because a substrate can saturate the enzyme easily at low salt, the salt–rate profile at

low salt would be similar to that of k_{cat}. At high salt, however, the salt–rate profile would be

similar to that of k_{cat}/K_M, because the substrate cannot saturate the enzyme. Consequently,

the salt optimum for catalysis by RNase A is a function of the substrate concentration. This

dependence of the salt optimum on the substrate concentration is analogous to the

dependence of the pH optimum on the substrate concentration. The pH optimum of k_{cat}/K_M

for cleavage of 2′,3′-cyclic CMP by RNase A is pH 6.0 (Findlay et al., 1961). The pH

optimum of k_{cat} for the same reaction is, however, pH 7.2. Therefore, the pH optimum for

RNase A catalysis is between pH 6.0 and pH 7.2, depending on the substrate concentration.

To define a salt optimum or a pH optimum, one must define the 'metabolic niche' where the

enzyme resides (Burbaum et al., 1989). Otherwise, a discussion on the salt optimum of

RNase A catalysis is arbitrary.

APPENDIX

A rigorous kinetic scheme for catalysis by RNase A includes the reverse reaction of the

chemistry step and the product-release steps.

$$\begin{array}{ccccc} k_1 & k_3 & & k_5 & k_7 \\ \mathrm{E+S} \rightleftarrows \mathrm{ES} & \rightleftarrows & \mathrm{EP_1P_2} & \rightarrow \mathrm{EP_2} & \rightarrow \mathrm{E} \\ k_2 & k_4 & & & \end{array}$$
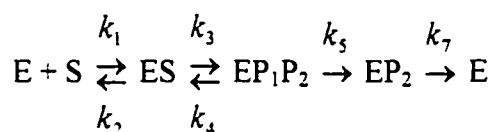
With this scheme, k_{cat}/K_M can be written:

$$k_{cat}/K_M = \frac{k_1 k_3 k_5}{k_2 k_4 + k_2 k_5 + k_3 k_5}$$

This k_{cat}/K_M can be simplified by the following two postulations. First, it is reasonable to

postulate the internal equilibrium constant (K_{int}) in ES $\rightleftarrows$ EP$_1$P$_2$ is greater than 1, that is, k_3

> k_4, because RNase A catalyzes the cleavage of RNA in an off-equilibrium state $in\ vivo$

(Burbaum et al., 1989). Second, the rate for the first product release is likely to be much

faster than the rate for the substrate release, that is, $k_5 >> k_2$. Since the length of either

product is half of the length of the substrate, the reduced Coulombic interactions of shorter

nucleotides with the enzyme would results in fater dissociation. By a rearrangement, k_{cat}/K_M

can be rewritten:

$$k_{cat}/K_M = \frac{k_1 k_3 k_5}{k_2 k_5 + k_3 \left(k_5 + k_2 \dfrac{k_4}{k_3} \right)}$$

Since the postulations above show that $k_2(k_4/k_3) \ll k_5$, k_{cat}/K_M can be approximated as in eq 4.1. Therefore, assuming the irreversibility of the catalysis step is unlikely to cause a significant deviation in the kinetic analyses.

Table 4.1: Parameters from Salt–Rate Profiles of Wild-Type Ribonuclease A and the K7A/R10A/K66A and K41R Variants.

Parameters[a]	Wild-type	K7A/R10A/K66A	K41R
n'	2.33 ± 0.05	1.37 ± 0.02	2.66 ± 0.08
K_{Na^-} (M)	0.025 ± 0.002	–	0.014 ± 0.002
$(k_{cat}/K_M)_{MAX}$ $(10^9 \text{ M}^{-1}\text{s}^{-1})$	3.3 ± 0.4	–	0.7 ± 0.2

[a]Parameters were determined by fitting the data in Figure 4.4 to eq 4.16 (wild-type ribonuclease A and K41R variant) or eq 4.14 (K7A/R10A/K66A ribonuclease A) by nonlinear regression. Errors of the parameters are standard errors from the regression analyses.

Table 4.2: Parameters from Salt–Rate Profiles of Wild-Type Ribonuclease A with Substrate 1–3.

Parameters[a]	Substrate 1	Substrate 2	Substrate 3
Number of phophoryl groups	3	5	7
n'	1.87 ± 0.07	2.33 ± 0.05	2.71 ± 0.11
K_{Na^-} (M)	0.025 ± 0.005	0.025 ± 0.002	0.044 ± 0.006
$(k_{cat}/K_M)_{MAX}$ $(\times 10^9\ M^{-1}s^{-1})$	0.8 ± 0.2	3.3 ± 0.4	1.7 ± 0.3

[a]Parameters were determined by fitting data in Figure 4.5 to eq 4.16 by nonlinear regression. Errors of the parameters are standard errors from the regression analyses.

Figure 4.1   Structure of the ribonuclease A•d(ApTpApApG) complex. The structure

(Protein Data Bank code : 1RCN) (Fontecilla-Camps et al., 1994) is depicted

in a ribbon diagram made with the program MOLSCRIPT (Kraulis, 1991).

Residues comprising phosphoryl group-binding subsites are shown in ball-

and-stick representation with labels. The ligand, d(ApTpApApG) is shown in

a solid line. Electron density was not apparent for the guanosine 5'-phosphate.

Lys7

Arg10

Lys41

His119

His12

Lys66

Arg85
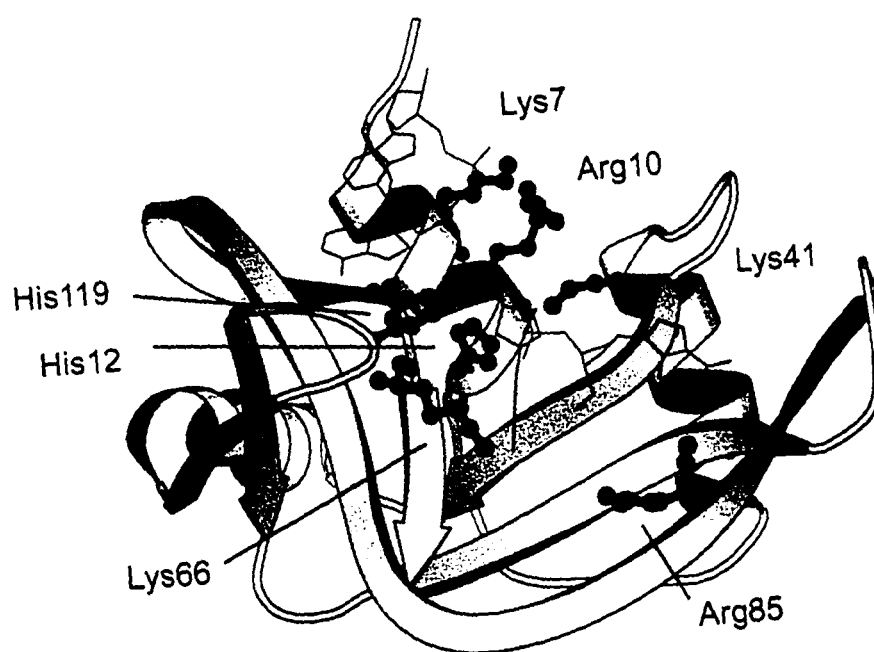
Figure 4.2   Notional free energy profile for catalysis by ribonuclease A. k_1, k_2, and k_3 are

the rate constants for the association, dissociation, and chemistry steps,

respectively. The solid line indicates the free energy profile when [Na$^+$] = 1.0

M. The dashed line shows the reaction free energy profile when [Na$^+$] < 1.0

M. The two profiles are normalized by setting the energies of E + S state

constant, for a facile comparison. $\Delta\Delta G_S°$, $\Delta\Delta G^{\ddagger}$, and $\beta\Delta\Delta G_S°$ indicate the

change of the free energies of the ES complex, the transition state for the

chemistry step, and the transition state for the substrate-binding step,

respectively, caused by decreasing [Na$^+$] from 1.0 M.

$$E+S \underset{k_2}{\overset{k_1}{\rightleftharpoons}} ES \overset{k_3}{\longrightarrow} EP$$
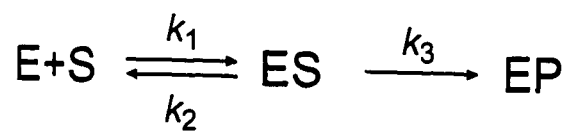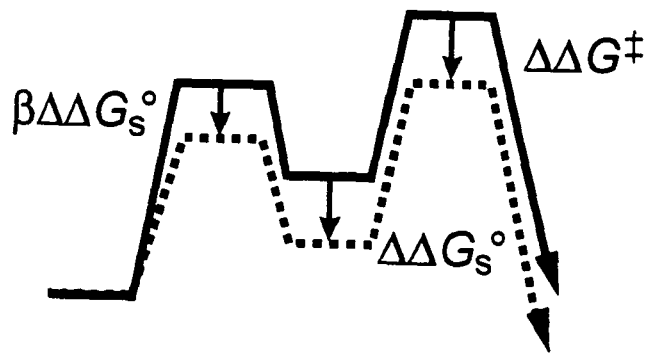
Figure 4.3   Schematic representation of a salt–rate profile. The plot is shown as

$\log(k_{cat}/K_M)$ versus $\log[Na^+]$. $(k_{cat}/K_M)_{MAX}$ is the physical limit of k_{cat}/K_M.

K_{Na^-} is the salt concentration where k_{cat}/K_M reaches half of its maximum. $-n'$

is the slope of the linear region.
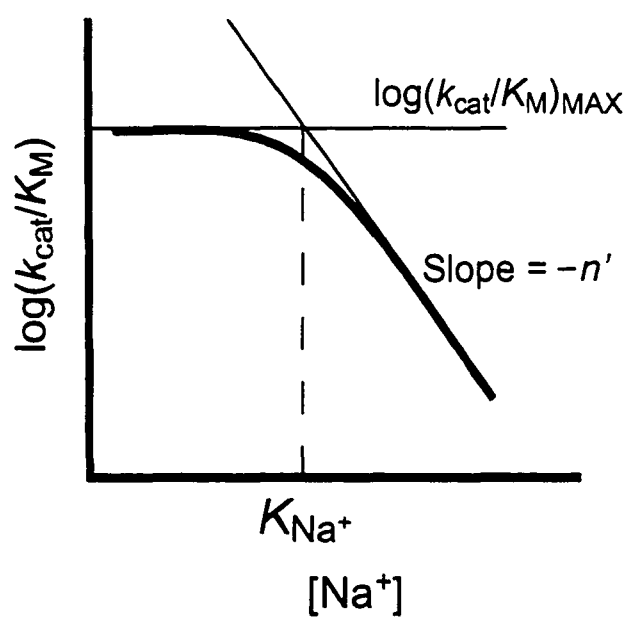
Figure 4.4   Salt–rate profiles of k_{cat}/K_M for the cleavage of substrate 2 by wild-type

ribonuclease A (■) and K41R (▲) and K7A/R10A/K66A (●) variants.

Assays were performed at 23 °C in 1.0 mM Bistris-HCl buffer (pH 6.0). Each

curve was fitted to eq 4.16 (for wild-type and K41R RNase A) or eq 4.14 (for

K7A/R10A/K66A RNase A) by nonlinear regression. Parameters determined

from the regression analysis are listed in Table 4.1.
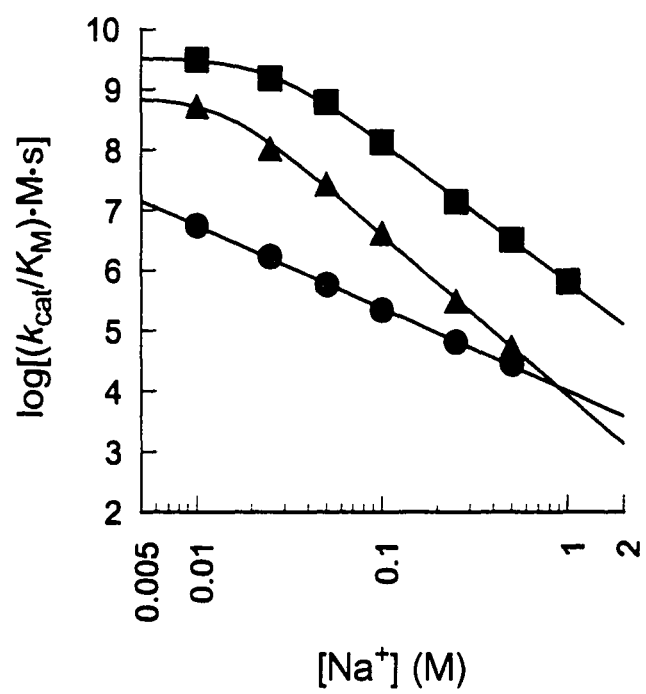
Figure 4.5   Effect of the length of substrates on the salt–rate profiles of k_{cat}/K_M. A. Salt–

rate profiles of k_{cat}/K_M for the cleavage of substrate 1 (■), substrate 2 (●),

and substrate 3 (▲) by wild-type ribonuclease A in 1.0 mM Bistris-HCl

buffer (pH 6.0). Each curve was fitted to eq 4.16 by nonlinear regression.

Parameters determined from the regression analysis are listed in Table 4.2.

B. Apparent dependence of n' determined from salt–rate profiles in Figure

4.5A on the number of phosphoryl groups. The numbers of phosphoryl

groups in substrate 1–3 are 3,5, and 7, respectively. The slope was

determined to be 0.21.

A

B
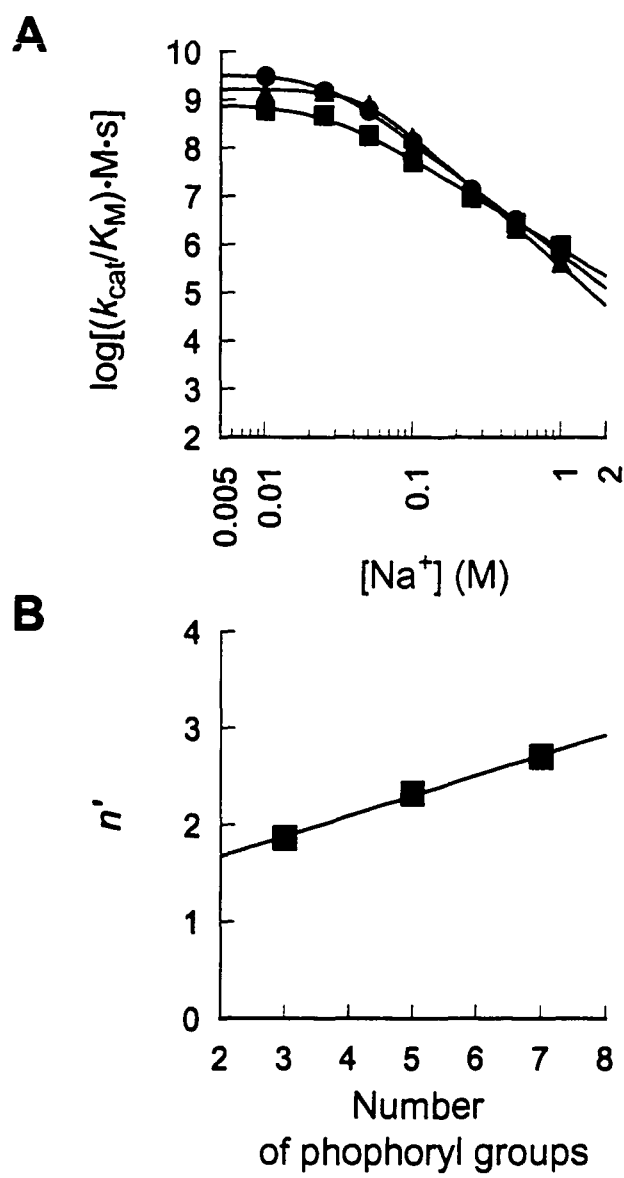
Chapter 5

Revisiting Energetics of Ribonuclease A Catalysis

by the Effects of pH, Salt, and Solvent Isotope

ABSTRACT

The energetics of catalysis by ribonuclease A (RNase A) is re-examined by determining the effects of pH, salt, and solvent isotope on the rate of cleavage of fluorogenic substrates by the enzyme. Oligomeric structures of these substrates allow us to assess the complete catalytic power of the enzyme, since the substrates can exploit extended subsites beyond the active site. The pK_a values from pH–k_{cat}/K_M profiles determined with a fluorogenic substrate, 6-FAM~dArU(dA)$_2$~4-DABCYL, at 0.010 M, 0.20 M, and 1.0 M NaCl are not consistent with macroscopic pK_a values of RNase A determined by NMR spectroscopy. Analysis of this abnormality in pH–k_{cat}/K_M profiles reveals that catalysis by RNase A is limited by the rate of substrate association even at 1.0 M NaCl. Solvent isotope effects also corroborate this finding. Moreover, independence of the rate of association at 0.010 M NaCl from pH and a comparison of k_{cat}/K_M with diffusion rates in model systems indicates that k_{cat}/K_M of RNase A reaches the limit of encounter at low salt. By integrating these effects of pH, salt and isotope, we propose a mechanism of substrate association by RNase A.

INTRODUCTION

Enzymes catalyze specific reactions with enormous rate enhancement (Radzicka & Wolfenden, 1995). Studies on the energetics of enzymatic catalysis reveal that, indeed, enzymes can evolve to become perfect catalysts (Knowles & Albery, 1977). Catalysis by a perfect enzyme is not limited by the rate of the chemical transformation of substrates to products. Rather, catalysis is limited by the rates of physical steps, like substrate association and product release. This perfection in enzymatic catalysis is achieved by optimizing the affinity of an enzyme for intermediates and transition states in its reaction pathway through evolutionary processes (Burbaum et al., 1989).

Ribonuclease A (RNase A; EC 3.1.27.5) could be a perfect enzyme. Studies on the energetics of cleavage of UpA by RNase A have shown that k_{cat}/K_M is limited by substrate desolvation and k_{cat} is partially limited by product release (Thompson et al., 1994; Thompson et al., 1995). Still, the lack of interactions with extended subsites of RNase A in UpA limits the menifestation of the full catalytic efficiency of RNase A. RNase A has a series of cationic residues that interact with the phosphoryl groups of RNA beyond the one bound in its active site (McPherson et al., 1986; Fontecilla-Camps et al., 1994). These residues contribute significantly to catalysis by forming Coulombic interactions with the polyanionic RNA substrates (Fisher et al., 1998b). Hence, the realistic assessment of catalytic power of RNase A demands the use of a substrate exploiting the pontential contributions of the subsites to catalysis. Oligomeric or polymeric RNA substrates are,

however, inadequate for rigorous kinetic analyses because of kinetic heterogeneity resulting from more than one cleavable site.

Recently, we developed an optimal fluorogenic DNA–RNA chimeric substrate, 6-carboxyfluorescein~dArU(dA)$_2$~6-carboxytetramethylrhodamine (6-FAM~dArU(dA)$_2$~6-TAMRA), for the sensitive detection of ribonucleolytic activity (Kelemen et al., 1999). The value of k_{cat}/K_M for cleavage of this substrates by RNase A (3.6 × 10^7 M^{-1}s^{-1}) is much greater than those determined with conventional substrates, like uridylyl(3'→5')adenosine (UpA) (2.3 × 10^6 M^{-1}s^{-1}) and poly(cytidylic acid) [poly(C)] (3.3 × 10^6 M^{-1}s^{-1}) (Schultz et al., 1998). Moreover, the value of k_{cat}/K_M reaches (2.7 ± 0.5) × 10^9 M^{-1}s^{-1} at 0.010 M NaCl (Park & Raines, 2001). This prodigious catalysis suggests that encounter rate of the enzyme and substrate determines k_{cat}/K_M at this salt concentration. This finding caused us to revisit the energetics of catalysis by RNase A. The effects of pH, salt, and solvent isotope determined with this optimal substrate reveals that RNase A catalysis is indeed limited by substrate association, even at 1.0 M NaCl.

MATERIALS AND METHODS

Materials. Wild-type RNase A and H12A variant were produced, folded and purified as described elsewhere (delCardayré et al., 1995; Park & Raines, 2000a). 6-FAM~dArU(dA)$_2$~4-DABCYL and 6-FAM~dArU(dA)$_2$~6-TAMRA were from Integrated DNA Technologies (Coralville, IA) (Kelemen et al., 1999; Park et al., 2000). UpA was a

generous gift of Dr. J. E. Thompson.

[Bis(2-Hydroxyethyl)amino]tris(hydroxymethyl)methane (Bistris) was from ICN

Biomedicals (Aurora, OH). 2-(N-Morpholino)ethanesulfonic acid (MES) was from Sigma

Chemical (St. Louis, MO). NaCl was from Fisher Scientific (Fair Lawn, NJ). D_2O was from

Cambridge Isotope Laboratories (Andover, MA). Concentrations of wild-type RNase A and

its variants were determined by ultraviolet spectroscopy using $\varepsilon = 0.72$ mL mg^{-1}cm^{-1} at

277.5 nm (Sela et al., 1957). Concentrations of 6-FAM~dArU(dA)$_2$~4-DABCYL and 6-

FAM~dArU(dA)$_2$~6-TAMRA were determined by ultraviolet spectroscopy using $\varepsilon = 77,180$

M^{-1}cm^{-1} and $\varepsilon = 102,400$ M^{-1}cm^{-1} at 260 nm, respectively. Concentrations of UpA was

determined by ultraviolet spectroscopy using $\varepsilon = 24,600$ M^{-1}cm^{-1} at 260 nm at pH 7.0.

General Procedure for Fluorimetric Assay. The catalytic activity of RNase A was

determined by monitoring the change of fluorescence intensity upon the cleavage of the

fluorogenic substrates (Kelemen et al., 1999; Park et al., 2000). Assays were performed at

23 °C with stirring in 2.00 mL of buffer containing NaCl (0.010–1.0 M), H12A RNase A

(5.0 nM), the fluorogenic substrates, and RNase A. H12A RNase A was added to reaction

mixtures to absorb any possible inhibitory contaminants from buffer solutions (Park &

Raines, 2000b). The catalytic contribution of 5.0 nM H12A RNase A was negligible in th

assays, because of its low catalytic activity (Thompson & Raines, 1995). Flourescence was

measured with a QuantaMaster 1 photon-counting fluorescence spectrometer from Photon

Technology International (South Brunswick, NJ), using 493 nm and 515 nm as excitation

and emission wavelengths, respectively. Values of k_{cat}/K_M were determined from the change

of fluorescence intensity, as described previously (Kelemen et al., 1999; Park et al., 2000).

pH–Rate Profiles. The effect of pH on the value of k_{cat}/K_M for cleavage of

6-FAM~dArU(dA)$_2$~4-DABCYL by wild-type RNase A was determined in 2.00 mL of 1.0

mM buffer containing NaCl (0.010–1.0 M), H12A RNase A (5.0 nM),

6-FAM~dArUdAdA~4-DABCYL, and wild-type RNase A (5.0 pM–0.50 nM). Buffers were

sodium formate–HCl (pH 3.54–pH 4.23), sodium acetate–HCl (pH 4.37–pH 5.61), Bistris–

NaOH (pH 5.87–pH 6.66), MOPS-NaOH (pH 6.93–pH 7.48), and Tris-HCl (pH 7.85–pH

8.71). The pH values of buffers were determined by a Φ40 pH meter from Beckman

instruments (Fullerton, CA). The pH values of reaction mixtures did not vary even after

complete cleavage of the substrates by RNase A. Salt effects on RNase A catalysis results

mainly from the specific interactions of cations with anionic RNA (Fisher et al., 1998b; Park

& Raines, 2001), and a constant ionic strength does not guarantee an identical salt

environment. Hence, buffer concentration was kept low (1.0 mM) to provide a nearly

identical salt environment at different pH's. 6-FAM~dArU(dA)$_2$~4-DABCYL was used

because of the greater chemical stability of 4-DABCYL than 6-TAMRA at acidic pH.

Higher concentrations of the substrate were used at acidic pH (24–47 nM) than at basic pH

(12 nM), because protonation of the fluorescein moiety of the substrate decreases its

fluorescence at acidic pH. (The pK_a of fluorescein in water = 6.5 (Goldberg & Baldwin,

1998).) pH–k_{cat}/K_M profiles were fitted to eq 5.1 by nonlinear regression analysis with the

program SIGMAPLOT 5.0 (SPSS; Chicago, IL).

$$k_{cat}/K_M = \frac{(k_{cat}/K_M)_{MAX}}{\dfrac{[H^+]}{K_1} + 1 + \dfrac{K_2}{[H^+]}}$$

(5.1)

where K_1 and K_2 are apparent macroscopic acid dissociation constants.

Solvent Isotope Effects. The effects of solvent isotope on k_{cat}/K_M for the cleavage of

6-FAM~dArU(dA)$_2$~6-TAMRA by wild-type RNase A (0.050 nM) were determined in 1.0

mM Bistris (pH 6.0) prepared in H_2O or D_2O containing NaCl (0.010–1.0 M) and H12A

RNase A (5.0 nM). To minimize the difference of ionization states of the active-site

histidines in the H_2O buffer and the D_2O buffer, k_{cat}/K_M values in D_2O were determined in

1.0 mM Bistris-HCl buffer prepared by diluting 0.10 M Bistris-HCl (pH 6.0) by 100-fold

with D_2O, assuming the effect of solvent isotope on the pK_a values of the histidine

imidazolium group is similar to that of Bistris cation. For k_{cat}/K_M determination in D_2O, an

enzyme solution was prepared with D_2O buffer and incubated at least overnight at ambient

temperature for complete isotope exchange. Further incubation of the enzyme in the D_2O

buffer did not show any noticeable difference. Solvent isotope effects were defined as the

ratio of k_{cat}/K_M determined in H_2O to the k_{cat}/K_M determined in D_2O. Determination of

solvent isotope effects was done in triplicate at each salt concentration.

The solvent isotope effects on RNase A catalysis were also studied with UpA. Cleavage

of UpA was monitored by following a decrease in absorbance at 286 nm by ultraviolet

spectroscopy ($\Delta\varepsilon = -620$ M^{-1}cm^{-1} (Thompson, 1995)). Assay was performed in 0.10 M

MES–NaOH buffer (pH 6.0 or pD 6.4), containing NaCl (0.10 M) and UpA (0.074–1.1

mM). The pD value of the D_2O buffer was calculated by adding 0.4 to the pH meter reading

(Quinn & Sutton, 1991). The concentrations of wild-type RNase A in reactions were 0.20

nM and 1.0 nM for assays in H_2O and D_2O, respectively. Kinetic parameters were

determined by fitting the observed reaction rates to the Michaelis–Menten equation by

nonlinear regression.

RESULTS

Effect of pH on Catalysis by RNase A. The values of k_{cat}/K_M for the cleavage of

6-FAM~dArU(dA)$_2$~4-DABCYL by RNase A were determined at varying pH at three

different salt concentrations (Table 5.1 and Figure 5.1). Parameters determined by fitting the

data in Table 5.1 to eq 5.1 are listed in Table 5.2. The pH–rate profile at 0.010 M NaCl

shows a wide plateau with pK_a's of 3.88 ± 0.06 and 7.47 ± 0.06. The $(k_{cat}/K_M)_{MAX}$ was

determined as $(2.8 ± 0.0) \times 10^9 \, M^{-1}s^{-1}$. The pH–rate profile determined at 0.20 M NaCl has a

narrower plateau than the one determined at 0.010 M NaCl. The pK_a's and $(k_{cat}/K_M)_{MAX}$ are

4.66 ± 0.09, 6.44 ± 0.08, and $(6.7 ± 0.9) \times 10^7 \, M^{-1}s^{-1}$. The pH–$k_{cat}/K_M$ profile determined at

0.20 M NaCl show an asymmetric bell-shaped pH–rate profile. The apparent slope of the

acidic arm is greater than that of the basic arm. This greater slope indicates that two titatable

groups affects catalysis below pH 4.0. The additional titration around pH 4 has also been

observed in pH–rate profiles determined with uridine 2′,3′-phosphate (cUMP) (Schultz et al.,

1998) and titration of His12 by NMR spectroscopy (Quirk & Raines, 1999). Though an equation with two basic groups and one acidic group improved the fitting to the profile (data not shown), the regression did not produce statistically meaningful pK_a's for both basic groups. The k_{cat}/K_M values determined at 1.0 M NaCl also produce a bell-shape pH–rate profile. The pK_a's and $(k_{cat}/K_M)_{MAX}$ are 4.88 ± 0.04, 6.95 ± 0.04, and $(1.4 \pm 0.1) \times 10^6 \text{ M}^{-1}\text{s}^{-1}$. These pK_a's are greater than those determined at 0.20 M NaCl.

These pK_a's determined from the pH–k_{cat}/K_M profiles do not agree with the macroscopic pK_a's of RNase A. Macroscopic pK_a's of an enzyme can be calculated from microscopic pK_a's of catalytically significant titratable groups of an enzyme (Tipton & Dixon, 1979). The macroscopic pK_a's of RNase A were estimated from the microscopic pK_a's of the active-site histidine residues determined by NMR spectroscopy (Fisher et al., 1998c) (Table 5.2). The macroscopic pK_a's of RNase A are 5.1 and 6.1 at 0.018 M NaCl. At a similar NaCl concentration (0.010 M), the pH–k_{cat}/K_M profile for cleavage of 6-FAM~dArU(dA)$_2$~4-DABCYL by RNase A shows pK_a's of 3.88 ± 0.06 and 7.47 ± 0.06 (Table 5.2), which are distinct from the microscopic pK_a's of the histidine residues. At 0.142 M NaCl, the macroscopic pK_a's of RNase A are increased to 5.6 and 6.6. The pH–k_{cat}/K_M profile determined at 0.20 M NaCl shows pK_a's of 4.66 ± 0.09 and 6.44 ± 0.08 (Table 5.2). Whereas the pK_2 from the pH–k_{cat}/K_M profile (6.44 ± 0.08) is close to the macroscopic pK_2 (6.6), the pK_1 from the pH–k_{cat}/K_M profile (4.66 ± 0.09) is distinct from the macroscopic pK_2 (5.6). The microscopic pK_a's of the histidine residues at 1.0 M are not known. From the effect of the increase of NaCl concentration from 0.018 M to 0.142 M on the macroscopic

pK_a's, the pK_a's at 1.0 M NaCl are expected to be higher by 0.4–0.5 unit than the pK_a's

determined at 0.142 M NaCl. The pH–k_{cat}/K_M profile determined at 1.0 M NaCl shows pK_a's

of 4.88 ± 0.04 and 6.95 ± 0.04 (Table 5.2). The pK_2 seems to be consistent with the

macroscopic pK_2, considering the expected increase of pK_a resulting from the increase of

salt concentration. The pK_1, however, is still not consistent with the macroscopic pK_1 of

RNase A.

Solvent Isotope Effects. Solvent isotope effects on k_{cat}/K_M of cleavage of 6-

FAM~dArU(dA)$_2$~6-TAMRA by RNase A were determined at three different salt

concentrations (Table 5.3). $^{D_2O}k_{cat}/K_M$ values are 1.18 ± 0.05, 1.40 ± 0.15, and 1.76 ± 0.02

at 0.010 M, 0.10 M, and 1.0 M NaCl, respectively. Isotope effects show a trend of gradual

increase as salt concentration increases.

Solvent isotope effects on k_{cat}/K_M and k_{cat} of cleavage of UpA by RNase A were also

determined (Table 5.4). $^{D_2O}k_{cat}/K_M$ was determined to be 3.9 ± 0.4, which is much greater

than the $^{D_2O}k_{cat}/K_M$ values determined with 6-FAM~dArU(dA)$_2$~6-TAMRA (Table 5.3).

$^{D_2O}k_{cat}$ was determined to be 1.6 ± 0.2 with UpA (Table 5.4).

DISCUSSION

Abnormality in pH–$k_{cat}K_M$ Profiles. RNase A cleaves RNA molecules by a concerted

general acid–general base mechanism using His12 and His119 in its active site (Findlay et

al., 1961; Roberts et al., 1969; Thompson & Raines, 1995; Sowa et al., 1997). The

requirement for a protonated histidine residue and an unprotonated histidine residue for efficient catalysis results in bell-shaped pH–k_{cat}/K_M profiles with two pK_a values near 6 (Findlay et al., 1961; Herries et al., 1962; del Rosario & Hammes, 1969). These pK_a's from pH–k_{cat}/K_M profiles are consistent with the microscopic pK_a's of the active-site histidine residues determined by NMR spectroscopy (Markley & Finkenstadt, 1975).

Apparent pK_a's determined from a pH–k_{cat}/K_M profile of an enzyme are generally believed to reflect the macroscopic pK_a's of catalytically significant titratable groups of the free enzyme. In this case, the pK_a's are independent from the substrate used to determine k_{cat}/K_M values, as shown in pH–k_{cat}/K_M profiles of transphosphorylation of UpA, UpU, and CpA (Witzel, 1963), and hydrolysis of cytidine 2',3'-cyclic phosphate (cCMP) (Herries et al., 1962; Eftink & Biltonen, 1983a) and cUMP (del Rosario & Hammes, 1969; Schultz et al., 1998) catalyzed by RNase A. This general statement that pH–k_{cat}/K_M profiles manifest macroscopic pK_a's of an enzyme, however, is based the assumption that the kinetic mechanism of an enzyme does not have parallel or diversionary pathways (Knowles, 1976; Brocklehurst, 1994). If this assumption is not satisfied, the pH–k_{cat}/K_M profile could present 'mirage' pK_a's, which do not reflect the pK_a's of catalytic residues. Hence, a direct deduction of pK_a values from pH–k_{cat}/K_M profiles could be misleading. The pH–k_{cat}/K_M profiles for cleavage of 6-FAM~dArU(dA)$_2$~4-DABCYL by RNase A in Figure 5.1 do not reflect the macroscopic pK_a values of RNase A. These inconsistencies between the pK_a values from pH–k_{cat}/K_M profiles and the macroscopic pK_a values of RNase A indicate that

the assumption in deducing macroscopic pK_a's of RNase A from $pH-k_{cat}/K_M$ profiles is not

valid in catalytic cleavage of 6-FAM~dArU(dA)$_2$~4-DABCYL by the enzyme.

Kinetic Mechanism of RNase A Catalysis. Two models for kinetic mechanisms of

RNase A catalysis are depicted in Figure 5.2. K_1 and K_2 are the macroscopic acid

dissociation constants of the free enzyme, and K_1' and K_2' are the macroscopic acid

dissociation constants of the ES complex. The proton-transfer steps are assumed to occur

rapidly, compared with the rates of other elementary steps. The rate constants for the

substrate-association steps are presented as k_1, k_1', and k_1'', according to the protonation

states of the free enzyme. The rate constants for the substrate-dissociation steps are also

presented as k_2, k_2', and k_2'', according to the protonation states of the ES complex. k_3

represents the rate constant for the chemistry step. The kinetic mechanism in Figure 5.2A

does not have parallel pathways, but the one in Figure 5.2B does. If the kinetic mechanism

in Figure 5.2A represents that of RNase A catalysis, then the $pH-k_{cat}/K_M$ profile would

always portray the macroscopic acid dissociation constants, K_1 and K_2 (Knowles, 1976;

Tipton & Dixon, 1979). The abnormal pK_a's from the $pH-k_{cat}/K_M$ profiles in Figure 5.1

indicate that the kinetic mechanism of RNase A catalysis does not fit to the model presented

in Figure 5.2A. The kinetic mechanism in Figure 5.2B seems to be the more proper

mechanism for RNase A catalysis. In this mechanism, substrates can bind to the enzyme

through parallel pathways even when the protonation state of the free enzyme is not

catalytically competent. The mechanism in Figure 5.2B does not, however, always show

abnormality in $pH-k_{cat}/K_M$ profiles. If the chemistry step is much slower than substrate

dissociation steps, kinetic mechanisms in Figure 5.2A and 5.2B are kinetically

indistinguishable. Because all the enzyme forms are in equilibrium, the existence of the

parallel pathways does not affect k_{cat}/K_M. Therefore, the abnormality in pH–k_{cat}/K_M profiles

implies 'stickiness' of the substrate, that is, $k_2 \ll k_3$ (Cleland, 1982).

Solvent Isotope Effects on RNase A Catalysis. With either mechanism in Figure 5.2, the

solvent isotope effect on k_{cat}/K_M at pH 6.0 can be written as eq 5.2 (Quinn & Sutton, 1991),

because the catalytically competent protonation state (EH$^+$) is prevalent at pH 6.0:

$$^{D_2O}k_{cat}/K_M = \frac{(k_{cat}/K_M)^{H_2O}}{(k_{cat}/K_M)^{D_2O}} = \frac{^{D_2O}k_3 + C_f}{1 + C_f} \qquad (5.2)$$

$^{D_2O}k_3$ is intrinsic isotope effect on the chemistry step and defined as the ratio of k_3 in H_2O to

k_3 in D_2O. C_f is a forward commitment factor, which is the ratio of k_3 to k_2 when the medium

is H_2O. If a substrate is sticky (*i.e.*, $C_f \gg 1$), then $^{D_2O}k_{cat}/K_M$ would be close to 1.

The value of $^{D_2O}k_{cat}/K_M$ for cleavage of UpA by RNase A is 3.9 ± 0.4 (Table 5.4),

which is close to the solvent isotope effect on k_{cat}/K_M and k_{cat} for the hydrolysis of cCMP

determined previously to be ~4 (Eftink & Biltonen, 1983a) and 3.1 (Matta & Vo, 1986),

respectively. $^{D_2O}k_3$ is likely to be greater than 3.9 ± 0.4, as substrate desolvation has been

proposed to limit the rate of cleavage of UpA by RNase A (Thompson et al., 1995). The

$^{D_2O}k_3$ for cleavage of UpA by RNase A is determined to be 1.6 ± 0.2 (Table 5.4), which

indicates that a step other than the chemistry step determines k_{cat}. This solvent isotope effect

on k_{cat} is consistent with the observation that product release is partially rate-limiting in the k_{cat} of UpA cleavage by RNase A (Thompson et al., 1994).

Solvent isotope effects on k_{cat}/K_M for cleavage of 6-FAM~dArU(dA)$_2$~4-DABCYL by RNase A are much smaller than $^{D_2O}k_{cat} / K_M$ for cleavage of UpA (Table 5.3). By assuming that $^{D_2O}k_3$ is 4 from the $^{D_2O}k_{cat} / K_M$ for cleavage of UpA (3.9 ± 0.4), C_f in cleavage of 6-FAM~dArU(dA)$_2$~4-DABCYL by RNase A is estimated to be 14 at 0.010 M NaCl and 3 at 1.0 M NaCl by eq 5.2. If $^{D_2O}k_3$ is greater than 4, the actual C_f will be greater than these estimated values. Therefore, the solvent isotope effects on k_{cat}/K_M for cleavage of 4-FAM~dArU(dA)$_2$~4-DABCYL by RNase A show that this substrate is sticky, even at 1.0 M NaCl.

Graphical Analysis of pH–k_{cat} K_M Profiles. When the kinetic mechanism in Figure 5.2B represents that of RNase A catalysis, a rigorous pH–k_{cat}/K_M profile equation includes seven rate constants and four acid equilibrium constants, as in eq 5.3 (Alberty & Bloomfield, 1963):

$$k_{cat}/K_M = \frac{\left(k_1{}' \dfrac{[H^+]}{K_1} + k_1 + k_1{}'' \dfrac{K_2}{[H^+]} \right) k_3}{\left(\dfrac{[H^+]}{K_1} + 1 + \dfrac{K_2}{[H^+]} \right) \left(k_2{}' \dfrac{[H^+]}{K_1{}'} + k_2 + k_2{}'' \dfrac{K_2{}'}{[H^+]} + k_3 \right)} \qquad (5.3)$$

This equation is impractical to use for fitting pH–k_{cat}/K_M profiles. The pattern of a pH–k_{cat}/K_M profile, however, can be assessed by a simple qualitative analysis of rate-limiting steps without considering eq 5.3. In the free energy profile depicted in Figure 5.3, two energy barriers determine k_{cat}/K_M. Each of these energy barrier corresponds to a pseudo first-order rate constant produced by multiplying a second-order rate constant and substrate concentration. $k_{association}[S]$ corresponds to the energy barrier from E + S to the transition state of the substrate-association step. $k_{chemistry}[S]$ corresponds to the energy barrier from E + S to the transition state of the chemistry step. k_{cat}/K_M of the reaction is determined by the smaller rate constant between $k_{association}$ and $k_{chemistry}$. $k_{association}$ is a weighted average of k_1, k_1', and k_1'', as in eq 5.4:

$$k_{association} = \frac{k_1' \dfrac{[H^+]}{K_1} + k_1 + k_1'' \dfrac{K_2}{[H^+]}}{\dfrac{[H^+]}{K_1} + 1 + \dfrac{K_2}{[H^+]}}$$

(5.4)

This pH dependence of $k_{association}$ is identical to that for k_{cat}/K_M in eq 5.3 if k_2, k_2', $k_2'' \ll k_3$ in eq 5.3. Assuming a fast equilibrium between free enzyme forms (E, EH^+, and EH_2^{2+}) and substrate-bound forms (E•S, EH^+•S, and EH_2^{2+}•S) does not affect $k_{chemistry}$. With this assumption, the kinetic mechanism in Figure 5.2B is kinetically indistinguishable from the mechanism in Figure 5.2A. Therefore, the pH dependence of $k_{chemistry}$ can be obtained by assuming that k_1', k_1'', k_2', and k_2'' are 0 in eq 5.3:

$$k_{\text{chemistry}} = \frac{k_1 k_3 / k_2}{\frac{[\text{H}^+]}{K_1} + 1 + \frac{K_2}{[\text{H}^+]}} = \frac{(k_{\text{cat}} / K_M)_{\text{MAX}}}{\frac{[\text{H}^+]}{K_1} + 1 + \frac{K_2}{[\text{H}^+]}}$$ (5.5)

where $(k_{\text{cat}}/K_M)_{\text{MAX}}$ is the k_{cat}/K_M when the enzyme is in the EH^+ form. Figure 5.4 depicts

possible pH–k_{cat}/K_M profiles for different values of $k_{\text{association}}$ and $k_{\text{chemistry}}$. K_1 and K_2 are

assumed to be close to each other. Figures 5.4A and 5.4B depicts pH–k_{cat}/K_M profiles when

the kinetic mechanism does not have a parallel pathway (Figure 5.2A). Because there is no

parallel path allowing the enzyme to bind to the substrate when the protonation state is not

catalytically competent, $k_{\text{association}}$ shows a bell-shaped pH-dependence. This pH-dependence

of $k_{\text{association}}$ can be shown by setting k_1' and k_1'' to 0 in eq 5.4. Chemistry and substrate

association are rate-determining in Figure 5.4A and 5.4B, respectively. In either case, pH–

k_{cat}/K_M profiles have a bell shape, representing macroscopic pK_a's of the enzyme. Figures

5.4C–5.4F depict pH–k_{cat}/K_M profiles when the kinetic mechanism has parallel pathways

(Figure 5.2B). In Figure 5.4C, chemistry is rate-determining. The pH–k_{cat}/K_M profile shows

the pH-dependence of $k_{\text{chemistry}}$ in eq 5.5, regardless of the pH-dependence of $k_{\text{association}}$.

Figure 5.4D shows a pH–k_{cat}/K_M profile when $k_{\text{association}}$ is smaller than the maximum of

$k_{\text{chemistry}}$ and when $k_{\text{association}}$ is pH-independent. This pH-dependence of $k_{\text{association}}$ can be

obtained by setting $k_1 = k_1' = k_1''$ in eq 5.4. This pH–k_{cat}/K_M profile has a wide plateau, and

the apparent pK_a's do not correspond to the actual pK_a's of an enzyme. The apparent pK_1

($pK_{apparent}$) can be expressed with the macroscopic pK_1 of the free enzyme as eq 5.6 (Cleland, 1982):

$$pK_{apparent} = pK_1 - \log\left(1 + \frac{k_3}{k_2}\right)$$ (5.6)

Figure 5.4E and 5.4F show pH–rate profiles when $k_{association}$ is smaller than the maximum of $k_{chemistry}$ and when $k_{association}$ is pH-dependent. The pH–k_{cat}/K_M profile in Figure 5.4E depicts an enzyme that associates with a substrate faster at acidic pH than at basic pH, that is, $k_1' >$ k_1''. For this enzyme, the pH–k_{cat}/K_M profile is asymmetric. The overall shape of this pH–k_{cat}/K_M profile is strongly dependent on the relative magnitudes of k_1, k_1', and k_1''. The pH–k_{cat}/K_M profile in Figure 5.4F depicts an enzyme that cannot associate with a substrate in its fully deprotonated form, that is, $k_1'' = 0$. For this enzyme, the pH–k_{cat}/K_M profile is symmetric, but shifted to the acidic region. The apparent pK_1 can also be expressed by eq 5.6. The apparent pK_2 is close to the actual macroscopic pK_a's of the free enzyme. According to the relative magnitudes of k_1 and k_1', the pH–k_{cat}/K_M profile could have a hump or a hollow near the macroscopic pK_a's of the enzyme (Cleland, 1986).

Interpretation of pH–k_{cat} K_M Profiles of RNase A. The pH–k_{cat}/K_M profiles determined with UpA and cCMP correspond to the case shown in Figure 5.4C. $k_{chemistry}$ determines k_{cat}/K_M. The apparent pK_a's from these profiles are the actual macroscopic pK_a's of the enzyme. Figure 5.4D corresponds to the pH–k_{cat}/K_M profile for cleavage of

6-FAM~dArU(dA)$_2$~4-DABCYL by RNase A at 0.010 M NaCl (Figure 5.1). $k_{\text{association}}$ is insensitive to the protonation state of the active-site histidine residues. The apparent pK_a's are shifted by 1.2–1.4 unit from the macroscopic pK_a's of RNase A (Table 5.2), which implies C_f is 15–24 according to eq 5.6. This estimated C_f is consistent with the minimal solvent isotope effect determined at this salt concentration ($^{D_2O}k_{\text{cat}} / K_M = 1.18 \pm 0.05$).

The pH–k_{cat}/K_M profiles determined at 0.20 M and 1.0 M NaCl (Figure 5.1) indicate that $k_{\text{association}}$ is dependent on pH, as in Figure 5.4E or 5.4F. The pK_1's from the pH–k_{cat}/K_M profiles are shifted to the acidic region, but the pK_2's from the pH–k_{cat}/K_M profiles are close to the macroscopic pK_a's of RNase A (Table 5.2) because of the effect of deprotonation of the histidine residues on $k_{\text{association}}$. The basic arms of the pH–rate profiles are straight lines with a slope of 1 without a curvature as in Figure 5.4E, which implies that k_1'' is much smaller than k_1'. Thought the magnitude of k_1'' is undeterminable because k_{cat}/K_M does not reach a minimum in the basic region, the lowest k_{cat}/K_M in the basic region is the upper limit of k_1'' at each salt concentration (4.7 × 10^5 M^{-1}s^{-1} at 0.20 M NaCl and 1.4 × 10^5 M^{-1}s^{-1} at 1.0 M NaCl). k_1 also seems to be smaller than k_1' from the absence of a hump around pH 6. The magnitude of k_1 is also undeterminable because two macroscopic pK_a's are close to each other. Nonetheless, it is clear that $k_{\text{association}}$ determines k_{cat}/K_M at pH 6.0 even at 0.20 M and 1.0 M NaCl, which is also consistent with the solvent isotope effects (Table 5.3). The stability of the complex of RNase A and a DNA ligand, 6-FAM~d(AUAA) shows a strong dependence on pH (Park et al., 2001). The dissociation equilibrium constant is increased from 0.038 ± 0.005 mM to 2.2 ± 0.2 mM as pH is increase from 4.0 to 8.0. The pH-

dependence of $k_{association}$ shows that protonation of the active-site histidine residues stabilizes the transition state for substrate binding (E:S to ES) as well as the ES state.

The pH-independence of $k_{association}$ at 0.010 M NaCl indicates that the mechanism of substrate association at this salt concentration is distinct from that at 0.10 M and 1.0 M NaCl. k_{cat}/K_M at this salt concentration has been proposed to be limited by the encounter of the enzyme and the substrate at this salt concentration (Park & Raines, 2001). The pH-independence of $k_{association}$ at 0.010 M NaCl supports this proposal, as the protonation state of the active-site histidine residues would not affect the rate of encounter.

Salt Effect on Substrate Association by Ribonuclease A. Salt effects on the k_{cat}/K_M of cleavage of 6-FAM~dArU(dA)$_2$~6-TAMRA by RNase A has been analyzed quantitatively with eq 5.7 (Park & Raines, 2001):

$$k_{cat}/K_M = \frac{(k_{cat}/K_M)_{MAX}}{1 + \left(\dfrac{[Na^+]}{K_{Na^-}}\right)^{n'}} \tag{5.7}$$

$(k_{cat}/K_M)_{MAX}$ is the maximum of k_{cat}/K_M. n' is the absolute value of the slope in the linear region of a $\log[Na^+]$–$\log(k_{cat}/K_M)$ plot. K_{Na^-} is the salt concentration where k_{cat}/K_M is half of its maximum. n' is related to n, the number of Na^+ ion released from a substrate upon binding as in eq 5.8:

$$\beta n < n' < n \tag{5.8}$$

where β is a correlation parameter for the salt effect on the free energy of the substrate-association transition state to that on the free energy of the ES state. $(k_{cat}/K_M)_{MAX}$, n', and K_{Na} for cleavage of 6-FAM~dArU(dA)$_2$~6-TAMRA by RNase A are $(3.3 \pm 0.4) \times 10^9$ $M^{-1}s^{-1}$, 2.33 ± 0.05, and (0.025 ± 0.002) M, respectively (Park & Raines, 2001).

Since pH–k_{cat}/K_M profiles and solvent isotope effects show that k_{cat}/K_M for cleavage for 6-FAM~dArU(dA)$_2$~4-DABCYL by RNase A is limited by the substrate-association rate, the salt effect on k_{cat}/K_M actually represents the salt effect on the substrate-association rate, that is, $n' = \beta n$. The n value is unknown, but can be estimated from the salt effect on k_{cat}/K_M of K41R RNase A. Because K41R RNase A is a sluggish variant (Messmore et al., 1995), n' of K41R RNase A (2.66 ± 0.08) seems to reflect n. By approximating n as 2.66 ± 0.08, β is estimated to be ~0.9.

This β value is consistent with the salt effects on the solvent isotope effects (Table 5.3). The forward commitment factor can be written as a function of [Na$^+$] (Park & Raines, 2001).

$$C_f = C_f^{\ominus}[\text{Na}^+]^{(\beta-1)n} \tag{5.9}$$

where $C_f^{\ominus}$ is the commitment factor when [Na$^+$] = 1.0 M. According to this equation, when β is close to 1, the salt effect on the commitment factor is minimal. The solvent isotope effect on cleavage of 6-FAM~dArU(dA)$_2$~6-TAMRA by RNase A does not vary

significantly, even though salt concentration is increased by 100-fold (Table 5.3). Therefore, the weak salt effect on the solvent isotope effect support β being close to 1.

This β value reveals the nature of the transition state of the substrate-binding step. If an association occurs without involving any intermediate complex, the salt effect on the association rate is expected to be minimal. The β value is normally ~0.1 for the single-step association of protein and nucleic acid (Lohman, 1986). This minor salt dependence on the association results mostly from the screening effect of salt ions. The β value of ~0.9 indicates that RNase A forms an intermediate complex with the substrate in the reaction pathway for substrate binding. This salt dependence of the association rate also shows that the interaction in the intermediate is Coulombic, but not as specific as the final enzyme–substrate complex.

Rate of the Encounter of RNase A with Substrates. The rate of substrate association by an enzyme is generally slower than the rate of encounter, because formation of a productive complex requires stringent orientational criteria (Berg & von Hippel, 1985). To form a productive complex, a substrate should collide with the *active site* of an enzyme with a proper orientation. Considering the proportion of the area of the active site to the total surface area of an enzyme, the probability of this proper binding would be very low. The $(k_{cat}/K_M)_{MAX}$ determined at 0.010 M NaCl (2.8×10^9 $M^{-1}s^{-1}$) implies, however, that the reaction is encounter-controlled at this salt concentration. A comparision with diffusion-controlled association rates for small ligands and single-stranded oligonucleotides also supports that the k_{cat}/K_M being encounter-controlled. Ca^{2+} was reported to associate with

A(pA)$_4$ with a bimolecular rate constant of 4.6 × 10^{10} M^{-1}s^{-1} (Pörschke, 1979). A tripeptide,

(Lys)$_3$, was also reported to associate with A(pA)$_4$ with a bimolecular rate constant of 1.4 ×

10^{10} M^{-1}s^{-1} (Pörschke, 1978). Both rate constants were determined at a low salt condition (1

mM sodium cacodylate). The smaller size of Ca^{2+} ion compared to that of RNase A

increases its diffusion rate significantly. The diffusion coefficient of Ca^{2+} ion is 7.92 × 10^{-6}

cm^{2}s^{-1} at 25 °C (American Institute of Physics, 1972), which is 6-fold greater than the

diffusion coefficient of RNase A, 1.19 × 10^{-6} cm^{2}s^{-1} at 20 °C (Tanford, 1961). Hence, the

k_{cat}/K_M of RNase A at 0.010 M NaCl is, indeed, comparable to the rate of an encounter-

controlled reaction. This consideration also implies that the substrate-association by

RNase A involves intermediates to enhance the association rate to the limit of encounter.

Enhancement of Association in Biological Systems. To enhance the rate of association,

biological systems frequently utilize special tactics, such as electronic guidance (Sharp et al.,

1987; Getzoff et al., 1992; Wade et al., 1998) and diffusion in reduced dimensions (Berg &

von Hippel, 1985; Northrup et al., 1988; von Hippel & Berg, 1989). Electronic guidance is

observed when an enzyme has an electrostatic potential gradient on its surface, which

facilitates the diffusion of a substrate to the active site. Computer simulation on the

association of superoxide anion to the protein superoxide dismutase revealed that electronic

guidance enhances the rate by a factor of 30 or more (Sharp et al., 1987). Moreover,

mutagenesis of a surface residue of the enzyme to improve the electrostatic guidance can

result in a better catalyst than the wild-type enzyme (Getzoff et al., 1992). Diffusion in

reduced dimensions facilitates the formation of a protein–protein or enzyme–substrate

complex by nonspecific association followed by movement in two-dimensions or one-dimension instead of three-dimensions to find a specific target. This tactic plays a significant role in the interaction of DNA-binding proteins with DNA. The association rate of *lac* repressor with its operator DNA target can reach 5×10^{10} $M^{-1}s^{-1}$, which surpasses the calculated association rate of 10^8 $M^{-1}s^{-1}$, based on a theoretical treatment of three-dimensional diffusion (von Hippel & Berg, 1989). Apparently, the *lac* repressor binds DNA nonspecifically, and then diffuses on the surface of DNA until it finds a specific target. The importance of electronically assisted nonspecific encounter has also been shown in the enhancement of the rate of protein–protein association. Simulation of the association of cytochrome c and cytochrome c peroxidase showed that nonspecific encounters are prolonged (100 ns), which allows the proteins to explore the surface of each protein by rotation to find the proper orientation (Northrup et al., 1988). Mutational analysis on the association rate of barnase and barstar also showed that the first step of the association process is the formation of a low-affinity nonspecific complex, which is held together by long-range Coulombic interactions, before the final complex is formed (Schreiber & Fersht, 1996).

Mechanism of Substrate Association by Ribonuclease A. Based on the results reported herein and the precedent in other systems, a mechanism for substrate binding by RNase A is envisaged in Figure 5.5. RNase A diffuses to a substrate and forms a short-lived complex (E:S) through nonspecific Coulombic interactions. Then, the substrate scans the surface of the enzyme by repeated nonelastic collisions (Berg & von Hippel, 1985). If the substrate

finds the active site of the enzyme before it dissociates from the enzyme, then the complex is stabilized by the specific interactions between the active-site residues and the substrate (ES). RNase A also seems to utilize electrostatic guidance to facilitate substrate binding. The pH-dependence of $k_{association}$ in the pH–k_{cat}/K_M profiles at 0.20 and 1.0 M NaCl shows that protonated active-site histidine residues facilitate substrate association. The localized cationic residues around the active site of RNase A could also play a role in 'steering' the substrate to the active site (E:S to ES) by providing an electrostatic potential on the surface. At 0.010 M NaCl, the transition state for the substrate-association step is stabilized significantly, and the encounter of the enzyme and the substrate (E+S to E:S) determines $k_{association}$, which is insensitive to salt concentration and pH, as shown in the salt–rate profile and pH–rate profile. The $(k_{cat}/K_M)_{MAX}$ determined at this salt concentration (2.8×10^9 $M^{-1}s^{-1}$) is the rate of encounter and the limit of RNase A catalysis.

Optimization of Catalytic Effectiveness of Ribonuclease A. The significant contribution of physical steps to the overall kinetics is a distinct characteristic of 'perfect' enzymes (Albery & Knowles, 1976; Knowles & Albery, 1977; Burbaum et al., 1989). For an enzyme to evolve into a perfect enzyme, the physical steps of the catalysis also need to be optimized. Once the transition state of a chemistry step is stabilized enough to be comparable with the transition state of a substrate-association step or a product-release step, further enhancement of the rate of the chemistry step does not improve overall catalytic effectiveness. In this case, substrate association (or product release) must be improved to the limit allowed by the Haldane relationship to maximize catalytic effectiveness. In other words, an enzyme's

having evolved to enhance substrate binding (or product release) is an indication that catalysis of the chemistry step has already been optimized fully.

The results reported herein show that catalysis of the chemistry step by RNase A is optimized enough for the substrate-association rate to determine k_{cat}/K_M. Also, the rate of the substrate-association step seems to have been elaborated by evolution to exploit 'electrostatic guidance' and 'diffusion in reduced dimension' by forming nonspecific intermediates. These features of the energetics of RNase A catalysis strongly suggest that RNase A is indeed a perfect enzyme.

Table 5.1: pH Dependence of k_{cat}/K_M Values for Cleavage of 6-FAM~dArU(dA)$_2$~4-DABCYL by Ribonuclease A at 0.010 M, 0.20 M and 1.0 NaCl.[a]

0.010 M NaCl		0.20 M NaCl		1.0 M NaCl	
pH	k_{cat}/K_M ($\times$ 10^9 M^{-1}s^{-1})	pH	k_{cat}/K_M ($\times$ 10^7 M^{-1}s^{-1})	pH	k_{cat}/K_M ($\times$ 10^5 M^{-1}s^{-1})
3.59	1.2 ± 0.2	3.54	0.25 ± 0.03		
3.85	1.1 ± 0.1	3.77	0.77 ± 0.09		
4.23	2.1 ± 0.1	4.13	2.6 ± 0.2	3.99	1.3 ± 0.0
4.68	2.3 ± 0.4	4.54	3.6 ± 0.2	4.37	3.6 ± 0.3
5.09	3.2 ± 0.4	4.94	5.3 ± 0.5	4.79	6.8 ± 0.2
5.61	2.2 ± 0.3	5.44	5.0 ± 0.1	5.30	9.7 ± 0.1
5.87	2.8 ± 0.2	5.91	4.1 ± 0.1	5.99	12 ± 1
6.53	3.0 ± 0.3	6.59	2.1 ± 0.1	6.66	8.3 ± 0.9
7.00	2.2 ± 0.5	6.93	1.4 ± 0.1	6.97	6.1 ± 0.5
7.43	1.2 ± 0.1	7.40	0.56 ± 0.03	7.48	2.9 ± 0.0
7.85	0.90 ± 0.05	7.89	0.26 ± 0.03	7.93	1.4 ± 0.0
		8.33	0.088 ± 0.010		
		8.71	0.047 ± 0.002		

[a]Assays were performed at 23 °C in 1.0 mM buffer containing NaCl. Buffers were sodium formate–HCl (pH 3.54–4.23), sodium acetate–HCl (pH 4.37–5.61), Bistris–NaOH (pH 5.87–6.66), MOPS-NaOH (pH 6.93–7.48), and Tris-HCl (pH 7.85–8.71). Errors are standard deviations of triplicate determinations.

Table 5.2: Parameters[a] Determined from pH Dependence of k_{cat}/K_M for Cleavage of 6-

FAM~dArU(dA)$_2$~4-DABCYL by Ribonuclease A at 0.010 M, 0.20 M, and 1.0 M NaCl.

[NaCl] (M)	pK_1	pK_2	$(k_{cat}/K_M)_{MAX}$ ($M^{-1}s^{-1}$)
0.010	3.88 ± 0.06 (5.1[b])	7.47 ± 0.06 (6.1[b])	$(2.8 \pm 0.0) \times 10^9$
0.20	4.66 ± 0.09 (5.6[b])	6.44 ± 0.08 (6.6[b])	$(6.7 \pm 0.9) \times 10^7$
1.0	4.88 ± 0.04	6.95 ± 0.04	$(1.4 \pm 0.1) \times 10^6$

[a]The parameters were determined by fitting the data in Table 5.1 to eq 5.1 by nonlinear

regression. The errors are standard errors from the nonlinear regression analyses.

[b]Macroscopic pK_a's of ribonuclease A calculated from microscopic pK_a's of His12 and

His119 determined by NMR spectroscopy under similar conditions (0.018 M or 0.142 M

NaCl without buffer) (Fisher et al., 1998c).

Table 5.3: Solvent Isotope Effects on the Cleavage of 6-FAM~dArU(dA)$_2$~6-TAMRA by Ribonuclease A.[a]

[NaCl] (M)	$^{D_2O}k_{cat}/K_M$ [b]
0.010	1.18 ± 0.05
0.10	1.40 ± 0.15
1.0	1.76 ± 0.02

[a]Assays were performed at 23 °C in 1.0 mM Bistris–HCl buffer (pH 6.0) containing NaCl in H$_2$O and D$_2$O. [b]$^{D_2O}k_{cat}/K_M$ is defined as the ratio of $(k_{cat}/K_M)^{H_2O}$ to $(k_{cat}/K_M)^{D_2O}$. Errors are standard deviations of triplicate determinations.

Table 5.4: Solvent Isotope Effects on the Cleavage of UpA by Ribonuclease A.[a]

Solvent	k_{cat}/K_M ($\times\ 10^6\ M^{-1}s^{-1}$)	k_{cat} ($\times\ 10^3\ s^{-1}$)
H_2O	3.5 ± 0.3	2.9 ± 0.3
D_2O	0.89 ± 0.04	1.8 ± 0.2
Isotope effects[b]	3.9 ± 0.4	1.6 ± 0.2

[a]Assays were performed at 25 °C in 0.10 M MES–NaOH (pH 6.0 or pD 6.4) containing NaCl (0.10 M) in H_2O and D_2O. [b]Isotope effects are defined as the ratio of kinetic parameters determined in H_2O to those determined in D_2O.

Figure 5.1   pH–k_{cat}/K_M profiles for cleavage of 6-FAM~dArU(dA)$_2$~4-DABCYL by

ribonuclease A at 0.010 M (●), 0.20 M (■), and 1.0 M (▲) NaCl. The assays

were performed at 23 °C in 1.0 mM buffer containing NaCl. Determination of

k_{cat}/K_M values at each pH were done in triplicate. Each curve was fitted to eq

5.1 by nonlinear regression. The apparent pK_a's and $(k_{cat}/K_M)_{MAX}$ are listed in

Table 5.2. Arrows indicate macroscopic pK_a's of ribonuclease A determined

at similar conditions (0.018 M and 0.142 M NaCl without buffer).
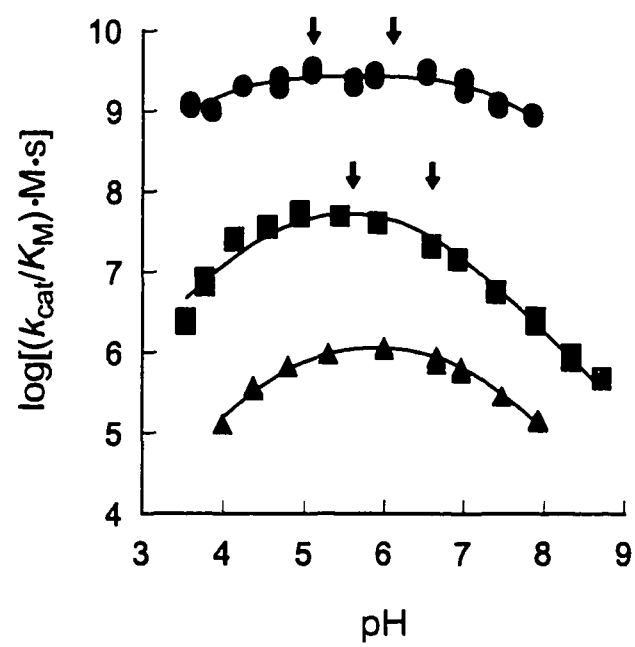
Figure 5.2   Kinetic mechanisms of ribonuclease A without (A) and with (B) parallel

pathways. K_1 and K_2 are the macroscopic acid dissociation constants of the

free enzyme, and K_1' and K_2' are the macroscopic acid dissociation constants

of the ES complex. k_1, k_1', and k_1'' are rate constants for substrate-association

steps. k_2, k_2', and k_2'' are rate constants for substrate-dissociation steps. k_3 is

the rate constant for the chemistry step.

A

$$EH_2^{2+}$$

$$\Big\updownarrow K_1$$

$$EH^+ \; \underset{k_2}{\overset{k_1[S]}{\rightleftarrows}} \; EH^+\!\bullet S \; \overset{k_3}{\longrightarrow} \; EH^+ + P_1 + P_2$$

$$\Big\updownarrow K_2$$

$$E$$

$$EH_2^{2+}\!\bullet S$$

$$\Big\updownarrow K_1{}'$$

$$\Big\updownarrow K_2{}'$$

$$E\!\bullet S$$

B

$$EH_2^{2+} \; \underset{k_2{}'}{\overset{k_1{}'[S]}{\rightleftarrows}} \; EH_2^{2+}\!\bullet S$$

$$\Big\updownarrow K_1 \qquad\qquad \Big\updownarrow K_1{}'$$

$$EH^+ \; \underset{k_2}{\overset{k_1[S]}{\rightleftarrows}} \; EH^+\!\bullet S \; \overset{k_3}{\longrightarrow} \; EH^+ + P_1 + P_2$$

$$\Big\updownarrow K_2 \qquad\qquad \Big\updownarrow K_2{}'$$

$$E \; \underset{k_2{}''}{\overset{k_1{}''[S]}{\rightleftarrows}} \; E\!\bullet S$$
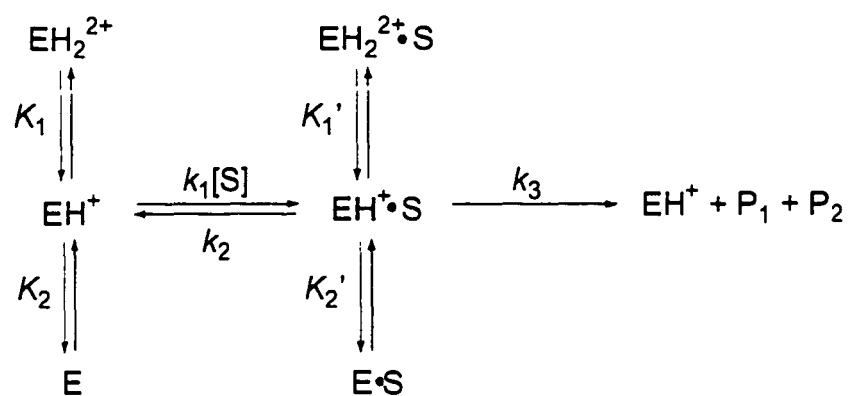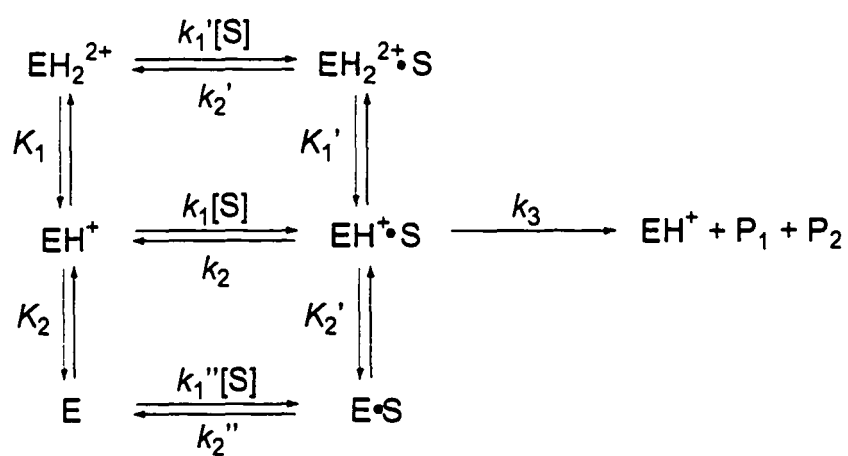
Figure 5.3 Notional free energy profile for enzymatic catalysis. The energy barriers

corresponding to two psuedo first-order rate constants, $k_{binding}[S]$ and

$k_{chemistry}[S]$, are represented with arrows.

$$E+S \underset{k_2}{\overset{k_1}{\rightleftharpoons}} ES \xrightarrow{k_3} EP$$
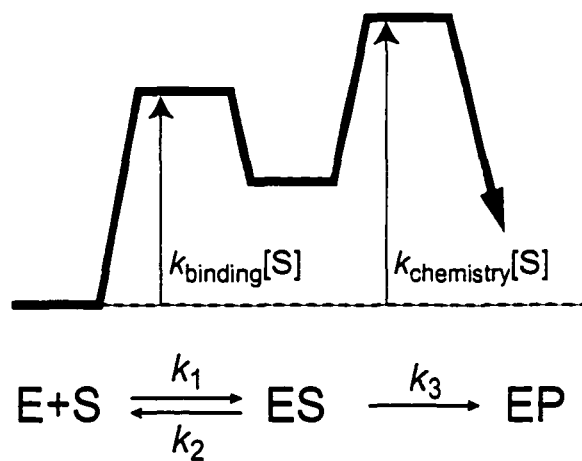
Figure 5.4 Possible pH–k_{cat}/K_M profiles for different cases of $k_{association}$ and $k_{chemistry}$. The

effect of pH on k_{cat}/K_M (solid line), $k_{association}$ (long-dashed line), and $k_{chemistry}$

(short-dashed line) are shown for cases that $k_{chemistry} < k_{association}$ without

parallel pathway (A), $k_{association} < k_{chemistry}$ without parallel pathway (B),

$k_{chemistry} < k_{association}$ with parallel pathways and $k_{association}$ is pH-independent

(C), $k_{association} < k_{chemistry}$ with parallel pathways and $k_{association}$ is pH-

independent (D), $k_{association} < k_{chemistry}$ with parallel pathways and $k_1' > k_1''$ (E),

and $k_{association} < k_{chemistry}$ with parallel pathways and $k_1'' = 0$ (F).
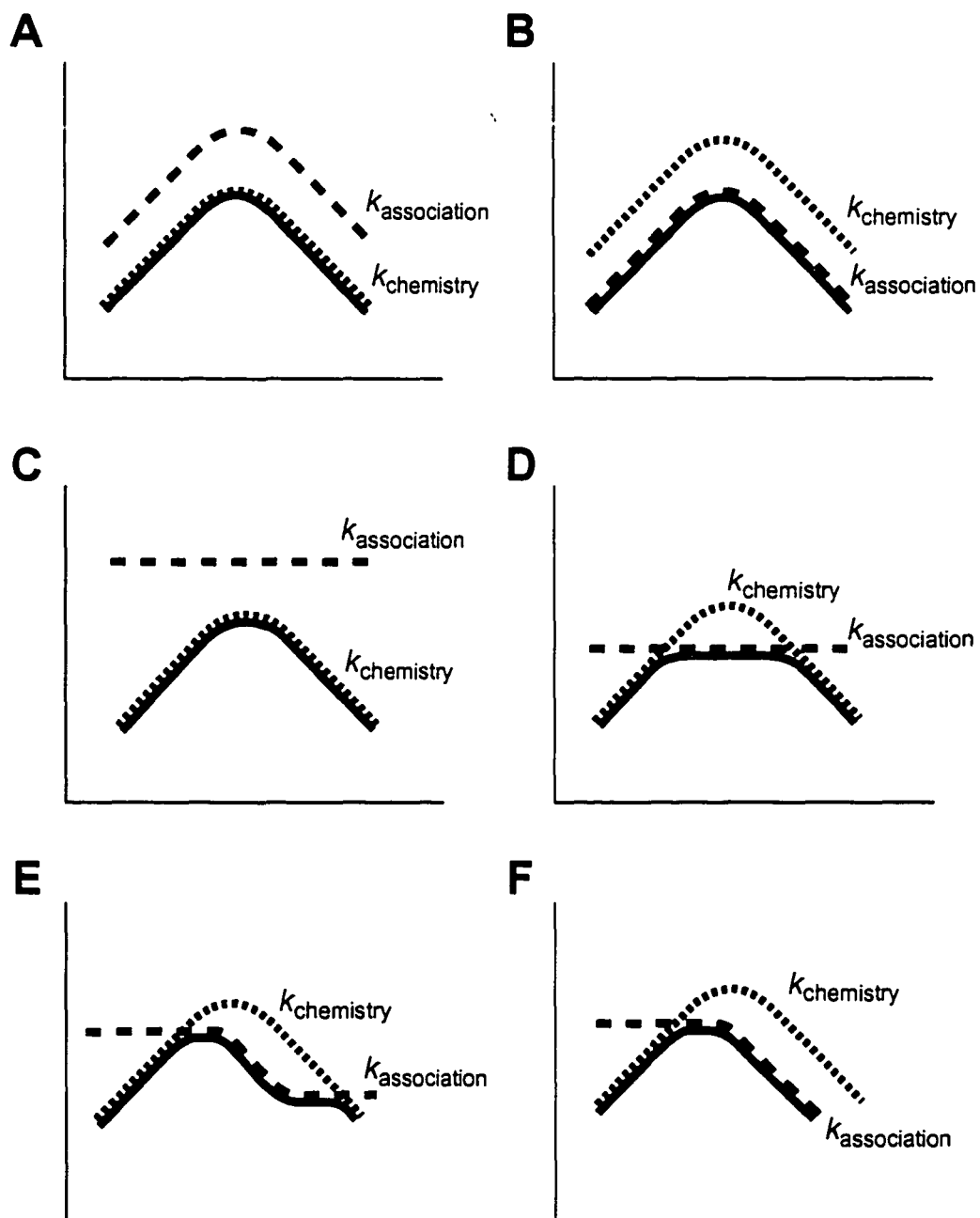
Figure 5.5   Mechanism of substrate association by ribonuclease A. The black circle with

a dent and the solid line represent ribonuclease A and a RNA substrate,

respectively. The dent of the black circle indicates the location of the

substrate-binding cleft on ribonuclease A. E:S is an intermediate formed by

nonspecific Coulombic interactions. ES is a productive complex formed by

specific interactions of the substrate with the substrate-binding cleft.

$$E+S \rightleftharpoons E:S \rightleftharpoons ES$$
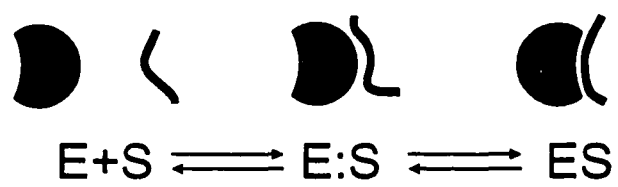
Chapter 6

Dimer Formation by a 'Monomeric' Protein

ABSTRACT

Dimeric proteins can arise by the swapping of structural domains between monomers. The prevalence of this occurrence is unknown. Ribonuclease A (RNase A) is assumed to be a monomer near physiological conditions. Here, this hypothesis is tested and found to be imprecise. The two histidine residues (His 12 and His 119) in the active site of RNase A arise from two domains (S-peptide and S-protein) of the protein. The H12A and H119A variants have 10^5-fold less ribonucleolytic activity than does the wild-type enzyme. Incubating a 1:1 mixture of the H12A and H119A variants at pH 6.5 and 65 °C results in a 10^3-fold increase in ribonucleolytic activity. A large quantity of active dimer can be produced by lyophilizing a 1:1 mixture of the H12A and H119A variants from acetic acid. At pH 6.5 and 65 °C, the ribonucleolytic activity of this dimer converges to that of the dimer formed by simply incubating the monomers, as expected for a monomer–dimer equilibrium. The equilibrium dissociation constant for the dimer is near 2 mM at both 65 and 37 °C. This value of K_d is only 20-fold greater than the concentration of RNase A in the cow pancreas, suggesting that RNase A dimers exist *in vivo*. The intrinsic ability of RNase A to form dimers under physiological conditions is consistent with a detailed model for the evolution of homodimeric proteins. Dimers of 'monomeric' proteins could be more prevalent than is usually appreciated.

INTRODUCTION

The assembly of oligomeric proteins from monomers by domain swapping is a recurrent theme (Bennett et al., 1995; Schlunegger et al., 1997). Bovine seminal ribonuclease (BS-RNase) is a quintessential example of a domain-swapped dimer (D'Alessio et al., 1997; D'Alessio, 1999a; D'Alessio, 1999b). Although ribonuclease A (RNase A) and BS-RNase share a similar three-dimensional structure as well as more than 80% of their amino acid residues, only BS-RNase is known to form a domain-swapped dimer naturally (Figure 6.1A) (Piccoli et al., 1992; Mazzarella et al., 1993). BS-RNase can also form a domain-swapped tetramer (Adinolfi et al., 1996).

RNase A can form domain-swapped dimers by an artificial procedure—lyophilization from a concentrated solution in 50% acetic acid (Crestfield et al., 1962; Crestfield et al., 1963). This dimer has been shown to have two different conformers (Gotte & Libonati, 1998; Sorrentino et al., 2000). The structure of one of these conformers has been determined (Liu et al., 1998), and is distinct from that of the BS-RNase dimer (Figure 6.1B). Dimeric RNase A is thermally unstable, dissociating to monomers irreversibly upon incubation at high temperature (Crestfield et al., 1962).

His 12 and His 119 are active-site residues near the N- and C-termini, respectively, of RNase A. The H12A and H119A variants have 10^5-fold lower ribonucleolytic activity than does the wild-type enzyme (Thompson & Raines, 1995). Dimerization of these variants by domain swapping should result in composite active sites and the regain of ribonucleolytic activity (Figure 6.2). Hence, an assay of enzymatic activity could be used to assess readily

and quantitatively the extent of domain swapping. Here, we use this method to analyze the thermodynamics and kinetics of dimer formation by RNase A. Most significantly, we find that RNase A spontaneously forms domain-swapped dimers *near neutral pH*. This discovery of a pre-evolved ability for domain swapping in a monomeric protein enables us to propose a detailed model for the evolution of dimeric proteins.

MATERIAL AND METHODS

Protein Production and Purification. Wild-type RNase A and its H12A and H119A variants (Thompson & Raines, 1995) were produced in *Escherichia coli* and purified as described elsewhere (delCardayré et al., 1995; Fisher et al., 1998b) with the following modifications. Inclusion bodies were resuspended in a minimal volume of solubilization buffer, which was 20 mM Tris-HCl buffer (pH 8.0) containing guanidine-HCl (7 M), EDTA (10 mM), and dithiothreitol (DTT; 0.10 M). This suspension was diluted 10-fold by adding 20 mM acetic acid slowly and with stirring. At this step, the dark brown solution turned turbid because of the precipitation of impurities. Reduced RNase A was still soluble after the dilution. The precipitant was removed by centrifugation for 30 min at 15000×g. The supernatant from the centrifugation was dialyzed against 20 mM acetic acid. The precipitant that developed during dialysis was also removed by centrifugation. The remaining supernatant was refolded as described (delCardayré et al., 1995). The removal of impurities

by diluting the solubilized inclusion body with 20 mM acetic acid increased the yield of pure

protein to 40–50 mg per 1 L of *E. coli* culture.

Preparation of the H12A RNase A•H119A RNase A Dimer. A dimer of H12A RNase A

and H119A RNase A was prepared as described elsewhere for the wild-type enzyme

(Crestfield et al., 1962; Liu et al., 1998). The variants (2.7 mg of each) were mixed, dialyzed

against distilled H_2O, and lyophilized. The lyophilized powder was dissolved in 50% (v/v)

acetic acid (0.50 mL) to give a final concentration of 11 mg/mL, and incubated at 4 °C

overnight. After the solution was lyophilized, the powder was dissolved in 0.50 mL of 0.20

M sodium phosphate buffer (pH 6.5) and loaded on a Pharmacia FPLC HiLoad 26/60

Superdex 75 gel filtration column, which had been equilibrated with 0.20 M sodium

phosphate buffer (pH 6.5). Fractions corresponding to dimers were collected, and the

concentration of dimer was determined spectroscopically by using $\varepsilon = 0.72$ mL mg^{-1} cm^{-1} at

277.5 nm (Sela et al., 1957). The yield of dimers was approximately 20%, which is similar

to a value reported recently (Liu et al., 1998).

Assays of Ribonucleolytic Activity. Ribonucleolytic activity was measured by monitoring

cleavage of poly(C) with ultraviolet spectroscopy. The buffer was composed of 50 mM

acetic acid, 50 mM MES, and 0.10 M Tris (Ellis & Morrison, 1982) containing NaCl (0.10

M). The pH was adjusted to pH 7.0 with aqueous HCl. After buffer (0.60 mL) containing

poly(C) (0.042–0.83 mM) was equilibrated at 25 °C, the reaction was initiated by addition

of enzyme. The increase in absorbance at 250 nm was monitored and used to calculate the

reaction rate with $\Delta\varepsilon = 2,380$ M^{-1}cm^{-1} (delCardayré & Raines, 1994). Kinetic parameters

were determined by nonlinear regression analysis of kinetic data with the program

SIGMAPLOT 5.0 (SPSS; Chicago, IL).

Assays of Dimer Dissociation. The dissociation of dimer was monitored by measuring

the loss of ribonucleolytic activity. A solution of the H12A RNase A•H119A RNase A

dimer (6 μM) in 0.20 M sodium phosphate buffer (pH 6.5) was heated to 37 °C or 65 °C. At

known time intervals, small aliquots were removed and assayed for ribonucleolytic activity.

When the dimer was incubated at 65 °C, the aliquots taken from the reaction were chilled on

ice before assaying activity to suppress further reaction. Assays of ribonucleolytic activity

were performed as described above, except that the concentration of poly(C) was 0.17 mM.

Specific activities were calculated by dividing the observed rates by the concentration of

enzyme monomer (0.20 μM) in the assay mixtures.

Assays of Dimer Formation at Neutral pH. The formation of dimers was monitored by

measuring the gain of ribonucleolytic activity. A mixture of H12A RNase A (6 μM) and

H119A RNase A (6 μM) were incubated at 37 °C and 65 °C in 0.20 M sodium phosphate

buffer (pH 6.5). Aliquots of the reaction were withdrawn at known time intervals and

assayed as described above.

Determination of K_d of the Dimer at Neutral pH. The concentration of dimer in the

mixture of H12A RNase A and H119A RNase A was determined from the ribonucleolytic

activities measured in the three-component buffer (pH 7.0) containing NaCl (0.10 M) and

poly(C) (0.17 mM). As a reference for 100% dimerization, the specific activity of the H12A

RNase A•H119A RNase A dimer formed by lyophilization was determined in the same

manner. Once the specific activity of a mixture of H12A RNase A and H119A RNase A was determined, the concentration of dimer, [D] was calculated with eq 6.1:

$$[D] = \frac{1}{2}\left(\frac{SA_{obs}}{SA_{ref}}[M]_{total}\right)$$ (6.1)

SA_{obs} and SA_{ref} are the observed specific activitiy at equilibrium and the maximal specific activity, respectively. $[M]_{total}$ is the total concentration of H12A RNase A and H119A RNase A. The K_d of the dimer was calculated with eq 6.2:

$$K_d = \frac{([M]_{total} - 2[D])^2}{[D]}$$ (6.2)

RESULTS

Detection of Dimers. Protein complementation by enzyme variants has been recognized as a useful tool to study the structure of multimeric enzymes with composite active sites (Larimer et al., 1987; Wente & Schachman, 1987; Tobias & Kahana, 1993; Li et al., 1997) or multiple domains (van Gent et al., 1993; Kao et al., 1996; Witkowski et al., 1996). Chemical modification of RNase A and BS-RNase had been used previously to show the existence of composite active sites by the formation of active dimers from inactive

monomers (Crestfield et al., 1963; Piccoli et al., 1992). Because of the residual catalytic

activity remaining after incomplete modification and purification, chemically-modified

enzymes do not allow for quantitation of domain swapping. Using H12A RNase A and

H119A RNase A, along with sensitive assays for ribonucleolytic activity, allowed us to

monitor accurately the dimerization of RNase A.

Enzymatic Activity. Steady-state kinetic parameters for the cleavage of poly(cytidylic

acid) [poly(C)] by the H12A RNase A•H119A RNase A dimer formed by lyophilization

from 50% acetic acid are listed in Table 6.1. Assays were performed at pH 7.0 instead at pH

6.0 (which is more typical), because the dimer was observed to lose its ribonucleolytic

activity slowly at pH 6.0. For comparison, steady-state kinetic parameters for monomers of

wild-type RNase A was also determined under the same conditions (Table 6.1). The values

of k_{cat} and k_{cat}/K_M for the H12A RNase A•H119A RNase A dimer are $(39 \pm 4)\%$ and

$(31 \pm 2)\%$ of those for the wild-type monomer, respectively. These values are close to 25%,

the relative activity expected from a theoretical 50% yield of dimers with 50% of the activity

of wild-type RNase A.

Dimer Dissociation. The dimer of H12A RNase A and H119A RNase A formed by

lyophilization lost its catalytic activity rapidly when incubated at 65 °C (Figure 6.3A). In

only 2 min, the specific activity decreased from 58 s^{-1} to 0.29 s^{-1}, which is a 99.5% decrease.

Surprisingly, the remaining activity increased slowly and converged to 0.82 s^{-1}, which is

10^3-fold higher than that of monomers of H12A RNase A or H119A RNase A. This

convergence indicates that the dimer does not convert to monomer completely upon

incubation at 65 °C.

The conformational stability of the dimer was also determined at 37 °C. The dimer was stable at 37 °C (Figure 6.3B). After a slight initial decrease, the activity remained constant for 90 min.

Monomer–Dimer Equilibrium at Neutral pH. To probe for the existence of a monomer–dimer equilibrium near neutral pH, an equimolar mixture of H12A RNase A and H119A RNase A was prepared and incubated at pH 6.5 and 65 °C. The catalytic activity of the mixture increased rapidly (Figure 6.3A). The specific activity reached 0.71 s^{-1} in 2 min, and did not change until 90 min. The average of the last three specific activities was (0.76 ± 0.06) s^{-1}. This value is within error of 0.82 s^{-1}, the activity remaining after the thermal inactivation of the dimer formed by lyophilization. This convergence to the same activity by heating the dimer to 65 °C or mixing the monomers at 65 °C indicates that a monomer–dimer equilibrium does indeed exist. By using SA_{obs} = (0.76 ± 0.06) s^{-1} as the observed specific activity at equilibrium, SA_{ref} = (58 ± 3) s^{-1} as the maximal specific activity (*vide supra*), and $[M]_{total}$ = 12 µM as the total concentration of H12A RNase A and H119A RNase A, the concentration of dimer at equilibrium was estimated to be [D] = (0.079 ± 0.007) µM by eq 6.1. With this concentration, the equilibrium dissociation constant was determined to be K_d = (1.8 ± 0.1) mM by eq 6.2 (Table 6.2).

To determine the equilibrium dissociation constant at physiological temperature, a mixture of H12A RNase A and H119A RNase A was likewise incubated at 37 °C (Figure 6.3B). The activity of this mixture also increased sharply and reached a specific activity of (0.50 ± 0.03) s^{-1}, which is similar to that of the mixture incubated at 65 °C. The concentration of dimer at equilibrium was calculated to be [D] = (0.052 ± 0.004) µM by

eq 6.1. The equilibrium dissociation constant was determined to be $K_d = (2.7 \pm 0.2)$ mM by

eq 6.2 (Table 6.2). The activity of the mixture did not change significantly after 20 h of

incubation (data not shown).

DISCUSSION

Protein Complementation by H12A and H119A Variants. The dimer formed by

lyophilization loses its catalytic activity rapidly at 65 °C (Figure 6.3A), as expected from the

reported instability of the dimer (Crestfield et al., 1962). Rapid inactivation can be a useful

property for practical applications of ribonucleases. The high thermal stability and folding

reversibility of RNase A make it impractical to inactivate the enzyme by heat treatment.

Thus, modulation of RNase A activity in vitro has been a problem attacked by both inhibitor

design (Hummel et al., 1987; Stowell et al., 1995; Russo & Shapiro, 1999) and protein

engineering (Messmore et al., 2000). The dimer of H12A RNase A and H119A RNase A

allows for facile regulation of ribonucleolytic activity in vitro. Rapid inactivation can be

achieved simply by heating to 65 °C without the addition of any chemical reagent.

Dimer of RNase A at Neutral pH. The formation of a dimer in a mixture of the H12A

and H119A variants demonstrates the existence of a monomer–dimer equilibrium, even at

neutral pH. This dimer has $K_d = (1.8 \pm 0.1)$ mM at 65 °C, and $K_d = (2.7 \pm 0.2)$ mM at 37 °C

(Table 6.2). A dimer of wild-type RNase A could have a slightly different K_d from those

measured with the H12A RNaseA•H119A RNase A dimer. The

H12A RNaseA•H119A RNase A dimer has one intact active site (with His 12 and His 119;

Figure 6.2) and one impaired active site (with Ala 12 and Ala 119). The T_m (which is the

temperature at the midpoint of the thermal transition between native and denatured states) of

the H12A/H119A variant of RNase A is lower by 9 °C than that of the wild-type enzyme

(T.A. Klink & R.T. Raines, unpublished results). In other words, the presence of Ala 12 and

Ala 119 diminishes conformational stability. Thus, it is reasonable to expect that the K_d for a

dimer of wild-type RNase A may actually be less than that for the H12A RNase A•H119A

RNase A dimer. Nevertheless, dimerization of wild-type RNase A near neutral pH had never

been observed previously, presumably because its K_d value is too high to allow for its

detection by conventional analytical methods (e.g., gel filtration chromatography, analytical

ultracentrifugation, calorimetry, and so forth).

The dimer formed near neutral pH seems to be distinct from that formed by

lyophilization from 50% acetic acid. The dissociation of the neutral-pH dimer at 37 °C is

markedly fast compared with that of the dimer formed by lyophilization from acetic acid

(Figure 6.3B). The monomer–dimer equilibrium can be written as A + B $\underset{\leftarrow}{\overset{\rightarrow}{}}$ AB, with an

association rate constant of k_a and a dissociation rate constant of k_d. The rate of dimer

formation can be written as:

$$\frac{d[\text{AB}]}{dt} = k_a[\text{A}][\text{B}] - k_d[\text{AB}] \qquad (6.3)$$

Because the initial concentration of homodimers in each solution of monomer is negligible, [A] and [B] are approximately equal to $[A]_{total}$ and $[B]_{total}$, respectively. By solving differential eq 6.3, [AB] can be written as:

$$[AB] \approx \frac{[A]_{total}[B]_{total}}{K_d}\left(1 - e^{-k_d t}\right) \qquad (6.4)$$

When the dimer formed by lyophilization dissociates, the initial contribution of $k_a[A][B]$ in eq 6.3 is negligible. At short times, [AB] can be written as:

$$[AB] \approx [AB]_0 e^{-k_d t} \qquad (6.5)$$

If the dimer formed at neutral pH has the same structure as the dimer formed by lyophilization, then the two dimers should have the same value of k_d. Nonlinear regression analysis of the data in Figure 6.3B with eq 6.4 (association) and eq 6.5 (dissociation), results in disparate values of k_d. The dimer formed at neutral pH has $k_d = (0.15 \pm 0.03)$ s^{-1}, whereas the dimer formed by lyophilization has $k_d = (0.002 \pm 0.001)$ s^{-1}. Thus, the dimer formed at neutral pH is distinct from the dimer formed by lyophilization. This result is consistent with the observation of an initial dip in ribonucleolytic activity when the dimer formed by lyophilization from 50% acetic acid was incubated at 65 °C (Figure 6.3A). The residual activity initially declines (to 0.29 s^{-1}) but slowly recovers (to 0.82 s^{-1}). Apparently, the dimer

formed by lyophilization (D) dissociates to monomers (M) first, then forms a dimer with a

different structure (D*) as in eq 6.6.

$$D \rightarrow 2M \rightleftarrows D^*$$ (6.6)
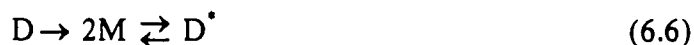
The dimer formed by lyophilization has been reported to have two distinct conformers

(Gotte & Libonati, 1998; Sorrentino et al., 2000). The above kinetic analysis shows that the

dimer formed at neutral pH is distinct from that of both conformers formed by lyophilization

(Table 6.3).

The dimer formed by RNase A at neutral pH could have a conformation similar to that

of the BS-RNase dimer (Figure 6.1A). The monomers of BS-RNase are crosslinked by two

intermolecular disulfide bonds (D'Alessio, 1995; Di Donato et al.. 1995; D'Alessio, 1999a;

D'Alessio, 1999b). With these disulfide bonds intact, the domain-swapped dimer (M×M) has

a free energy equivalent to that of the covalently-linked dimer without domain swapping

(M=M) (Piccoli et al., 1992; Kim et al., 1995b). The formation of a BS-RNase-like dimer by

RNase A has a precedent. The K31C/S32C variant of RNase A forms two intermolecular

disulfide bonds and swaps its S-peptide domain in the resulting dimer (Di Donato et al.,

1995; Ciglic et al., 1998).

Domain swapping has been shown to endow BS-RNase with distinct biochemical and

physiological characteristics, such as allostericity (Piccoli et al., 1992) and cytotoxicity

(Cafaro et al., 1995; Kim et al., 1995a). Due to the structural similarity between BS-

RNase and RNase A, engineering RNase A to form dimers like BS-RNase has also been used to endow new biological functions (Di Donato et al., 1994; Cafaro et al., 1998) or to explore the molecular evolution of BS-RNase (Di Donato et al., 1995; Ciglic et al., 1998). RNase A as well as its human homolog have been engineered to form dimers, and the cytotoxicity of those variants approaches that of BS-RNase (Cafaro et al., 1998; Piccoli et al., 1999). Given that the engineered dimeric structure confers cytotoxicity to RNase A, the endogenous concentration of dimeric RNase A *in vivo* is of significant interest. The concentration of RNase A in bovine pancreas has been estimated to be 0.1 mM (Barnard, 1969). With the assumption that the K_d of 2.7 mM determined here for dimer dissociation at 37 °C is still valid *in vivo*, the concentration of domain-swapped RNase A dimer in bovine pancreas is 3 μM. This value is comparable to the IC_{50} value of BS-RNase for transformed cell lines (Kim et al., 1995b). This finding could have important implications in understanding the biological role of RNase A.

Evolution of homodimeric proteins. The evolution of homodimeric proteins is a topic of much current interest in molecular evolution (Bennett et al., 1995; Ciglic et al., 1998). Because multiple mutations are necessary to provide a complimentary intermolecular interface, the mechanism for the evolution of a stable dimeric protein is enigmatic. Domain swapping has been proposed to explain how an intermolecular interface can evolve without changing multiple residues (Bennett et al., 1995). In the domain swapping model, a monomeric protein swaps one of its domains with another monomer to form a homodimer. Then, residues can be replaced to stabilize the nascent dimer.

The intermolecular interface in a domain-swapped homodimer has two components. A "C–interface" is the intermolecular interface that evolves from the closed intramolecular interface in each monomer. An "O–interface" is the new intermolecular interface, which was an open surface in each monomer. Hence, the evolution of a domain-swapped homodimer uses a pre-evolved interface in the monomer. Domain swapping of monomeric proteins under harsh, non-physiological conditions has been proposed as evidence for the use of this pre-evolved interface. For example, RNase A dimerizes upon lyophilization from 50% acetic acid (Crestfield et al., 1962), and diphtheria toxin dimerizes upon freezing in phosphate buffer (Carroll et al., 1988). Our detection of an RNase A dimer at neutral pH demonstrates that RNase A has an intrinsic ability to form a domain-swapped dimer, even without harsh treatment.

The dimerization of RNase A also has an interesting implication for the evolution of composite active sites. As mentioned above, protein complementation experiments have been used to identify proteins with composite active sites (Larimer et al., 1987; Wente & Schachman, 1987; Tobias & Kahana, 1993; Li et al., 1997). The fusion of single-domain proteins has been proposed as a mechanism for the evolution of composite active sites (Bennett et al., 1995). According to this proposal, an active site develops at a domain interface after a primitive monomer with two domains is formed by the fusion of genes encoding two single-domain proteins.

We propose an alternative mechanism for the evolution of homodimers with composite active sites. Our mechanism is shown in Figure 6.4. This mechanism is based on our detection of an RNase A dimer at neutral pH, the known ability of the S-protein and S-

peptide fragments to form a stable noncovalent complex (Richards, 1955; Richards & Vithayathil, 1959), and physicochemical considerations.

We begin with protein I (Figure 6.4), which is a primitive protein that has no biological activity. An active site evolves by natural selection, to give protein II. The evolution of the active site is likely to destabilize the protein for the following reasons. First, active-site residues tend to be hydrophilic so as to provide the Brønsted acids, Brønsted bases, nucleophiles, hydrogen bonds, and Coulombic interactions needed for function (Warshel, 1998). The evolution of a hydrophilic active site creates a solvent-accessible concave surface, which is likely to be less favorable to conformational stability than a hydrophobic core. Second, active-site residues can have pK_a values that differ by several units from their intrinsic pK_a values [for a dramatic example, see: (Highbarger et al., 1996)]. Conformational stability must be sacrificed to perturb the pK_a values of these residues. Finally, proteins often have clusters of cationic or anionic residues at their active sites [e.g., the cationic residues of RNase A (Fisher et al., 1998b; Fisher et al., 1998c)] to enhance Coulombic interactions with their ligand (e.g., the anionic phosphoryl groups of RNA). This clustering is unfavorable to conformational stability because of repulsive Coulombic forces (Grimsley et al., 1999; Loladze et al., 1999; Perl et al., 2000; Spector et al., 2000). Hence, the evolution of an active site likely destabilizes a protein. Indeed, when His 119 of RNase A is mutated to an alanine residue, the conformational stability of the protein is increased by 0.3 kcal/mol at pH 6.0 and 1.1 kcal/mol at pH 1.2 (Quirk et al., 1998). This destabilization by active-site residues allows the protein to open along the interface defining the active site to form protein II_o. The evolution of an active site could thus define the domain structure of a protein.

Protein II is vulnerable to denaturation via protein II_o. The open conformation of protein II_o has fewer favorable intramolecular interactions than does the closed conformation of protein II. Protein III and protein III_o have evolved stable domains without compromising the active site, as depicted by the shaded boxes in Figure 6.4. The stabilized domains could form a noncovalent complex, protein $III_N\cdot$protein III_C, after proteolytic cleavage between the two domains. The individual domains, protein III_N and protein III_C, could even be stable (or metastable) independently.

RNase S is an example of the protein $III_N\cdot$protein III_C complex. S-Protein, which is an example of protein III_C, has a partially disordered but native-like structure (Graziano et al., 1996). Disulfide bonds seem to be responsible for the conformational stability of S-protein, as S-protein cannot form correct disulfide bonds once it is reduced in the absence of S-peptide (Harber & Anfinsen, 1961), which is an example of protein III_N. S-Peptide also tends to fold into its native conformation, an α-helix (Shoemaker et al., 1987).

The equilibrium between protein III and protein III_o allows for the formation of protein III_2, which is a primitive domain-swapped dimer with composite active sites but a high K_d. The unstable RNase A dimer formed near neutral pH is an example of protein III_2. Lyophilization of RNase A from 50% acetic acid induces dimerization because the acidic pH increases the population of the open conformation, protein III_o; and the lyophilization process increases the concentration of protein, which favors its dimerization to form protein III_2. Dehydration could also enhance dimer formation by desolvating the C- and O-interfaces and thereby favoring intermolecular association. Lyophilization from 50%

acetic acid is likely to produce dimers in several different conformations, but only the

metastable conformers are observed routinely (Gotte & Libonati, 1998).

Domain swapping provides a dimerization interface without the need for multiple

mutations in a monomer (Bennett et al., 1995). Still, domain swapping alone is unlikely to

endow a dimer with stability. Swapping intramolecular interactions for identical

intermolecular interactions in a domain-swapped dimer is likely to be isoenthalpic, and

dimerization itself has a substantial entropic cost. If there were a phenotypic selection for the

dimer, then its K_d could become lower through mutations that stabilize the dimer (e.g.,

development of an O-interface or evolution of intermolecular disulfide bonds) or destabilize

the monomer (e.g., deletion of residues between the two domains). The efficacy of this latter

strategy was demonstrated recently with human pancreatic ribonuclease, which forms a

homodimer with $K_d = 1.5$ μM upon removal of five residues in the loop that links the S-

peptide and S-protein domains (Russo et al., 2000). The result is protein **IV**, which is a

stable domain-swapped dimer.

The role of domain swapping in the dimerization of BS-RNase has been controversial

(D'Alessio, 1995; D'Alessio, 1999a; D'Alessio, 1999b). If the integrity of the BS-RNase

dimer is paramount, then the intermolecular disulfide bonds are most responsible for

dimerization. After all, the dissociation energy of a disulfide bond far exceeds that of any

known noncovalent interaction. Although domain swapping plays only a minor role in the

stabilization of dimeric BS-RNase, it does dictate the location of the dimerization interface.

Moreover, the cytotoxicity of BS-RNase originates from domain swapping, and not from the

intermolecular disulfide bonds (Cafaro et al., 1995; Kim et al., 1995b).

The lack of evidence for unstable dimers, such as protein III_2 (Figure 6.4), had suggested that stable dimers evolve directly from stable monomers. In contrast, we have discovered that RNase A has a predisposition [perhaps even a preadaptation (Gould, 1977)] to form a dimer, albeit an unstable one, at neutral pH. The intrinsic ability of RNase A to form an unstable dimer indicates that evolution of a dimeric quaternary structure can be a continuous process. Assigning a particular mutation as being responsible for dimerization in such a continuous process would be arbitrary. Proteins have been subjected to natural selection as a result of the evolutionary pressures on the organisms that contain them (Burbaum et al., 1989). Hence, it would be most appropriate to ask: Which mutation provided a selectable phenotype for dimerization?

Table 6.1: Steady-State Kinetic Parameters for the Cleavage of Poly(cytidylic acid) by Wild-Type Ribonuclease A and the Dimer of the H12A and H119A Variants Formed by Lyophilization from 50% (v/v) Acetic Acid.[a]

Ribonuclease A	k_{cat} (s^{-1})	k_{cat}/K_M (10^6 M^{-1}s^{-1})	K_M (mM)
Wild-type	880 ± 80	1.6 ± 0.1	0.55 ± 0.06
Dimer	340 ± 20	0.50 ± 0.02	0.68 ± 0.05

[a]Parameters were calculated from nonlinear regression analysis of data collected at pH 7.0 and 25 °C.

Table 6.2: Properties of the Dimer Formed by H12A Ribonuclease A and H119A

Ribonuclease A at pH 6.5.

Method	Specific activity $(s^{-1})^a$	[Dimer] $(\mu M)^b$	K_d $(mM)^b$
Quenched on ice after incubation at 65 $^{\circ}$C	0.76 ± 0.06	0.079 ± 0.007	1.8 ± 0.1
Incubated at 37 °C	0.50 ± 0.03	0.052 ± 0.004	2.7 ± 0.2

[a]Specific activities are expressed as the mean (± SE) of last three time points in Figure 6.3A

and 6.3B. [b]The values of [Dimer] and K_d were calculated by using eq 6.1 and eq 6.2.

Table 6.3: Stability and Structure of Dimers of Ribonuclease A.

Dimers	Conformational Stability	Structure
Dimer formed by lyophilization (Conformer I[a])	Metastable	Unknown
Dimer formed by lyophilization (Conformer II[a])	Metastable	(Liu et al., 1998)
Dimer formed at neutral pH	Unstable	Unknown

[a]The designation is from (Sorrentino et al., 2000).

Figure 6.1   Structures of BS RNase and RNase A dimer. Ribbon diagram of bovine

seminal ribonuclease [A; Protein Data Bank entry 1BSR (Mazzarella et al.,

1993)] and the ribonuclease A dimer formed by lyophilization [B; Protein

Data Bank entry 1A2W (Liu et al., 1998)]. The diagram was made with the

program MOLSCRIPT (Kraulis, 1991).

A
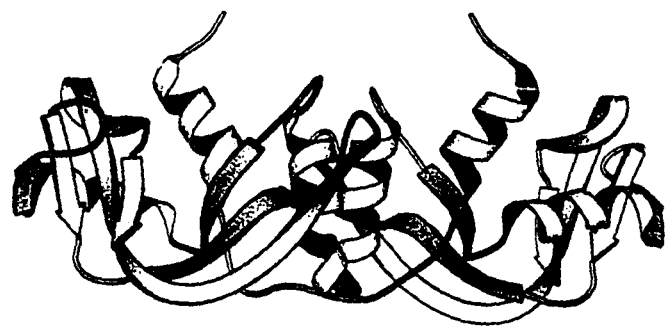
B

Figure 6.2   Scheme for the dimerization of H12A ribonuclease A and H119A

ribonuclease A. RNase A is depicted as a complex of the S-peptide and S-

protein domains connected by a flexible loop. The location of the histidine

residues that are absent in the H12A (black) and H119A (white) variants are

denoted with an indent. In the H12A RNase A•H119A RNase A dimer, only

one active site is intact.

H12A·H12A
Inactive

H12A
Inactive

H119A
Inactive

H12A·H119A
Active

H119A·H119A
Inactive
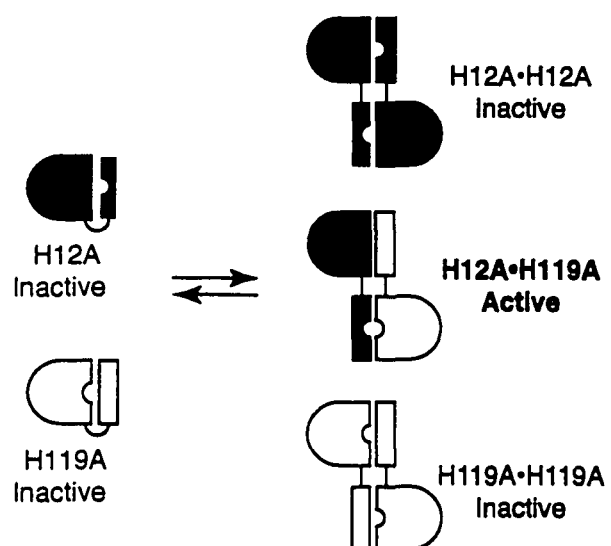
Figure 6.3   Dissociation and formation of a dimer of H12A ribonuclease A and H119A

ribonuclease A at 65 °C (A) and 37 °C (B). Dimers were formed by

lyophilization from 50% acetic acid (●), or by mixing at pH 6.5 (O). Specific

activities were determined by monitoring catalysis of poly(C) cleavage. The

specific activity of the mixture of H12A RNase A and H119A RNase A at 0

min is the average of the specific activity of each variant.
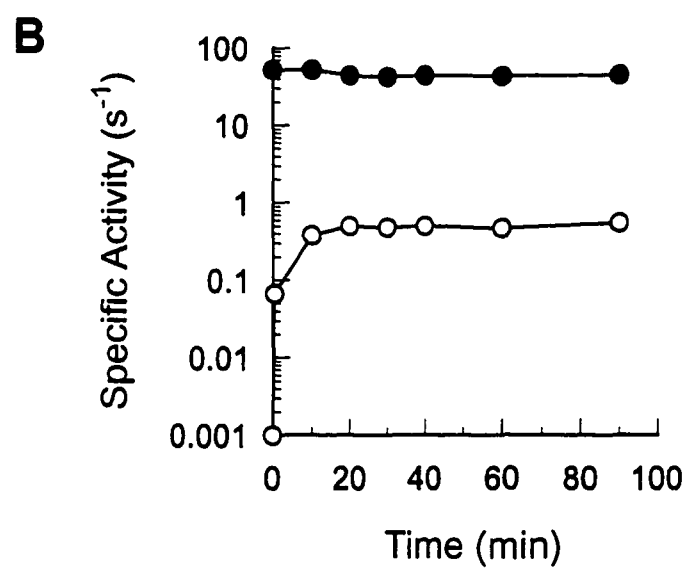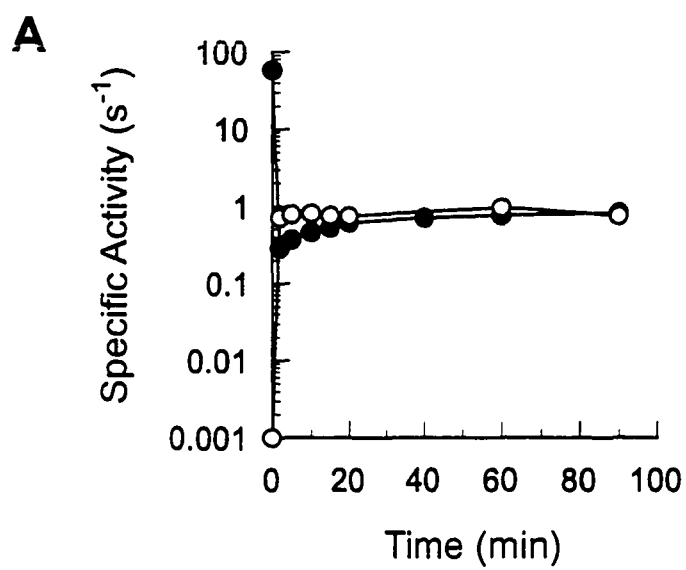
Figure 6.4 Putative mechanism for the evolution of domain-swapped dimer with

composite active sites. The primitive monomer does not have an active site

(protein I). The evolution of the active site ($\bullet$) destabilizes the protein,

allowing equilibration between an intact conformation (protein II) and an

open conformation (protein II_o). Stable domains evolve to increase

conformational stability (protein III). In a side reaction, proteolytic cleavage

between the domains results in a noncovalent complex (protein $III_N \bullet$ protein

III_C) that dissociate into its two components (protein III_N and protein III_C).

The protein with stable domains (protein III) forms a primitive domain-

swapped dimer (protein III_2). A stable dimer evolves by favorable changes in

the dimeric interface (protein IV). The steps in this mechanism are shown to

be sequential, but could also occur in concert.
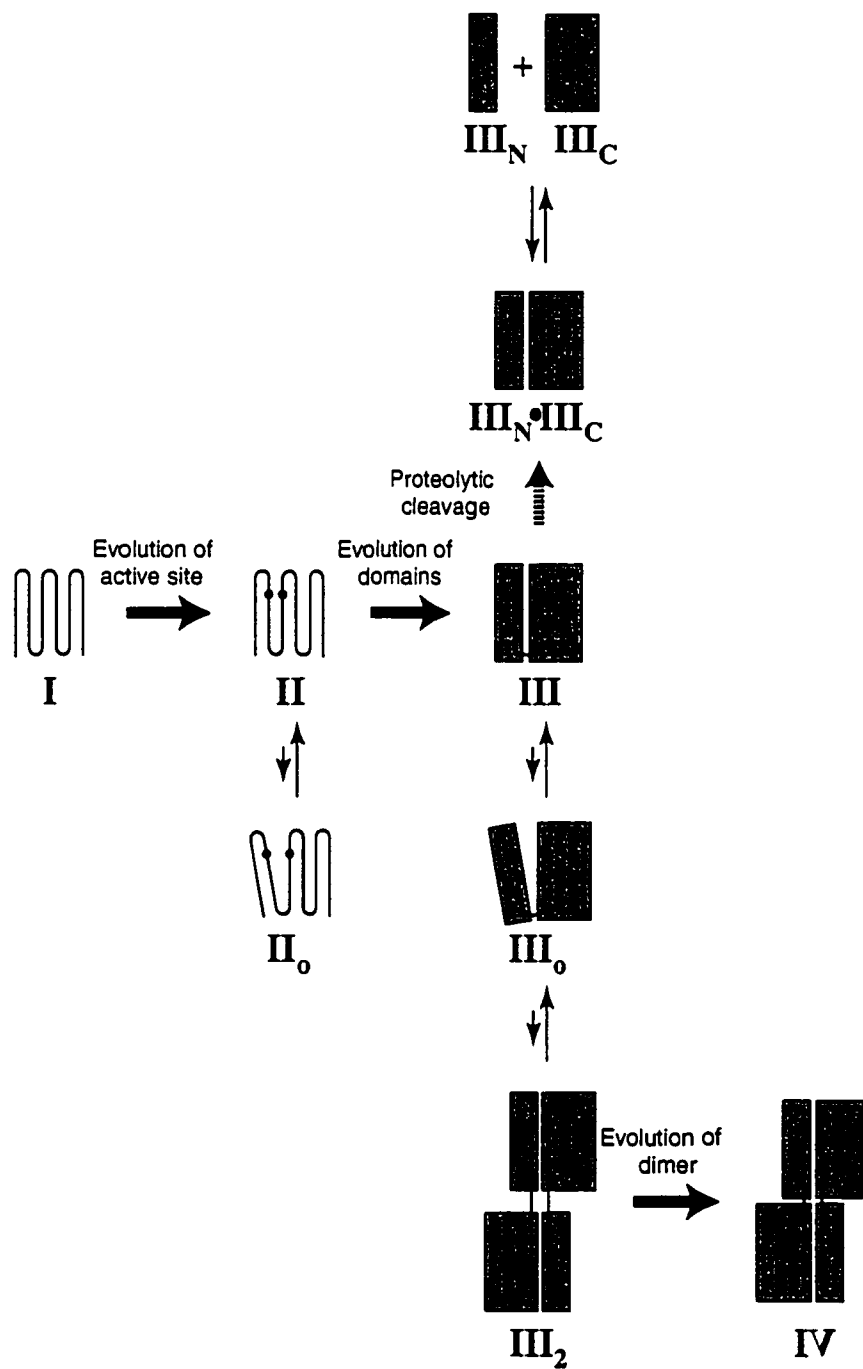
Chapter 7

Adjacent Cysteine Residues as a Redox Switch

ABSTRACT

Oxidation of adjacent cysteine residues into a cystine forms a strained eight-membered ring. This motif was tested as the basis for an enzyme with an artificial redox switch. Adjacent cysteine residues were introduced into two different structural contexts in ribonuclease A by site-directed mutagenesis to produce the A5C/A6C and S15C/S16C variants. Ala5 and Ala6 are located in an α-helix, whereas Ser15 and Ser16 are located in a surface loop. Only A5C/A6C ribonuclease A had the desired property. The catalytic activity of this variant decreases by 70% upon oxidation. The new disulfide bond also decreases the conformational stability of the A5C/A6C variant. Reduction with dithiothreitol restores full enzymatic activity. Thus, the insertion of adjacent cysteine residues in a proper context can be used to modulate enzymatic activity.

INTRODUCTION

The modulation of enzymatic activity is of great importance in biology (Cleland &

Craik, 1996; Alberghina, 1999). The non-equilibrium nature of biological systems

necessitates temporal or spatial suppression or enhancement of specific biochemical

pathways according to cellular metabolism or exogenous signals. For example,

conformational regulation by phosphorylation is a recurring theme in cellular signal

transduction pathways (Munico & Miras-Portugal, 1996; Sefton & Hunter, 1998). Indeed, it

is common to find that an enzymatic activity is enhanced significantly by phosphorylation of

a single residue. Such *in vivo* regulation through conformational change inspired us to

devise a new "on–off" switch.

Adjacent cysteines residues in a protein form a strained eight-membered ring upon

oxidation to a cystine (Figure 7.1). The amide bond in the eight-membered ring was

predicted by an early theoretical calculation to have a *cis* conformation (Chandrasekaran &

Balasubramanian, 1969). Studies with model peptides showed, however, that this amide

bond is in a conformational equilibrium, with either the *cis* conformation (Sukumaran et al.,

1991) or the *trans* conformation (Garcia-Echeverría & Rich, 1997) preferred according to

context. In either conformation, the ring alters the structure of the polypeptide chain (Figure

7.1).

The oxidation of naturally occurring adjacent cysteine residues can impair protein

function. For example, oxidation of Cys558 and Cys559 in the active site of mercuric

reductase abolishes its catalytic activity (Miller et al., 1989). When the disulfide bond is

reduced with dithiothreitol (DTT), the enzyme recovers its activity. Oxidation of adjacent

cysteine residues can also destabilize protein conformation. The oxidation of cysteine

residues in human ribonuclease inhibitor (hRI) inactivates the protein. Of the 32 cysteine

residues in hRI, four belong to two pairs of adjacent cysteine residues: Cys94, Cys95,

Cys328 and Cys329. When either pair is replaced with alanines, the resistance of the protein

to oxidation is enhanced (Kim et al., 1999). Disulfide bonds between adjacent cysteine

residues are known to exist even in the native conformation of proteins. The structure of

crystalline methanol dehydrogenase from *Methylobacterium extorquens* has an eight-

membered ring with a *cis* amide bond formed by adjacent cysteine residues in its active site

(Blake et al., 1994). The eight-membered ring is necessary for catalytic activity, as the

enzyme loses its activity when the disulfide bond is reduced by DTT. A regulatory role for

the disulfide bond between adjacent cysteine residues in the ligand-binding site of

acetylcholine receptor has also been proposed (Kao & Karlin, 1986; Mosckovitz &

Gershoni, 1988). Interestingly, a disulfide bond between adjacent cysteine residues is more

stable to reduction than is one in a CXC motif, two cysteines with one intervening residue

(Zhang & Snyder, 1989).

Together, these studies suggested to us that adjacent cysteines could serve as an artificial

"redox switch" by which enzymatic activity is turned on and off according to the reduction

potential of the medium. If the native conformation of a protein necessitates the *trans*

conformation of an amide bond, imposing a *cis* conformation by the oxidation of adjacent

cysteine residues would lead to inactivation. Reduction of the disulfide bond between

adjacent cysteines would switch the protein back to its native conformation.

To explore the use of this motif as a redox switch, we introduced adjacent cysteine residues into ribonuclease A (RNase A; EC 3.1.27.5), a pyrimidine-specific ribonuclease from bovine pancreas (D'Alessio & Riordan, 1997; Raines, 1998). The plethora of information available on the structure and catalytic mechanism of this enzyme makes RNase A a suitable model system for designing and testing artificial switches (Hamachi et al., 2000; Messmore et al., 2000). We created two RNase A variants with adjacent cysteines residues: A5C/A6C RNase A and S15C/S16C RNase A (Figure 7.2). Each has a pair of adjacent cysteine residues within a distinct context of the three-dimensional structure. We report the effect of oxidation and reduction on the catalytic activity and conformational stability of the variants.

MATERIAL AND METHODS

Production of A5C A6C and S15C S16C Variants. Plasmids that direct the production of the two variants, A5C/A6C RNase A and S15C/S16C RNase A, were created by site-directed mutagenesis (Kunkel et al., 1987) using oligonucleotides CTACCGCTCAAACTTGCAGCATGCAGTTTCCTTGCC (for A5C/A6C) and GGAGCTGCTGGCAGCACTAGTACAACAGTCCATGTGCTG (for S15C/S16C). The proteins were produced, folded, and purified as described elsewhere (delCardayré et al., 1995; Park & Raines, 2000a), with the following modification. After the protein was folded overnight in a solution containing reduced glutathione (GSH; 1.5 mM) and oxidized glutathione (GSSG; 0.3 mM), DTT was added to 1 mM to reduce any mixed disulfides

between the newly introduced sulfhydryl groups and glutathione or disulfide bonds formed

by adjacent cysteines. The buffers for chromatography also contained 1 mM DTT to keep

the introduced sulfhydryl groups reduced during purification. The catalytic activity of

RNase A (and, presumably, the integrity of its native disulfide bonds) is not affected by 1

mM DTT.

Assays of Enzymatic Activity. RNase A catalyzes the cleavage of poly(cytidylic acid)

[poly(C)]. Poly(C) was purified by ethanol precipitation. Assays of poly(C) cleavage were

performed at 25 °C in 0.10 M MES–NaOH (pH 6.0) containing 0.10 M NaCl. Rates of

poly(C) cleavage were determined by monitoring absorption at 250 nm and using $\Delta\varepsilon$ =

2,380 $M^{-1}cm^{-1}$ (delCardayré et al., 1994). Enzyme concentrations were determined by using

ε = 0.72 mL $mg^{-1}cm^{-1}$ at 277.5 nm (Sela et al., 1957). Kinetic parameters were determined

by nonlinear regression analysis using the Michaelis–Menten kinetic mechanism.

Inactivation of A5C A6C and S15C S16C Variants by Oxidation. The effect of oxidation

on the enzymatic activity of wild-type RNase A, A5C/A6C RNase A, and S15C/S16C

RNase A was determined as follows. Enzymes were incubated at 50 °C for 1 h in 0.10 M

Tris–HCl buffer (pH 8.0) with oxidants. The elevated temperature was used to facilitate any

conformational changes necessary to effect cystine formation. The low enzyme

concentration, 10 nM, was used to prevent intermolecular disulfide bond formation. Three

distinct oxidation conditions were used: (1) $O_2(g)$ dissolved naturally in the buffer, (2)

oxidized glutathione (GSSG; 20 nM), and (3) 5,5'-dithiobis(2-nitrobenzoic acid) (DTNB;

20 nM). Only a twofold excess of GSSG and DTNB was used to minimize the formation of

mixed disulfides between the enzyme and the oxidant. After oxidation, the remaining

ribonucleolytic activity of each sample was determined by monitoring the cleavage of

poly(C).

Oxidation of A5C A6C Variant by Dialysis. Oxidized A5C/A6C RNase A was prepared

in large quantity as follows. The A5C/A6C variant (40 µM) was dialyzed overnight against

0.10 M Tris–HCl buffer (pH 8.0) with bubbling air at ambient temperature. To remove any

dimer formed by intermolecular disulfide bonds, the dialyzed solution was applied to a gel

filtration column that had been equilibrated with 0.050 M sodium acetate buffer (pH 5.0)

containing 0.10 M NaCl. Monomeric protein was applied to a cation–exchange column that

had been equilibrated with 0.050 M sodium acetate buffer (pH 5.0), and protein was eluted

with a gradient of NaCl. One peak in the chromatogram from the cation–exchange column

accounted for >90% of the total protein. The protein in this peak was used for further study.

Carboxymethylation of Oxidized A5C A6C Variant. The completeness of the oxidation

of A5C/A6C RNase A upon dialysis overnight was determined by carboxymethylation.

Iodoacetic acid was neutralized with one equivalent of sodium hydroxide prior to use. The

resulting sodium iodoacetate was added to a final concentration of 0.010 M to A5C/A6C

RNase A that had been oxidized by overnight dialysis. After incubation for 15 min at

ambient temperature, the protein was purified as described above.

Determination of Conformational Stability of A5C A6C Variant. As RNase A is

denatured, its six tyrosine residues become exposed to solvent and its molar absorptivity

near 280 nm decreases significantly. Protein solutions were dialyzed against 0.10 M Tris–

HCl buffer (pH 8.0) with bubbling Ar(g), which prevents oxidation. The dialyzed protein

solutions were sealed in Quartz cuvettes with stopcocks. Conformational stability was

assessed by monitoring the change in absorbance at 286 nm as the temperature was

increased from 20 to 75 °C by 0.2 °C/min.

RESULTS AND DISCUSSION

Design of a Ribonuclease A Variant with a Redox Switch. To minimize the adverse

effect imposed by the engineered cysteines in their reduced state, we selected alanine and

serine residues as mutagenesis targets (Figure 7.2). Ala5 and Ala6 in the N-terminal helix of

RNase A were replaced with cysteine residues to create A5C/A6C RNase A. The α-helix

formed by residues 3–13 contains His12, which is critical for enzymatic activity (Thompson

& Raines, 1995). Thus, a *cis* conformation of the amide bond between Cys5 and Cys6 was

expected to diminish catalysis. Ser15 and Ser16 were also replaced with cysteine residues to

create S15C/S16C RNase A. Ser15 and Ser16 are located in a long surface loop. Because of

the likely flexibility of this loop, disulfide bond formation between the adjacent cysteine

residues in S15C/S16C RNase A was not expected to disturb catalytic activity significantly.

Catalytic Activity of A5C A6C and S15C S16C Variants. The designed variants,

A5C/A6C RNase A and S15C/S16C RNase A, were produced by site-directed mutagenesis.

The extra sulfhydryl groups did not interfere significantly with the proper folding of the

variants. After purification, the activities of the reduced variants were determined with

poly(C) as substrate. The k_{cat} values of A5C/A6C RNase A and S15C/S16C RNase A were ~80% that of wild-type RNase A. The catalytic activities of the variants indicate that the interference caused by the introduced cysteines is negligible when these residues are reduced.

Modulation of Catalytic Activity by Oxidation. Three distinct methods were used to oxidize the engineered variants. Wild-type RNase A and the two variants were oxidized at 50 °C by dissolved $O_2(g)$, GSSG, and DTNB. The catalytic activity of A5C/A6C RNase A decreased to 20% of its initial value, whereas the activities of wild-type RNase A and the S15C/S16C variant were unaffected (Figure 7.3). The efficiencies of the three different oxidation methods were indistinguishable.

To reactivate A5C/A6C RNase A oxidized by GSSG, DTT was added to a final concentration of 1 mM. The variant recovered 52% of its original activity 1 min after adding DTT. In 20 min, the recovered activity reached 61% (Table 7.1). These data suggest that the loss of catalytic activity by oxidized A5C/A6C RNase A results from the formation of a disulfide bond between Cys5 and Cys6 and that the reduction of this disulfide bond leads to the recovery of activity. Still, reactivation was not complete.

Incubation at 50 °C could cause irreversible inactivation of an oxidized variant. Hence, reduced A5C/A6C RNase A was also oxidized at 23 °C by overnight dialysis against an alkaline buffer with bubbling air. After purification, the activity of the oxidized A5C/A6C RNase A was 28% of its original activity. The oxidized A5C/A6C RNase A recovered 80% of its original activity within 1 min when DTT was added to a final concentration of 1 mM.

After incubation with 1 mM DTT for 45 min, the variant recovered full activity (Table 7.1).

Thus, the loss in activity upon oxidation is fully reversible, as expected for the formation (by

oxidation) and reduction of a disulfide bond between the side chains of Cys5 and Cys6

(Figure 7.1).

Verification of Completeness of Oxidation. Carboxymethylation of a sulfhydryl group

adds an extra negative charge to a protein near neutral pH. When oxidized A5C/A6C

RNase A so treated was subjected to cation–exchange chromatography after gel filtration,

only one protein eluted and this protein appeared at the salt concentration at which the

oxidized variant elutes normally. The protein had 32% of the activity of reduced A5C/A6C

RNase A. This activity increased to 105% when DTT was added to 1 mM (Table 7.1). These

activities are virtually identical to those of the oxidized and reactivated variant prepared

without carboxymethylation, indicating that the amount of reduced enzyme is undetectable

after overnight dialysis against alkaline buffer.

Effect of Oxidation on Conformational Stability. The difference in the activities

recovered from a 1-h incubation at 50 °C and from dialysis overnight implied that the

oxidized variant may denature irreversibly at 50 °C (Table 7.1). Thermal denaturation of

reduced and oxidized A5C/A6C RNase A in 0.10 M Tris–HCl buffer (pH 8.0) were

monitored with UV spectroscopy. Reduced A5C/A6C RNase A was observed to have a

well-defined T_m, which is the temperature at the midpoint of the thermal denaturation, of 55

°C. Oxidized A5C/A6C RNase A, however, showed an unusual non-cooperative thermal

denaturation pattern (data not shown), and its T_m could not be determined with a two-state

unfolding model. Moreover, oxidized A5C/A6C RNase A denatures irreversibly at high

temperature. This irreversibility, as well as the inability of the heated, oxidized enzyme to recover full activity (Table 7.1), indicates that the conformational stability of A5C/A6C RNase A has been compromised by oxidation.

Cis–Trans Isomerization of the Peptide Bond between Adjacent Cysteine Residues. The catalytic activity of oxidized A5C/A6C RNase A is ~30% that of the reduced enzyme. This residual activity could result from the interconversion of the *trans* and *cis* isomers of the peptide bond within the eight-membered ring of the oxidized enzyme. An NMR analysis of a heptapeptide with oxidized adjacent cysteines showed that an equilibrium exists between *trans* and *cis* isomers, and that (30 ± 5)% of the oxidized heptapeptide has a *trans* conformation (Sukumaran et al., 1991). Interestingly, this value is similar to the residual activity of the oxidized A5C/A6C RNase A. Nonetheless, this similarity is likely to be a coincidence, as the *cis–trans* equilibrium in a peptide is likely to differ from that in a folded protein. Moreover, it is unlikely that the *trans* isomer of oxidized A5C/A6C RNase A has the same catalytic activity as the reduced variant, as the two have different conformations (Figure 7.1).

Conclusions. Engineering novel disulfide bonds in proteins has been used to increase conformational stability or to regulate enzymatic activity (Perry & Wetzel, 1984; Matsumura & Matthews, 1989; Klink & Raines, 2000). Recently, thiol–disulfide interchange has also been identified as an *in vivo* molecular on–off switch in signal transduction pathways that control gene expression (Kim & Mayfield, 1997; Zheng et al., 1998). Here, we demonstrated that adjacent cysteine residues are also capable of acting as an

on–off redox switch to modulate enzymatic activity. The effectiveness of the regulation by adjacent cysteine residues is sensitive to the structural context of the motif. The adjacent cysteines in A5C/A6C RNase A do indeed modulate enzymatic activity upon oxidation and reduction. In contrast, those in S15C/S16C RNase A do not have any influence, despite their proximity to a critical active-site residue. We anticipate that other contexts could produce an even greater reduction in enzymatic activity.

Table 7.1: Enzymatic Activity of Oxidized and Reactivated A5C/A6C Ribonuclease A Prepared with Different Methods.

Oxidation Method	Enzymatic Activity (Relative)[a]	
	After Oxidation	After Reactivation
1 h at 50 °C with GSSG	19%	61%
Overnight dialysis at 23 °C	28%	100%
Carboxymethylation after overnight dialysis	32%	105%

[a]Enzymatic activity was determined with 0.12 mM poly(C) in 0.10 M MES–NaOH buffer (pH 6.0) containing 0.10 M NaCl. Relative activity is the ratio of activity remaining to that before oxidation.

Figure 7.1   Depiction of adjacent cysteine residues in a model peptide, AcCysCysNH$_2$,

as a redox switch. The structure of reduced AcCysCysNH$_2$ is based on the ϕ

and ψ main-chain dihedral angles of Ala5 and Ala6 in crystalline

ribonuclease A (PDB entry 1RCN). The structures of oxidized

AcCysCysNH$_2$ have a trans or cis peptide bond, and are depicted in a

conformation of minimal energy according to the MMFF94 force field in

MacSpartan Pro v1.3.5 (Wavefunction, Irvine, CA). The *trans* and *cis* forms

have C$^\beta$SSC$^\beta$ dihedral angles of $-84°$ and $+80°$, respectively. The green bars

denote the direction of the peptide chain as it extends from C$^\alpha$ of each

cysteine residue.

reduced   oxidation / reduction   trans   +   cis
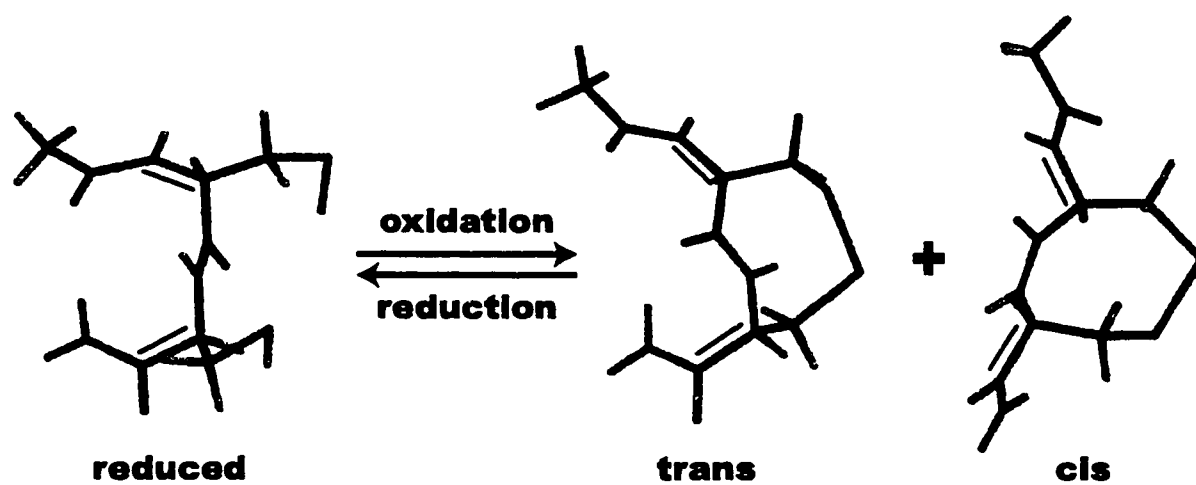
Figure 7.2   *N*-Terminal amino acid sequence of wild-type ribonuclease A and the

A5C/A6C and S15C/S16C variants. The engineered adjacent cysteine

residues and His12, a critical active-site residue, are underlined. Residues 3–

13, which form an α-helix, are in bold-faced type.

```
                                              1               2
                                 12345678901234567890
Wild-type RNase A                KETAAAKFERQHMDSSTSAA...
A5C/A6C RNase A                  KETACCKFERQHMDSSTSAA...
S15C/S16C RNase A                KETAAAKFERQHMDCCTSAA...
```

Figure 7.3   Effect of oxidation on the ribonucleolytic activity of wild-type RNase A and

the A5C/A6C and S15C/S16C variants. Each enzyme (10 nM) was incubated

at 50 °C for 1 h with dissolved oxygen (hatched), oxidized glutathione (20

nM; solid), or dithionitrobenzoic acid (20 nM; horizontal strip) as an oxidant.

Remaining activities were determined with 0.12 mM poly(C) as substrate in

0.10 M MES–NaOH buffer (pH 6.0) containing 0.10 M NaCl. The relative

activities are the ratios of the remaining activities to the original activities

determined before oxidation.
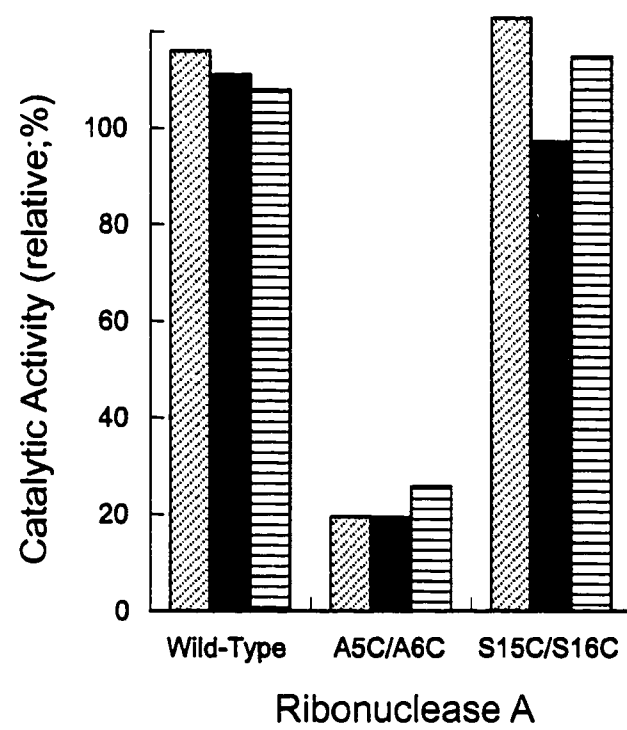
BIBLIOGRAPHY

Adinolfi, S., Piccoli, R., Sica, F. & Mazzarella, L. (1996). BS-RNase tetramers: An example of domain-swapped oligomers. *FEBS Lett.* **398**(2-3), 326-332.

Alberghina, L., Ed. (1999). *Protein Engineering in Industrial Biotechnology.* Newark, NJ: Gordon & Breach Science.

Alberty, R. A. & Bloomfield, V. (1963). Multiple intermediates in steady state enzyme kinetics. *J. Biol. Chem.* **238**, 2804-2810.

Albery, W. J. & Knowles, J. R. (1976). Evolution of enzyme funciton and the development of catalytic efficiency. *Biochemistry* **15**, 5631-5640.

American Institute of Physics. (1972). *American Institute of Physics Handbook* (Gray, D. E., Ed.), McGraw-Hill, New York.

Anderson, D. E., Becktel, W. J. & Dahlquist, F. W. (1990). pH-induced denaturation of proteins: A single salt bridge contributes 3–5 kcal/mol to the free energy of folding of T4 lysozyme. *Biochemistry* **29**(9), 2403-2408.

Anfinsen, C. B. (1973). Principles that govern the folding of protein chains. *Science* **181**, 223-230.

Anslyn, E. & Breslow, R. (1989). On the mechanism of catalysis by ribonuclease: cleavage and isomerization of the dinucleotide UpU catalyzed by imidazole buffers. *J. Am. Chem. Soc.* **111**, 4473-4482.

Atkins, P. W. (1990). *Physical chemistry*, Oxford University Press, Oxford, U.K.

Barnard, E. A. (1969). Biological function of pancreatic ribonuclease. *Nature* **221**, 340-344.

Beaven, G. H., Holiday, E. R. & Johnson, E. A. (1955). Optical properties of nucleic acids and thier components. In *The Nucleic Acids: Chemistry and Biology* (Chargaff, E. & Davison, J. D., eds.), Vol. 1, pp. 493-553. 3 vols. Academic Press, New York.

Bennett, M. J., Schlunegger, M. P. & Eisenberg, D. (1995). 3D domain swapping: A mechanism for oligomer assembly. *Protein Sci.* **4**(12), 2455-2468.

Berg, O. G. & von Hippel, P. H. (1985). Diffusion-controlled macromolecular interactions. *Annu. Rev. Biophys. Biophys. Chem.* **14**, 131-160.

Blake, C. C., Ghosh, M., Harlos, K., Avezoux, A. & Anthony, C. (1994). The active site of methanol dehydrogenase contains a disulphide bridge between adjacent cysteine residues. *Nat. Struct. Biol.* 1(2), 102-105.

Boix, E., Nogues, M. V., Schein, C. H., Benner, S. A. & Cuchillo, C. M. (1994). Reverse transphosphorylation by ribonuclease A needs an intact P2-binding site. Point mutations at Lys-7 and Arg-10 alter the catalytic properties of the enzyme. *J. Biol. Chem.* 269(4), 2529-2534.

Boix, E., Wu, Y., Vasandani, V. M., Saxena, S. K., Ardelt, W., Ladner, J. & Youle, R. J. (1996). Role of the N-terminus in RNase A homologues: Differences in catalytic activity, ribonuclease inhibitor interaction and cytotoxicity. *J. Mol. Biol.* 257, 992-1007.

Borkakoti, N., Moss, D. S. & Palmer, R. A. (1982). Ribonuclease A: Least squares refinement of structure at 1.45 Å resolution. *Acta Crystallogr.* B38, 2210-2217.

Brocklehurst, K. (1994). A sound basis for pH-dependent kinetic studies on enzymes. *Protein Eng.* 7(3), 291-299.

Burbaum, J. J., Raines, R. T., Albery, W. J. & Knowles, J. R. (1989). Evolutionary optimization of the catalytic effectiveness of an enzyme. *Biochemistry* 28, 9293-9305.

Cacace, M. G., Landau, E. M. & Ramsden, J. J. (1997). The Hofmeister series: Salt and solvent effects on interfacial phenomenon. *Q. Rev. Biophys.* 30, 241-277.

Cafaro, V., Bracale, A., Di Maro, A., Sorrentino, S., D'Alessio, G. & Di Donato, A. (1998). New muteins of RNase A with enhanced antitumor action. *FEBS Lett.* 437(1-2), 149-152.

Cafaro, V., De Lorenzo, C., Piccoli, R., Bracale, A., Mastronicola, M. R., Di Donato, A. & D'Alessio, G. (1995). The antitumor action of seminal ribonuclease and its quaternary conformations. *FEBS Lett.* 359(1), 31-34.

Cambillau, C., Roussel, A., Inisan, A. G. & Knoops-Mouthay, E. (1997). TURBO-FRODO OpenGL.1 edit. CNRS/Universite Aix-Marseille II, Marseille, France.

Carbeck, J. D., Colton, I. J., Gao, J. & Whitesides, G. M. (1998). Protein charge ladders, capillary electrophoresis, and the role of electrostatics in biomolecular recognition. *Acc. Chem. Res.* 31, 343-350.

Carroll, S. F., Barbieri, J. T. & Collier, R. J. (1988). Diphtheria toxin: Purification and properties. *Methods Enzymol.* 165, 68-76.

Chandrasekaran, R. & Balasubramanian, R. (1969). Stereochemical studies of cyclic peptides: VI. Energy calculation of the cyclic disulfide cysteinylcysteine. *Biochim. Biophys. Acta* **188**, 1-9.

Ciglic, M. I., Jackson, P. J., Raillard, S. A., Haugg, M., Jermann, T. M., Opitz, J. G., Trabesinger-Ruf, N. & Benner, S. A. (1998). Origin of dimeric structure in the ribonuclease superfamily. *Biochemistry* **37**(12), 4008-4022.

Cleland, J. L. & Craik, C. S., Eds. (1996). *Protein Engineering: Principles and Practice.* New York: Wiley–Liss.

Cleland, W. W. (1979). Substrate inhibition. *Methods Enzymol.* **63**, 500-513.

Cleland, W. W. (1982). The use of pH studies to determine chemical mechanisms of enzyme-catalyzed reactions. *Methods Enzymol.* **87**, 390-405.

Cleland, W. W. (1986). Enzyme kinetics as a tool for determination of enzyme mechanisms. In *Investigations of rates and mechanisms of reactions* 4th edit. (Bernasconi, C. F., ed.), Vol. 6, pp. 791-870. John Wiley & Sons, New York.

Crestfield, A. M. & Stein, W. H. (1963). Alkylation and identification of the histidine residues at the active site of ribonuclease. *J. Biol. Chem.* **238**, 2413.

Crestfield, A. M., Stein, W. H. & Moore, S. (1962). On the aggregation of bovine pancreatic ribonuclease. *Arch. Biochem. Biophys.* **Supplement 1**, 217-222.

Crestfield, A. M., Stein, W. H. & Moore, S. (1963). Properties and conformaiton of the histidine residues at the active site of ribonuclease. *J. Biol. Chem.* **238**(7), 2421-2428.

D'Alessio, G. (1995). Oligomer evolution in action? *Nat. Struct. Biol.* **2**(1), 11-13.

D'Alessio, G. (1999a). Evolution of oligomeric proteins. The unusual case of a dimeric ribonuclease. *Eur. J. Biochem.* **266**(3), 699-708.

D'Alessio, G. (1999b). The evolutionary transition from monomeric to oligomeric proteins: Tools, the environment, hypotheses. *Prog. Biophys. Mol. Biol.* **72**(3), 271-298.

D'Alessio, G., Di Donato, A., Mazzarella, L. & Piccoli, R. (1997). Seminal ribonuclease: The importance of diversity. In *Ribonuclease: Structures and function* (D'Alessio, G. & Riordan, J., eds.), pp. 383-423. Academic Press, New York.

D'Alessio, G. & Riordan, J. F. (1997). *Ribonucleases: Structure and Functions*, Academic Press, New York.

Davis, F. F. & Allen, F. W. (1955). The action of ribonuclease on synthetic substrates. *J. Biol. Chem.* **217**, 13-21.

del Rosario, E. J. & Hammes, G. G. (1969). Kinetic and equilibrium studies of the ribonuclease-catalyzed hydrolysis of uridine 2',3'-cyclic phosphate. *Biochemistry* **8**, 1884-1889.

delCardayré, S. B. & Raines, R. T. (1994). Structural determinants of enzymatic processivity. *Biochemistry* **33**, 6032-6037.

delCardayré, S. B. & Raines, R. T. (1995). A residue–residue hydrogen bond mediates the specificity of ribonuclease A. *J. Mol. Biol.* **252**, 328-336.

delCardayré, S. B., Ribo, M., Yokel, E. M., Quirk, D. J., Rutter, W. J. & Raines, R. T. (1995). Engineering ribonuclease A: Production, purification, and characterization of wild-type enzyme and mutants at Gln11. *Protein Eng.* **8**(3), 261-273.

delCardayré, S. B., Thompson, J. T. & Raines, R. T. (1994). Altering substrate specificity and detecting processivity in nucleases. In *Techniques in Protein Chemistry V* (Crabb, J. W., ed.), pp. 313-320. Academic Press, San Diego, CA.

Di Cera, E., Guinto, E. R., Vindigni, A., Dang, Q. D., Ayala, Y. M., Wuyi, M. & Tulinsky, A. (1995). The Na^+ binding site of thrombin. *J. Biol. Chem.* **270**(38), 22089-22092.

Di Donato, A., Cafaro, V. & D'Alessio, G. (1994). Ribonuclease A can be transformed into a dimeric ribonuclease with antitumor activity. *J. Biol. Chem.* **269**, 17394-17396.

Di Donato, A., Cafaro, V., Romeo, I. & D'Alessio, G. (1995). Hints on the evolutionary design of a dimeric RNase with special bioactions. *Protein Sci.* **4**(8), 1470-1477.

Dickman, S. R., Aroskar, J. P. & Kropf, R. B. (1956). Activation and inhibition of beef pancreas ribonuclease. *Biochem. Biophys. Acta* **21**, 539-545.

Dickman, S. R. & Ring, B. (1958). Effects of ionic strength on ribonucleic acid structure and ribonulclease activity. *J. Biol. Chem.* **231**, 741-750.

Edelhoch, H. & Coleman, J. (1956). The kinetics of the enzymatic hydrolysis of ribonucleic acid. *J. Biol. Chem.* **219**, 351-363.

Eftink, M. R. & Biltonen, R. L. (1983a). Energetics of ribonuclease A catalysis. 1. pH, ionic strength, and solvent isotope dependence of the hydrolysis of cytidine cyclic 2',3'-phosphate. *Biochemistry* **22**, 5123-5134.

Eftink, M. R. & Biltonen, R. L. (1983b). Energetics of ribonuclease A catalysis. 3. Temperature dependence of the hydrolysis of cytidine cyclic 2',3'-phosphate. *Biochemistry* 22(22), 5140-5150.

Eftink, M. R. & Biltonen, R. L. (1987). Pancreatic ribonuclease A: The most studied endoribonuclease. In *Hydrolytic Enzymes* (Neuberger, A. & Brocklehurst, K., eds.), pp. 333-375. Elsevier, New York.

Ellis, K. J. & Morrison, J. F. (1982). Buffers of constant ionic strength for studying pH-dependent processes. *Methods Enzymol.* 87, 405-426.

Fersht, A. (1985). *Enzyme Structure and Mechanism*, Freeman, New York.

Findlay, D., Herries, D. G., Mathias, A. P., Rabin, B. R. & Ross, C. A. (1961). The active site and mechanism of action of bovine pancreatic ribonuclease. *Nature* 190, 781-784.

Fisher, B. M., Grilley, J. E. & Raines, R. T. (1998a). A new remote subsite in ribonuclease A. *J. Biol. Chem.* 273(51), 34134-34138.

Fisher, B. M., Ha, J.-H. & Raines, R. T. (1998b). Coulombic forces in protein-RNA interactions: Binding and cleavage by ribonuclease A and variants at Lys7, Arg10 and Lys66. *Biochemistry* 37(35), 12121-12132.

Fisher, B. M., Schultz, L. W. & Raines, R. T. (1998c). Coulombic effects of remote subsites on the active site of ribonuclease A. *Biochemistry* 37(50), 17386-17401.

Flogel, M., Albert, A. & Biltonen, R. L. (1975). The magnitude of electrostatic interactions in inhibitor binding and during catalysis by ribonuclease A. *Biochemistry* 14(12), 2616-2621.

Flogel, M. & Biltonen, R. L. (1975a). Calorimetric and potentiometric characterization of the ionization behavior of ribonuclease A and its complex with 3'-cytosine monophosphate. *Biochemistry* 14(12), 2603-2609.

Flogel, M. & Biltonen, R. L. (1975b). The pH dependence of the thermodynamics of the interaction of 3'- cytidine monophosphate with ribonuclease A. *Biochemistry* 14(12), 2610-2615.

Fontecilla-Camps, J. C., de Llorens, R., le Du, M. H. & Cuchillo, C. M. (1994). Crystal structure of ribonuclease A•d(ApTpApApG) complex. *J. Biol. Chem.* 269, 21526-21531.

Fridovich, I. (1963). Inhibition of acetoacetic decarboxylase by anions: The Hofmeister lyotropic series. *J. Biol. Chem.* 238(2), 592-598.

Garcia-Echeverría, C. & Rich, D. H. (1997). Solution conformations of the cyclic Cys=Cys disulfide strucutural motif. In *Peptides—Chemistry, Structure, and Biology: Proceedings of theThe thirteenth American Peptide Symposium* (Hodges, R. S. & Smith, J. A., eds.), pp. 782-784. Kluwer Academic, Norwell, MA.

Getzoff, E. D., Cabelli, D. E., Fisher, C. L., Parge, H. E., Viezzoli, M. S., Banci, L. & Hallewell, R. A. (1992). Faster superoxide dismutase mutants designed by enhancing electrostatic guidance. *Nature* **358**(6384), 347-351.

Goldberg, J. M. & Baldwin, R. L. (1998). Kinetic mechanism of a partial folding reaction. 1. Properties of the reaction and effects of denaturants. *Biochemistry* **37**(8), 2546-2555.

Gotte, G. & Libonati, M. (1998). Two different forms of aggregated dimer of ribonuclease A. *Biochim. Biophys. Acta* **1386**, 106-112.

Gould, S. J. (1977). *Ever since Darwin: Reflections in Natural History*, W.W. Norton & Company, New York.

Graziano, G., Catanzano, F., Giancola, C. & Barone, G. (1996). DSC study of the thermal stability of S-protein and S-peptide/S-protein. *Biochemistry* **35**(41), 13386-13392.

Grimsley, G. R., Shaw, K. L., Fee, L. R., Alston, R. W., Huyghues-Despointes, B. M., Thurlkill, R. L., Scholtz, J. M. & Pace, C. N. (1999). Increasing protein stability by altering long-range coulombic interactions. *Protein Sci.* **8**(9), 1843-1849.

Hamachi, I., Eboshi, R., Watanabe, J. & Shinkai, S. (2000). Guest-induced umpolung on a protein surface: A strategy for regulation of enzymatic activity. *J. Am. Chem. Soc.* **122**(18), 4530-4531.

Harber, E. & Anfinsen, C. A. (1961). Regeneration of enzyme activity by air oxidation of reduced subtilisin-modified ribonuclease. *J. Biol. Chem.* **236**, 422-426.

Herries, D. G., Mathias, A. P. & Rabin, B. R. (1962). The active site and mechanism of action of bovine pancreatic ribonuclease: 3. The pH-dependence of the kinetic parameters for the hydrolysis of cytidine 2',3'-phosphate. *Biochem. J.* **85**, 127-134.

Herschlag, D. (1994). Ribonuclease revisited: Catalysis via the classical genera acid–base mechanism or a triester-like mechanism. *J. Am. Chem. Soc.* **116**, 11631-11635.

Highbarger, L. A., Gerlt, J. A. & Kenyon, G. L. (1996). Mechanism of the reaction catalyzed by acetoacetate decarboxylase. Importance of lysine 116 in determining the pK_a of active-site lysine 115. *Biochemistry* **35**(1), 41-46.

Honig, B. & Nicholls, A. (1995). Classical electrostatics in biology and chemistry. *Science* **268**(5214), 1144-1149.

Hummel, C. F., Pincus, M. R., Brandt-Rauf, P. W., Frei, G. M. & Carty, R. P. (1987). Reaction of (bromoacetamido)nucleoside affinity labels with ribonuclease A: Evidence for steric control of reaction specificity and alkylation rate. *Biochemistry* **26**, 135-146.

Irie. M. (1965). Effects of salts on the reaction of bovine pancreatic ribonuclease. *J. Biochem (Tokyo)* **57**, 355-362.

Jackson, D. Y., Burnier, J., Quan, C., Stanley, M., Tom, J. & Wells, J. A. (1994). A designed peptide ligase for total synthesis of ribonuclease A with unnatural catalytic residues. *Science* **266**, 243-247.

Jackson, S. E. & Fersht, A. R. (1993). Contribution of long-range electrostatic interactions to the stabilization of the catalytic transition state of the serine protease subtilisin BPN'. *Biochemistry* **32**(50), 13909-13916.

Jencks, W. P. (1987). *Catalysis in Chemistry and Enzymology*, Dover, Mineola, NY.

Jensen, D. E. & von Hippel, P. H. (1976). DNA "melting" proteins. *J. Biol. Chem.* **251**, 7198-7214.

Kabsch, W. (1988). Evaluation of single-crystal X-ray-diffraction data from a position-sensitive detector. *J. Appl. Crystallogr.* **21**, 916-924.

Kabsch, W. (1998). Automatic-indexing of rotation diffraction patterns. *J. Appl. Crystallogr.* **21**, 67-71.

Kalnitsky, G., Hummel, J. P., Resnick, H., Carter, J. R., Barnett, L. B. & Dierks, C. (1959). The relation of structure to enzymatic activity in ribonuclease. *Ann. N. Y. Acad. Sci.* **81**, 541-566.

Kao, C. M., Pieper, R., Cane, D. E. & Khosla, C. (1996). Evidence for two catalytically independent clusters of active sites in a functional modular polyketide synthase. *Biochemistry* **35**(38), 12363-12368.

Kao, P. N. & Karlin, A. (1986). Acetylcholine receptor binding site contains a disulfide cross-link between adjacent half-cystinyl residues. *J. Biol. Chem.* **261**(18), 8085-8088.

Kartha, G., Bello, J. & Harker, D. (1967). Tertiary structure of ribonuclease. *Nature* **213**, 862-865.

Kelemen, B. R., Klink, T. A., Behlke, M. A., Eubanks, S. R., Leland, P. A. & Raines, R. T. (1999). Hypersensitive substrate for ribonucleases. *Nucleic Acids Res.* **27**, 3696-3701.

Kelemen, B. R., Schultz, L. W., Sweeney, R. Y. & Raines, R. T. (2000). Excavating an active site: The nucleobase specificity of ribonuclease A. *Biochemistry*, In Press.

Kim, B.-M., Schultz, L. W. & Raines, R. T. (1999). Variants of ribonuclease inhibitor that resist oxidation. *Protein Sci.* **8**(2), 430-434.

Kim, J. & Mayfield, S. P. (1997). Protein disulfide isomerase as a regulator of chloroplast translational activation. *Science* **278**(5345), 1954-1957.

Kim, J.-S., Soucek, J., Matousek, J. & Raines, R. T. (1995a). Catalytic activity of bovine seminal ribonuclease is essential for its immunosuppressive and other biological activities. *Biochem. J.* **308**, 547-550.

Kim, J.-S., Soucek, J., Matousek, J. & Raines, R. T. (1995b). Structural basis for the biological activities of bovine seminal ribonuclease. *J. Biol. Chem.* **270**, 10525-10530.

Klink, T. A. & Raines, R. T. (2000). Conformational stability is a determinant of ribonuclease A cytotoxicity. *J. Biol. Chem.* **275**(23), 17463-17467.

Klug, D., Rabani, J. & Fridovich, I. (1972). A direct demonstration of the catalytic action of superoxide dismutase through the use of pulse radiolysis. *J. Biol. Chem.* **247**(15), 4839-4842.

Knowles, J. R. (1976). The intrinsic pK_a-values of functional groups in enzymes: Improper deductions from the pH-dependence of steady-state parameters. *CRC Crit. Rev. Biochem.* **4**(2), 165-173.

Knowles, J. R. & Albery, W. J. (1977). Perfection in enzyme catalysis: The energetics of triosephosphate isomerase. *Acc. Chem. Res.* **10**, 105-111.

Kraulis, P. J. (1991). MOLSCRIPT: A program to produce both detailed and schematic plots of protein structures. *J. Appl. Crystallogr.* **24**, 946-950.

Kunkel, T. A., Roberts, J. D. & Zakour, R. A. (1987). Rapid and efficient site-specific mutagenesis without phenotypic selection. *Methods Enzymol.* **154**, 367-382.

Larimer, F. W., Lee, E. H., Mural, R. J., Soper, T. S. & Hartman, F. C. (1987). Intersubunit location of the active site of ribulose-bisphosphate carboxylase/oxygenase as determined by in vivo hybridization of site-directed mutants. *J. Biol. Chem.* **262**(32), 15327-15329.

Larsen, T. M., Laughlin, L. T., Holden, H. M., Rayment, I. & Reed, G. H. (1994). Structure of rabbit muscle pyruvate kinase complexed with Mn^{2+}, K^+, and pyruvate. *Biochemistry* 33(20), 6301-6309.

Li, Y., Feng, L. & Kirsch, J. F. (1997). Kinetic and spectroscopic investigations of wild-type and mutant forms of apple 1-aminocyclopropane-1-carboxylate synthase. *Biochemistry* 36(49), 15477-15488.

Libonati, M. & Sorrentino, S. (1992). Rivisiting the action of bovine ribonuclease A and pancreatic-type ribonucleases on double-stranded RNA. *Mol. Cell. Biochem.* 117, 139-151.

Liu, Y., Hart, P. J., Schlunegger, M. P. & Eisenberg, D. (1998). The crystal structure of a 3D domain-swapped dimer of RNase A at a 2.1 Å resolution. *Proc. Natl. Acad. Sci. U.S.A.* 95(7), 3437-3442.

Lohman, T. M. (1986). Kinetics of protein-nucleic acid interactions: Use of salt effects to probe mechanisms of interaction. *CRC Crit. Rev. Biochem.* 19(3), 191-245.

Loladze, V. V., Ibarra-Molero, B., Sanchez-Ruiz, J. M. & Makhatadze, G. I. (1999). Engineering a thermostable protein via optimization of charge–charge interactions on the protein surface. *Biochemistry* 38(50), 16419-16423.

Markley, J. L. & Finkenstadt, W. R. (1975). Correlation proton magnetic resonance studies at 250 MHz of bovine pancreatic ribonuclease. III. Mutual electrostatic interaction between histidine residues 12 and 119. *Biochemistry* 14(16), 3562-3566.

Matsumura, M. & Matthews, B. W. (1989). Control of enzyme activity by an engineered disulfide bond. *Science* 243(4892), 792-794.

Matta, M. S. & Vo, D. T. (1986). Proton inventory of the second step of ribonuclease catalysis. *J. Am. Chem. Soc.* 108, 5316-5318.

Mayr, L. M. & Schmid, F. X. (1993). Stabilization of a protein by guanidinium chloride. *Biochemistry* 32(31), 7994-7998.

Mazzarella, L., Capasso, S., Demasi, D., Di Lorenzo, G., Mattia, C. A. & Zagari, A. (1993). Bovine seminal ribonuclease: Structure at 1.9 Å resolution. *Acta Crystallogr.* D49, 389-402.

McPherson, A., Brayer, G., Cascio, D. & Williams, R. (1986). The mechanism of binding of a polynucleotide chain to pancreatic ribonuclease. *Science* 232, 765-768.

Merrifield, R. B. (1984). Solid phase synthesis. *Science* 232, 341-347.

Messmore, J. M. (1999). Ph.D. Thesis, University of Wisconsin-Madison.

Messmore, J. M., Fuchs, D. N. & Raines, R. T. (1995). Ribonuclease A: Revealing structure–function relationships with semisynthesis. *J. Am. Chem. Soc.* 117(31), 8057-8060.

Messmore, J. M., Holmgren, S. K., Grilley, J. E. & Raines, R. T. (2000). Sulfur shuffle: Modulating enzymatic activity by thiol–disulfide interchange. *Bioconjug. Chem.* 11(3), 408-413.

Miller, S. M., Moore, M. J., Massey, V., Williams, C. H., Jr., Distefano, M. D., Ballou, D. P. & Walsh, C. T. (1989). Evidence for the participation of Cys558 and Cys559 at the active site of mercuric reductase. *Biochemistry* 28(3), 1194-1205.

Moore, S. & Stein, W. H. (1973). Chemical structures of pancreatic ribonuclease and deoxyribonuclease. *Science* 180, 458-464.

Mosckovitz, R. & Gershoni, J. M. (1988). Three possible disulfides in the acetylcholine receptor alpha-subunit. *J. Biol. Chem.* 263(2), 1017-1022.

Moussaoui, M., Guasch, A., Boix, E., Cuchillo, C. M. & Nogués, M. V. (1995). The role of non-catalytic binding subsites in the endonuclease activity of bovine pancreatic ribonuclease A. *J. Biol. Chem.* 271(9), 4687-3692.

Munico, A. M. & Miras-Portugal, M. T., Eds. (1996). *Cell Signal Transduction, Second Messengers, and Protein Phosphorylation in Health and Disease.* Dordreicht, The Netherlands: Plenum.

Nogues, M. V., Moussaoui, M., Boix, E., Vilanova, M., Ribo, M. & Cuchillo, C. M. (1998). The contribution of noncatalytic phosphate-binding subsites to the mechanism of bovine pancreatic ribonuclease A. *Cell. Mol. Life Sci.* 54(8), 766-774.

Nolte, H. J., Rosenberry, T. L. & Neumann, E. (1980). Effective charge on acetylcholinesterase active sites determined from the ionic strength dependence of association rate constants with cationic ligands. *Biochemistry* 19(16), 3705-3711.

Northrup, S. H., Boles, J. O. & Reynolds, J. C. (1988). Brownian dynamics of cytochrome c and cytochrome c peroxidase association. *Science* 241(4861), 67-70.

Park, C., Kelemen, B. R., Klink, T. A., Sweeney, R. Y., Behlke, M. A., Eubanks, S. R. & Raines, R. T. (2000). Fast, facile, and hypersensitive Assays for ribonucleolytic activity. *Methods in Enzymol.*, In Press.

Park, C. & Raines, R. T. (2000a). Dimer formation by a 'monomeric' protein. *Protein Sci.* 9, 2026-2033.

Park, C. & Raines, R. T. (2000b). Origin of the "inactivation" of ribonuclease A at low salt concentration. *FEBS Lett.* **468**, 199-202.

Park, C. & Raines, R. T. (2001). Quantitative analysis of the effects of salt concentration on enzymatic catalysis. *Biochemistry*, In Preparation.

Park, C., Schultz, L. W. & Raines, R. T. (2001). Contribution of the active-site histidine residues of ribonuclease A to nucleic acid binding. *Biochemistry*, In Preparation.

Perl, D., Mueller, U., Heinemann, U. & Schmid, F. X. (2000). Two exposed amino acid residues confer thermostability on a cold shock protein. *Nat. Struct. Biol.* **7**(5), 380-383.

Perry, L. J. & Wetzel, R. (1984). Disulfide bond engineered into T4 lysozyme: Stabilization of the protein toward thermal inactivation. *Science* **226**(4674), 555-557.

Perutz, M. F. (1978). Electrostatic effects in proteins. *Science* **201**, 1187-1191.

Piccoli, R., Di Gaetano, S., De Lorenzo, C., Grauso, M., Monaco, C., Spalletti-Cernia, D., Laccetti, P., Cinatl, J., Matousek, J. & D'Alessio, G. (1999). A dimeric mutant of human pancreatic ribonuclease with selective cytotoxicity toward malignant cells. *Proc. Natl. Acad. Sci. U.S.A.* **96**(14), 7768-7773.

Piccoli, R., Tamburrini, M., Piccialli, G., Di Donato, A., Parente, A. & D'Alessio, G. (1992). The dual-mode quaternary structure of seminal RNase. *Proc. Natl. Acad. Sci. U.S.A.* **89**, 1870-1874.

Pörschke, D. (1978). Thermodynamic and kinetic parameters of oligonucleotide-oligopeptide interactions. Specificity of arginine•inosine association. *Eur. J. Biochem.* **86**(1), 291-299.

Pörschke, D. (1979). The mode of Mg^{++} binding to oligonucleotides. Inner sphere complexes as markers for recognition? *Nucleic Acids Res.* **6**(3), 883-898.

Quinn, D. M. & Sutton, L. D. (1991). Theoretical basis and mechanistic utility of solvent isotope effects. In *Enzyme mechanism from isotope effects* (Cook, P. F., ed.), pp. 73-126. CRC Press, Boca Raton, FL.

Quirk, D. J., Park, C., Thompson, J. E. & Raines, R. T. (1998). His...Asp catalytic dyad of ribonuclease A: Conformational stability of the wild-type, D121N, D121A, and H119A enzymes. *Biochemistry* **37**(51), 17958-17964.

Quirk, D. J. & Raines, R. T. (1999). His...Asp catalytic dyad of ribonuclease A: Histidine pK_a values in the wild-type, D121N, and D121A enzymes. *Biophys. J.* **76**(3), 1571-1579.

Radzicka, A. & Wolfenden, R. (1995). A proficient enzyme. *Science* **267**, 90-92.

Raines, R. T. (1998). Ribonuclease A. *Chem. Rev.* **98**(3), 1045-1066.

Record, M. T., Jr., Lohman, M. L. & De Haseth, P. (1976). Ion effects on ligand–nucleic acid interactions. *J. Mol. Biol.* **107**(2), 145-158.

Record, M. T., Jr., Zhang, W. & Anderson, C. F. (1998). Analysis of effects of salts and uncharged solutes on protein and nucleic acid equilibria and processes: A practical guide to recognizing and interpreting polyelectrolyte effects, Hofmeister effects, and osmotic effects of salts. *Adv. Protein. Chem.* **51**, 281-353.

Richards, F. M. (1955). Titration of amino groups released during the digestion of ribonuclease by subtilisin. *C. R. Trav. Lab Carlsberg Ser. Chim.* **29**, 322-328.

Richards, F. M. & Vithayathil, P. J. (1959). The preparation of subtilisin-modified ribonuclease and the separation of the peptide and protein components. *J. Biol. Chem.* **234**, 1459-1465.

Richards, F. M. & Wyckoff, H. W. (1971). Bovine pancreatic ribonuclease. In *The Enzymes* (Boyer, P. D., ed.), Vol. IV, pp. 647-806. Academic Press, New York.

Roberts, G. C. K., Dennis, E. A., Meadows, D. H., Cohen, J. S. & Jardetsky, O. (1969). The mechanism of action of ribonuclease. *Proc. Natl. Acad. Sci. U.S.A.* **62**, 1151-1158.

Russo, N., Antignani, A. & D'Alessio, G. (2000). In vitro evolution of a dimeric variant of human pancreatic ribonuclease. *Biochemistry* **39**(13), 3585-3591.

Russo, N. & Shapiro, R. (1999). Potent inhibition of mammalian ribonucleases by 3', 5'-pyrophosphate-linked nucleotides. *J. Biol. Chem.* **274**(21), 14902-14908.

Schlunegger, M. P., Bennett, M. J. & Eisenberg, D. (1997). Oligomer formation by 3D domain swapping: A model for protein assembly and misassembly. *Adv. Protein. Chem.* **50**, 61-122.

Schreiber, G. & Fersht, A. R. (1996). Rapid, electrostatically assisted association of proteins. *Nat. Struct. Biol.* **3**(5), 427-431.

Schultz, L. W., Quirk, D. J. & Raines, R. T. (1998). His...Asp catalytic dyad of ribonuclease A: Structure and function of the wild-type, D121N, and D121A enzymes. *Biochemistry* **37**(25), 8886-8898.

Sefton, B. M. & Hunter, T., Eds. (1998). *Protein Phosphorylation.* New York: Academic Press.

Sela, M., Anfinsen, C. B. & Harrington, W. F. (1957). The correlation of ribonuclease activity with specific aspects of tertiary structure. *Biochim. Biophys. Acta* **26**, 502-512.

Sharp, K., Fine, R. & Honig, B. (1987). Computer simulations of the diffusion of a substrate to an active site of an enzyme. *Science* **236**(4807), 1460-1463.

Shoemaker, K. R., Fairman, R., Kim, P. S., York, E. J., Stewart, J. M. & Baldwin, R. L. (1987). The C-peptide helix from ribonuclease A considered as an autonomous folding unit. *Cold Spring Harb. Symp. Quant. Biol.* **52**, 391-398.

Sorrentino, S., Barone, R., Bucci, E., Gotte, G., Russo, N., Libonati, M. & D'Alessio, G. (2000). The two dimeric forms of RNase A. *FEBS Lett.* **466**(1), 35-39.

Sowa, G. A., Hengge, A. C. & Cleland, W. W. (1997). ^{18}O Isotope effects support a concerted mechanism for ribonuclease A. *J. Am. Chem. Soc.* **119**, 2319-2320.

Spector, S., Wang, M., Carp, S. A., Robblee, J., Hendsch, Z. S., Fairman, R., Tidor, B. & Raleigh, D. P. (2000). Rational modification of protein stability by the mutation of charged surface residues. *Biochemistry* **39**(5), 872-879.

Stowell, J. K., Widlanski, T. S., Kutateladze, T. G. & Raines, R. T. (1995). Mechanism-based inactivation of ribonuclease A. *J. Org. Chem.* **60**, 6930-6936.

Suelter, C. H. (1970). Enzymes activated by monovalent cations. *Science* **168**(933), 789-795.

Sukumaran, D., Prorok, M. & Lawrence, D. (1991). A molecular constraint that generates a cys peptide bond. *J. Am. Chem. Soc.* **113**, 706-707.

Tanford, C. (1961). *Physical Chemistry of Macromolecules*, John Wiley & Sons, New York.

Thompson, J. E. (1995). Ph. D. Thesis, University of Wisconsin-Madison.

Thompson, J. E., Kutateladze, T. G., Schuster, M. C., Venegas, F. D., Messmore, J. M. & Raines, R. T. (1995). Limits to catalysis by ribonuclease A. *Bioorg. Chem.* **23**, 471-481.

Thompson, J. E. & Raines, R. T. (1995). Value of general acid-base catalysis to ribonuclease A. *J. Am. Chem. Soc.* **116**, 5467-5467.

Thompson, J. E., Venegas, F. D. & Raines, R. T. (1994). Energetics of catalysis by ribonucleases: Fate of the 2',3'-cyclic intermediate. *Biochemistry* **33**, 7408-7414.

Tipton, K. F. & Dixon, H. B. (1979). Effects of pH on enzymes. *Methods Enzymol.* **63**, 183-234.

Tobias, K. E. & Kahana, C. (1993). Intersubunit location of the active site of mammalian ornithine decarboxylase as determined by hybridization of site-directed mutants. *Biochemistry* **32**(22), 5842-5847.

Toney, M. D., Hohenester, E., Cowan, S. W. & Jansonius, J. N. (1993). Dialkylglycine decarboxylase structure: Bifunctional active site and alkali metal sites. *Science* **261**(5122), 756-759.

Tronrud, D. E., Ten-Eyck, L. F. & Matthews, B. W. (1987). An efficient general-purpose least-squares refinement program for macromolecular structures. *Acta Crystallogr.* **A43**, 489-501.

Ui, N. (1971). Isoelectricpoints and conformation of proteins. II. Isoelectric focusing of alpha-chymotrypsin and its inactive derivative. *Biochim. Biophys. Acta* **229**, 567-581.

van Gent, D. C., Vink, C., Groeneger, A. A. & Plasterk, R. H. (1993). Complementation between HIV integrase proteins mutated in different domains. *EMBO J.* **12**(8), 3261-3267.

von Hippel, P. H. & Berg, O. G. (1989). Facilitated target location in biological systems. *J. Biol. Chem.* **264**(2), 675-678.

von Hippel, P. H. & Schleich, T. (1969a). The effects of neutral salts on the structure and confomational stability of macromolecules in solution. In *Biological Macromolecules* (Timasheff, S. & Fasman, G., eds.), Vol. 2, pp. 417-574. Marcel Dekker, New York.

von Hippel, P. H. & Schleich, T. (1969b). Ion effects on the solution strucuture of biological macromolecules. *Acc. Chem. Res.* **2**, 257-265.

von Hippel, P. H. & Wong, K.-Y. (1965). On the conformational stability of globular proteins: The effects of various electrolytes and nonelectrolytes on the thermal ribonuclease transition. *J. Biol. Chem.* **240**, 3909-3923.

Wade, R. C., Gabdoulline, R. R., Ludemann, S. K. & Lounnas, V. (1998). Electrostatic steering and ionic tethering in enzyme-ligand binding: insights from simulations. *Proc. Natl. Acad. Sci. U.S.A.* **95**(11), 5942-5949.

Warren, J. C. & Cheatum, S. G. (1966). Effect of neutral salts on enzyme activity and structure. *Biochemistry* **5**(5), 1702-1707.

Warren, J. C., Stowring, L. & Morales, M. F. (1966). The effect of structure-disrupting ions on the activity of myosin and other enzymes. *J. Biol. Chem.* **241**(2), 309-316.

Warshel, A. (1998). Electrostatic origin of the catalytic power of enzymes and the role of preorganized active sites. *J. Biol. Chem.* **273**(42), 27035-27038.

Wente, S. R. & Schachman, H. K. (1987). Shared active sites in oligomeric enzymes: Model studies with defective mutants of aspartate transcarbamoylase produced by site-directed mutagenesis. *Proc. Natl. Acad. Sci. U.S.A.* **84**(1), 31-35.

Winstead, J. A. & Wold, F. (1965). The effect of high concentrations of salt on kinetic properties of pancreatic ribonuclease. *J. Biol. Chem.* **240**, PC3694-PC3696.

Wiseman, T., Williston, S., Brandts, J. F. & Lin, L.-N. (1989). Rapid measurement of bindind constants and heat using a new titration calorimeter. *Anal. Biochem.* **179**, 131-137.

Witkowski, A., Joshi, A. & Smith, S. (1996). Fatty acid synthase: In vitro complementation of inactive mutants. *Biochemistry* **35**(32), 10569-10575.

Witzel, H. (1963). The function of the pyrimidine base in the ribonuclease reaction. *Progr. Nucleic Acid Res.* **2**, 221-258.

Witzel, H. & Barnard, E. A. (1962). Mechanism and binding sites in the ribonuclease reaction II. Kinetic studies of the first step of the reaction. *Biochem. Biophys. Res. Com.* **7**(4), 295-299.

Zegers, I., Maes, D., Dao-Thi, M. H., Poortmans, F., Palmer, R. & Wyns, L. (1994). The structures of RNase A complexed with 3'-CMP and d(CpA): Active site conformation and conserved water molecules. *Protein Sci.* **3**(12), 2322-2339.

Zhang, R. M. & Snyder, G. H. (1989). Dependence of formation of small disulfide loops in two-cysteine peptides on the number and types of intervening amino acids. *J. Biol. Chem.* **264**(31), 18472-19479.

Zheng, M., Aslund, F. & Storz, G. (1998). Activation of the OxyR transcription factor by reversible disulfide bond formation. *Science* **279**(5357), 1718-1721.